

Classical Quantum Mechanics

Randell L. Mills

Abstract

Despite its successes, quantum mechanics (QM) has remained mysterious to all who have encountered it. Starting with Bohr and progressing into the present, the departure from intuitive, physical reality has widened. The connection between QM and reality is more than just a "philosophical" issue. It reveals that QM is not a correct or complete theory of the physical world and that inescapable internal inconsistencies and incongruities arise when attempts are made to treat it as physical as opposed to a purely mathematical "tool." Some of these issues are discussed in a review by F. Laloë [Am. J. Phys. 69, 655 (2001)]. In an attempt to provide some physical insight into atomic problems and starting with the same essential physics as Bohr of e^- moving in the Coulombic field of the proton and the wave equation as modified by Schrödinger, a classical approach is explored that yields a remarkably accurate model and provides insight into physics on the atomic level. The proverbial view, deeply seated in the wave-particle duality notion, that there is no large-scale physical counterpart to the nature of the electron may not be correct. Physical laws and intuition may be restored when dealing with the wave equation and quantum-mechanical problems. Specifically, a theory of classical quantum mechanics (CQM) is derived from first principles that successfully applies physical laws on all scales. Rather than using the postulated Schrödinger boundary condition " $\Psi \rightarrow 0$ as $r \rightarrow \infty$," which leads to a purely mathematical model of the electron, the constraint is based on experimental observation. Using Maxwell's equations, the classical wave equation is solved with the constraint that the bound ($n = 1$)-state electron cannot radiate energy. By further application of Maxwell's equations to electromagnetic and gravitational fields at particle production, the Schwarzschild metric is derived from the classical wave equation, which modifies general relativity to include conservation of space-time in addition to momentum and matter/energy. The result gives a natural relationship among Maxwell's equations, special relativity, and general relativity. CQM holds over a scale of space-time of 85 orders of magnitude — it correctly predicts the nature of the universe from the scale of the quarks to that of the cosmos. A review is given by G. Landvogt [Internat. J. Hydrogen Energy 28, 1155 (2003)].

Key words: Maxwell's equations, nonradiation, quantum theory, special and general relativity, particle masses, cosmology, wave equation

1. INTRODUCTION

The hydrogen atom is the only real problem for which the Schrödinger equation can be solved without approximations; however, it only provides three quantum numbers, not four, and inescapable disagreements between observation and predictions arise from the later postulated Dirac equation as well as the Schrödinger equation.⁽³⁻⁵⁾ Furthermore, physical laws, such as Maxwell's equations, have a physical basis,

unlike Dirac's and Schrödinger's equations, which must be accepted without any underlying physical basis for fundamental observables such as the stability of the hydrogen atom in the first place, which is always disconcerting to those that study quantum mechanics (QM). In this instance, a circular argument regarding definitions for parameters in the wave equation solutions and the Rydberg series of spectral lines replaces a prediction of those lines based on first principles.⁽³⁻⁵⁾ Nevertheless, the application of the

Schrödinger equation to real problems has provided useful approximations for physicists and chemists. Schrödinger interpreted $e\Psi^*(x)\Psi(x)$ as the charge density or the amount of charge between x and $x + dx$ (Ψ^* is the complex conjugate of Ψ). Presumably, then, he pictured the electron to be spread over large regions of space. Max Born, who was working with scattering theory, later found that Schrödinger's interpretation led to inconsistencies, so he replaced it with the probability of finding the electron between x and $x + dx$ as

$$\int \Psi(x)\Psi^*(x)dx. \quad (1)$$

Born's interpretation is generally accepted. Nonetheless, interpretation of the wave-function is a never-ending source of confusion and conflict. Many scientists have solved this problem by conveniently adopting the Schrödinger interpretation for some problems and the Born interpretation for others. This duality allows the electron to be everywhere at one time — yet have no volume. Alternatively, the electron can be viewed as a discrete particle that moves here and there (from $r = 0$ to $r = \infty$), and $\Psi\Psi^*$ gives the time average of this motion. Despite its successes, after decades of futility, QM and the intrinsic Heisenberg uncertainty principle have not yielded a unified theory, are still purely mathematical, and have yet to be shown to be based on reality.⁽⁵⁾ Both are based on circular arguments that the electron is a point with no volume with a vague probability wave requiring that the electron have multiple positions and energies including negative and infinite energies simultaneously. It may be time to revisit the 75-year-old notion that fundamental particles such as the electron are one- or zero-dimensional and obey different physical laws than objects comprising fundamental particles and the even more disturbing view that fundamental particles don't obey physical laws — rather they obey mathematics devoid of physical laws. Perhaps mathematics does not determine physics. It only models physics.

The Schrödinger equation was originally postulated in 1926 as having a solution of the one-electron atom. It gives the principal energy levels of the hydrogen atom as eigenvalues of eigenfunction solutions of the Laguerre differential equation. But, when the principal quantum number n is much greater than 1, the eigenfunctions become nonsensical since they are sinusoidal over all space; thus they are nonintegrable, cannot be normalized, and are infinite.⁽⁶⁾ Despite its wide acceptance, on deeper inspection, the

Schrödinger equation solution is plagued with many failings as well as difficulties in terms of a physical interpretation that have caused it to remain controversial since its inception. Only the one-electron atom may be solved without approximations, but the equation fails to predict electron spin and leads to models with nonsensical consequences such as negative energy states of the vacuum, infinities, and negative kinetic energy. In addition to many predictions, which simply do not agree with observations, the Schrödinger equation and succeeding extensions predict noncausality, nonlocality, spooky actions at a distance or quantum telepathy, perpetual motion, and many internal inconsistencies where contradicting statements have to be taken true simultaneously.⁽³⁻⁵⁾

It was reported previously⁽⁵⁾ that the behavior of free electrons in superfluid helium has again forced the issue of the meaning of the wave-function. Electrons form bubbles in superfluid helium, which reveal that the electron is real and that a physical interpretation of the wave-function is necessary. Furthermore, when irradiated with light of energy of about 0.5 to several electron volts,⁽⁷⁾ the electrons carry current at different rates as if they exist with different sizes. It has been proposed that the behavior of free electrons in superfluid helium can be explained in terms of the electron breaking into pieces at superfluid helium temperatures.⁽⁷⁾ Yet the electron has proved to be indivisible even under particle accelerator collisions at 90 GeV (Large Electron Positron Collider II). The nature of the wave-function needs to be addressed. It is time for the physical rather than the mathematical nature of the wave-function to be determined.

From the time of its inception, QM has been controversial because its foundations are in conflict with physical laws and are internally inconsistent. Interpretations of QM such as hidden variables, multiple worlds, consistency rules, and spontaneous collapse have been put forward in an attempt to base the theory in reality. Unfortunately, many theoreticians ignore the requirement that the wave-function be real and physical in order for it to be considered a valid description of reality. For example, regarding this issue, Fuchs and Peres believe,⁽⁸⁾ "Contrary to those desires, quantum theory does *not* describe physical reality. What it does is provide an algorithm for computing *probabilities* for macroscopic events ('detector ticks') that are the consequences of our experimental interventions. This strict definition of the scope of quantum theory is the only interpretation ever needed, whether by experimenters or theorists."

With Penning traps, it is possible to measure transitions including those with hyperfine levels of electrons of single ions. This case can be experimentally distinguished from statistics over equivalent transitions in many ions. Whether many or one, the transition energies are always identical within the resonant line width. So *probabilities* have no place in describing atomic energy levels. Moreover, quantum theory is incompatible with probability theory since it is based on underlying unknown, but determined, outcomes, as discussed previously.⁽⁵⁾

The Copenhagen interpretation provides another meaning of QM. It asserts that what we observe is all we can know; any speculation about what an electron, photon, atom, or other atomic-sized entity is really or what it is doing when we are not looking is just that — speculation. The postulate of quantum measurement asserts that the process of measuring an observable forces it into a state of reality. In other words, reality is irrelevant until a measurement is made. In the case of electrons in superfluid helium, the fallacy with this position is that the “ticks” (migration times of electron bubbles) reveal that the electron is real before a measurement is made. Furthermore, experiments on transitions on single ions such as Ba^+ in a Penning trap under continuous observation demonstrate that the postulate of quantum measurement of QM is experimentally disproved, as discussed previously.^(5,9) These issues and other such flawed philosophies and interpretations of experiments that arise from QM were discussed previously.⁽³⁻⁵⁾

QM gives correlations with experimental data. It does not explain the mechanism for the observed data. But it should not be surprising that it gives good correlations given that the constraints of internal consistency and conformance to physical laws are removed for a wave equation with an infinite number of solutions, where the solutions may be formulated as an infinite series of eigenfunctions with variable parameters. There are no physical constraints on the parameters. They may even correspond to unobservables such as virtual particles, hyperdimensions, effective nuclear charge, polarization of the vacuum, worm holes, spooky action at a distance, infinities, parallel universes, and faster than light travel. If the constraints of internal consistency and conformance to physical laws are invoked, QM has never successfully solved a physical problem.

Throughout the history of quantum theory, wherever there was an advance to a new application, it was necessary to repeat a trial-and-error experiment to find which method of calculation gave the right answers. Often the textbooks present only the successful

procedure as if it followed from first principles and do not mention the actual method by which it was found. In electromagnetic theory based on Maxwell's equations, one deduces the computational algorithm from the general principles. In quantum theory, the logic is just the opposite. One chooses the principle to fit the empirically successful algorithm. For example, we know that it required a great deal of art and tact over decades of effort to get correct predictions out of quantum electrodynamics (QED). For the right experimental numbers to emerge, one must do the calculation (i.e. subtract off the infinities) in one particular way and not in some other way that appears in principle equally valid. There is a corollary, noted by Kallen: from an inconsistent theory, any result may be derived.

Reanalysis of old experiments and many new experiments including electrons in superfluid helium challenge the Schrödinger equation predictions. Many noted physicists have rejected QM. Feynman also attempted to use first principles including Maxwell's equations to discover new physics to replace QM.⁽¹⁰⁾ Other great physicists of the 20th century have searched: “Einstein ... insisted ... that a more detailed, wholly deterministic theory must underlie the vagaries of quantum mechanics.”⁽¹¹⁾ He felt that scientists were misinterpreting the data. These issues and the results of many experiments, such as the wave-particle duality, the Lamb shift, anomalous magnetic moment of the electron, transition and decay lifetimes, and experiments invoking interpretations of spooky action at a distance such as the Aspect experiment, entanglement, and double-slit-type experiments, are shown to be absolutely predictable and physical in the context of a theory of classical quantum mechanics (CQM) derived from first principles.⁽³⁻⁵⁾ Using the classical wave equation with the constraint of nonradiation based on Maxwell's equations, CQM gives closed-form physical solutions for the electron in atoms, the free electron, and the free electron in superfluid helium, which match the observations without requiring that the electron be divisible. Moreover, unification of atomic and large-scale physics — the ultimate objective of natural theory — is enabled. CQM holds over a scale of space-time of 85 orders of magnitude — it correctly predicts the nature of the universe from the scale of the quarks to that of the cosmos.

2. CLASSICAL QUANTUM THEORY OF THE ATOM BASED ON MAXWELL'S EQUATIONS THAT HOLDS OVER ALL SCALES

In this paper the old view that the electron is a zero- or one-dimensional point in an all-space probability wave-function $\Psi(x)$ is not taken for granted. The theory of CQM, derived from first principles, must successfully and consistently apply physical laws on all scales.⁽³⁻⁵⁾ Historically, the point at which QM broke with classical laws can be traced to the issue of non-radiation of the one-electron atom that was addressed by Bohr with a postulate of stable orbits in defiance of the physics represented by Maxwell's equations.⁽³⁻⁵⁾ Later, physics was replaced by "pure mathematics" based on the notion of the inexplicable wave-particle duality nature of electrons, which lead to the Schrödinger equation, where the consequences of radiation predicted by Maxwell's equations were ignored. Ironically, both Bohr and Schrödinger used the electrostatic Coulomb potential of Maxwell's equations but abandoned the electrodynamic laws. Physical laws may indeed be the root of the observations thought to be "purely quantum mechanical," and it may have been a mistake to make the assumption that Maxwell's electrodynamic equations must be rejected at the atomic level. Thus, in the present approach, the classical wave equation is solved with the constraint that a bound ($n = 1$)-state electron cannot radiate energy.

Thus, here, derivations consider the electrodynamic effects of moving charges as well as the Coulomb potential, and the search is for a solution representative of the electron where there is acceleration of charge motion without radiation. The mathematical formulation for zero radiation based on Maxwell's equations follows from a derivation by Haus.⁽¹²⁾ The function that describes the motion of the electron must not possess space-time Fourier components that are synchronous with waves traveling at the speed of light. Similarly, nonradiation is demonstrated based on the electron's electromagnetic fields and the Poynting power vector.

In this paper a summary of the results of CQM^(3,13,14) is presented. (The details of the derivations are given in Ref. 3.) Specifically, CQM gives closed-form solutions for the atom including the stability of the $n = 1$ state and the instability of the excited states, the equation of the photon and electron in excited states, and the equation of the free electron and photon, which predict the wave-particle duality behavior of particles and light. The current and charge density functions of the electron may be directly

physically interpreted. For example, spin angular momentum results from the motion of negatively charged mass moving systematically, and the equation for angular momentum, $\mathbf{r} \times \mathbf{p}$, can be applied directly to the wave-function (a current density function) that describes the electron. The magnetic moment of a Bohr magneton, Stern-Gerlach experiment, g factor, Lamb shift, resonant line width and shape, selection rules, correspondence principle, wave-particle duality, excited states, reduced mass, rotational energies, momenta, orbital and spin splitting, spin-orbital coupling (fine structure), Knight shift, spin-nuclear coupling (hyperfine structure), muonium hyperfine structure interval, ionization energies of multi-electron atoms, elastic electron scattering from helium atoms, and nature of the chemical bond are derived in closed-form equations based on Maxwell's equations. The calculations agree with experimental observations.

For any kind of wave advancing with limiting velocity and capable of transmitting signals, the equation of front propagation is the same as the equation for the front of a light wave. By applying this condition to electromagnetic and gravitational fields at particle production, the Schwarzschild metric (SM) is derived from the classical wave equation, which modifies general relativity to include conservation of space-time as a consequence of (175) (See Ref. 3, Chap. 23, and footnote 7 of Chap. 23), in addition to momentum and matter/energy. The result gives a natural relationship between Maxwell's equations, special relativity, and general relativity. It gives gravitation from the atom to the cosmos. The universe is time harmonically oscillatory in matter energy and space-time expansion and contraction with a minimum radius that is the gravitational radius. In closed-form equations with fundamental constants only, CQM gives the deflection of light by stars, the precession of the perihelion of Mercury, the particle masses, the Hubble constant, the age of the universe, the observed acceleration of the expansion, the power of the universe, the power spectrum of the universe, the microwave background temperature, the uniformity of the microwave background radiation at 2.7 K with the microkelvin spatial variation observed by the degree angular scale interferometer (DASI), the observed violation of the GZK cutoff, the mass density, the large-scale structure of the universe, and the identity of dark matter, which matches the criteria for the structure of galaxies. In a special case where the gravitational potential energy density of a black hole equals that of the Planck mass, matter converts to

energy and space-time expands with the release of a gamma-ray burst. The singularity in the SM is eliminated.

3. ONE-ELECTRON ATOMS

One-electron atoms include the hydrogen atom, He^+ , Li^{2+} , Be^{3+} , and so on. The mass energy and angular momentum of the electron are constant; this requires that the equation of motion of the electron be temporally and spatially harmonic. Thus the classical wave equation applies and

$$\left(\nabla^2 - \frac{1}{v^2} \frac{\partial^2}{\partial t^2} \right) \rho(r, \theta, \phi, t) = 0, \quad (2)$$

where $\rho(r, \theta, \phi, t)$ is the time-dependent charge density function of the electron in time and space. In general, the wave equation has an infinite number of solutions. To arrive at the solution that represents the electron a suitable boundary condition must be imposed. It is well known from experiments that each single atomic electron of a given isotope radiates to the same stable state. Thus the physical boundary condition of nonradiation of the bound electron was imposed on the solution of the wave equation for the time-dependent charge density function of the electron.⁽³⁾ The condition for radiation by a moving point charge given by Haus⁽¹²⁾ is that its space-time Fourier transform possess components that are synchronous with waves traveling at the speed of light. Conversely, it is proposed that the condition for nonradiation by an ensemble of moving point charges that makes up a current density function is as follows:

For nonradiative states, the current density function must not possess space-time Fourier components that are synchronous with waves traveling at the speed of light.

The time, radial, and angular solutions of the wave equation are separable. The motion is time harmonic with frequency ω_n . A constant angular function is a solution to the wave equation. Solutions of the Schrödinger wave equation making up a radial function radiate according to Maxwell's equation, as shown previously by application of Haus's condition.⁽³⁾ In fact, it was found that any function that permitted radial motion gave rise to radiation. A radial function that satisfies the boundary condition is a radial delta function

$$f(r) = \frac{1}{r^2} \delta(r - r_n). \quad (3)$$

This function defines a constant charge density on a spherical shell where $r_n = nr_1$, where n is an integer in an excited state as given in Section 13, and (2) becomes the two-dimensional wave equation plus time with separable time and angular functions. Given time harmonic motion and a radial delta function, the relationship between an allowed radius and the electron wavelength is given by

$$2\pi r_n = \lambda_n, \quad (4)$$

where the subscript n is determined during photon absorption as given by (77). Using the observed de Broglie relationship for the electron mass, where the coordinates are spherical (this relationship is derived in Chap. 3 of Ref. 3), we have

$$\lambda_n = \frac{h}{p_n} = \frac{h}{m_e v_n}, \quad (5)$$

and the magnitude of the velocity for every point on the orbitsphere is

$$v_n = \frac{\hbar}{m_e r_n}. \quad (6)$$

The sum of the $|\mathbb{L}_i|$, the magnitude of the angular momentum of each infinitesimal point of the orbitsphere of mass m_i , must be constant. The constant is \hbar :

$$\Sigma |\mathbb{L}_i| = \Sigma |\mathbf{r} \times m_i \mathbf{v}| = m_e r_n \frac{\hbar}{m_e r_n} = \hbar. \quad (7)$$

Thus an electron is a spinning, two-dimensional spherical surface (zero thickness¹), called an *electron orbitsphere*, that can exist in a bound state at only specified distances from the nucleus, as shown in Fig. 1. The corresponding current function shown in Fig. 2, which gives rise to the phenomenon of *spin*, is derived in Section 4. (See the Appendix of this paper and the Orbitsphere Equation of Motion for $\ell = 0$ section of Ref. 3 at Chap. 1.)

Nonconstant functions are also solutions for the angular functions. To be a harmonic solution of the wave equation in spherical coordinates, these angular functions must be spherical harmonic functions.⁽¹⁵⁾ A

zero of the space-time Fourier transform of the product function of two spherical harmonic angular functions, a time harmonic function, and an unknown radial function is sought. The solution for the radial function that satisfies the boundary condition is also a delta function given by (3). Thus bound electrons are described by a charge density (mass density) function that is the product of a radial delta function, two angular functions (spherical harmonic functions), and a time harmonic function:

$$\begin{aligned}\rho(r, \theta, \phi, t) &= f(r) A(\theta, \phi, t) \\ &= \frac{1}{r^2} \delta(r - r_n) A(\theta, \phi, t), \\ A(\theta, \phi, t) &= Y(\theta, \phi) k(t).\end{aligned}\quad (8)$$

In these cases the spherical harmonic functions correspond to a traveling charge density wave confined to the spherical shell, which gives rise to the phenomenon of orbital angular momentum. The orbital functions that modulate the constant "spin" function shown graphically in Fig. 3 are given in Section 5.

4. SPIN FUNCTION

The orbitsphere spin function comprises a constant charge (current) density function with moving charge confined to a two-dimensional spherical shell. The current pattern of the orbitsphere spin function comprises an infinite series of correlated orthogonal great circle current loops where each point charge (current) density element moves time harmonically with constant angular velocity

$$\omega_n = \frac{\hbar}{m_e r_n^2}. \quad (9)$$

The uniform current density function $Y_0^0(\theta, \phi)$, the orbitsphere equation of motion of the electron (14)–(15), corresponding to the constant charge function of the orbitsphere that gives rise to the spin of the electron, is generated from a basis set current vector field defined as the orbitsphere current vector field (orbitsphere-cvf). This in turn is generated over the surface by two complementary steps of an infinite series of nested rotations of two orthogonal great circle current loops, where the coordinate axes rotate with the two orthogonal great circles that serve as a basis set. The algorithm to generate the current density function rotates the great circles and the corresponding $x'y'z'$ coordinates relative to the xyz frame. Each infinitesimal

rotation of the infinite series is about the new i' axis and new j' axis resulting from the preceding such rotation. Each element of the current density function is obtained with each conjugate set of rotations. In Appendix III of Ref. 3, the *continuous* uniform electron current density function $Y_0^0(\theta, \phi)$ ((14) and (15)) is then exactly generated from this orbitsphere-cvf as a basis element by a convolution operator comprising an autocorrelation-type function.

For Step 1, the current density elements move counterclockwise on the great circle in the $y'z'$ plane and clockwise on the great circle in the $x'z'$ plane. The great circles are rotated by an infinitesimal angle $\pm\Delta\alpha_y$ (a positive rotation around the x' axis and a negative rotation about the z' axis for Steps 1 and 2, respectively) and then by $\pm\Delta\alpha_z$ (a positive rotation around the new y' axis and a positive rotation about the new x' axis for Steps 1 and 2, respectively). The coordinates of each point on each rotated great circle (x', y', z') are expressed in terms of the first (x, y, z) coordinates by the following transforms, where clockwise rotations and motions are defined as positive looking along the corresponding axis. Note the abbreviations of c for cosine and s for sine to save space.

Step 1:

$$\begin{aligned}\begin{bmatrix} x \\ y \\ z \end{bmatrix} &= \begin{bmatrix} c(\Delta\alpha_y) & 0 & -s(\Delta\alpha_y) \\ 0 & 1 & 0 \\ s(\Delta\alpha_y) & 0 & c(\Delta\alpha_y) \end{bmatrix} \\ &\quad \times \begin{bmatrix} 1 & 0 & 0 \\ 0 & c(\Delta\alpha_x) & s(\Delta\alpha_x) \\ 0 & -s(\Delta\alpha_x) & c(\Delta\alpha_x) \end{bmatrix} \begin{bmatrix} x' \\ y' \\ z' \end{bmatrix} \\ &= \begin{bmatrix} c(\Delta\alpha_y) & s(\Delta\alpha_y)s(\Delta\alpha_x) & -s(\Delta\alpha_y)c(\Delta\alpha_x) \\ 0 & c(\Delta\alpha_x) & s(\Delta\alpha_x) \\ s(\Delta\alpha_y) & -c(\Delta\alpha_y)s(\Delta\alpha_x) & c(\Delta\alpha_y)c(\Delta\alpha_x) \end{bmatrix} \begin{bmatrix} x' \\ y' \\ z' \end{bmatrix}.\end{aligned}\quad (10)$$

Step 2:

$$\begin{aligned}
\begin{bmatrix} x \\ y \\ z \end{bmatrix} &= \begin{bmatrix} 1 & 0 & 0 \\ 0 & c(\Delta\alpha_x) & s(\Delta\alpha_x) \\ 0 & -s(\Delta\alpha_x) & c(\Delta\alpha_x) \end{bmatrix} \begin{bmatrix} c(\Delta\alpha_z) & s(\Delta\alpha_z) & 0 \\ -s(\Delta\alpha_z) & c(\Delta\alpha_z) & 0 \\ 0 & 0 & 1 \end{bmatrix} \begin{bmatrix} x' \\ y' \\ z' \end{bmatrix} \\
&= \begin{bmatrix} c(\Delta\alpha_z) & s(\Delta\alpha_z) & 0 \\ -c(\Delta\alpha_x)s(\Delta\alpha_z) & c(\Delta\alpha_x)c(\Delta\alpha_z) & s(\Delta\alpha_x) \\ s(\Delta\alpha_x)s(\Delta\alpha_z) & -s(\Delta\alpha_x)c(\Delta\alpha_z) & c(\Delta\alpha_x) \end{bmatrix} \begin{bmatrix} x' \\ y' \\ z' \end{bmatrix}. \quad (11)
\end{aligned}$$

The angular sum in (10) and (11) is

$$\lim_{\Delta\alpha \rightarrow 0} \sum_{n=1}^{\frac{\sqrt{2}\pi}{2\Delta\alpha}} |\Delta\alpha_{i,j}| = \frac{\sqrt{2}}{2} \pi.$$

The orbitsphere-cvf is given by n reiterations of (10) and (11) for each point on each of the two orthogonal great circles during each of Steps 1 and 2. The output given by the nonprimed coordinates is the input of the next iteration corresponding to each successive nested rotation by the infinitesimal angle $\pm\Delta\alpha_i$ or $\pm\Delta\alpha_j$, where the magnitude of the angular sum of the n rotations about the i' axis and the j' axis is $(\sqrt{2}/2)\pi$. Half of the orbitsphere-cvf is generated during each of Steps 1 and 2.

Following Step 2, in order to match the boundary condition that the magnitude of the velocity at any given point on the surface is given by (6), the output half of the orbitsphere-cvf is rotated clockwise by an angle of $\pi/4$ about the z axis. Using (11) with $\Delta\alpha_z = \pi/4$ and $\Delta\alpha_x = 0$ gives the rotation. Then the one half of the orbitsphere-cvf generated from Step 1 is superimposed with the complementary half obtained from Step 2 following its rotation about the z axis of $\pi/4$ to give the basis function to generate $Y_0^0(\theta, \phi)$, the orbitsphere equation of motion of the electron, by convolution about the resultant angular momentum axis.

The current pattern of the orbitsphere-cvf generated by the nested rotations of the orthogonal great circle current loops is a continuous and total coverage of the spherical surface, but it is shown as a visual representation using 6° increments of the infinitesimal angular variable $\pm\Delta\alpha_i$ or $\pm\Delta\alpha_j$ of (10) and (11) from the perspective of the z axis in Fig. 2. In each case, the complete orbitsphere current pattern corresponds to all the orthogonal great circle elements generated by the rotation of the basis set according to (10) and (11), where $\pm\Delta\alpha_i$ and $\pm\Delta\alpha_j$ approach zero and the summation of the infinitesimal angular rotations of $\pm\Delta\alpha_i$ and

$\pm\Delta\alpha_j$ about the successive i' axes and j' axes is $(\sqrt{2}/2)\pi$ for each step.

The resultant angular momentum projections of $L_{xy} = \hbar/4$ and $L_z = \hbar/2$ meet the boundary condition for the unique current with angular velocity magnitude at each point on the surface given by (6) and give rise to the Stern-Gerlach experiment, as shown in Ref. 3. The further constraint that the current density is uniform such that the charge density is uniform, corresponding to an equipotential, minimum energy surface, is satisfied by using the orbitsphere-cvf as a basis element to generate $Y_0^0(\theta, \phi)$ using a convolution operator comprising an autocorrelation-type function, as given in Appendix III of Ref. 3. The operator comprises the convolution of each great circle current loop of the orbitsphere-cvf designated as the primary orbitsphere-cvf with a second orbitsphere-cvf designated as the secondary orbitsphere-cvf having its angular momentum matched to that of each convoluted current loop such that the resulting exact uniform current distribution obtained from the convolution has the same components of $L_{xy} = \hbar/4$ and $L_z = \hbar/2$ as those of the orbitsphere-cvf used as a primary basis element. The current pattern gives rise to the phenomenon corresponding to the spin quantum number. The details of the derivation of the spin function are given in the Appendix of this paper and in Chapter 1 of Ref. 3.

5. ANGULAR FUNCTIONS

The time, radial, and angular solutions of the wave equation are separable. Also, based on the radial solution, the angular charge and current density functions of the electron, $A(\theta, \phi, t)$, must be a solution of the wave equation in two dimensions (plus time):

$$\left[\nabla^2 - \frac{1}{v^2} \frac{\partial^2}{\partial t^2} \right] A(\theta, \phi, t) = 0, \quad (12)$$

where $\rho(r, \theta, \phi, t) = f(r)A(\theta, \phi, t) = (1/r^2)\delta(r - r_n)A(\theta, \phi, t)$ and $A(\theta, \phi, t) = Y(\theta, \phi)k(t)$:

$$\left[\frac{1}{r^2 \sin \theta} \frac{\partial}{\partial \theta} \left(\sin \theta \frac{\partial}{\partial \theta} \right)_{r,\phi} + \frac{1}{r^2 \sin^2 \theta} \left(\frac{\partial^2}{\partial \phi^2} \right)_{r,\theta} - \frac{1}{v^2} \frac{\partial^2}{\partial t^2} \right] A(\theta, \phi, t) = 0, \quad (13)$$

where v is the linear velocity of the electron. The charge density functions including the time function factor are

$$\rho(r, \theta, \phi, t) = \frac{e}{8\pi r^2} [\delta(r - r_n)] [Y_0^0(\theta, \phi) + Y_l^m(\theta, \phi)] \quad (14)$$

for $\ell = 0$ and

$$\rho(r, \theta, \phi, t) = \frac{e}{4\pi r^2} [\delta(r - r_n)] [Y_0^0(\theta, \phi) + \text{Re}\{Y_l^m(\theta, \phi)e^{i\omega_n t}\}] \quad (15)$$

for $\ell \neq 0$, where $Y_l^m(\theta, \phi)$ are the spherical harmonic functions that spin about the z axis with angular frequency ω_n with $Y_0^0(\theta, \phi)$ the constant function. $\text{Re}\{Y_l^m(\theta, \phi)e^{i\omega_n t}\} = P_l^m(\cos \theta) \cos(m\phi + \omega_n t)$, where, to keep the form of the spherical harmonic as a traveling wave about the z axis, $\omega_n' = m\omega_n$.

6. ACCELERATION WITHOUT RADIATION

6.1 Special Relativistic Correction to the Electron Radius

The relationship between the electron wavelength and its radius is given by (4), where λ is the de Broglie wavelength. For each current density element of the spin function, the distance along each great circle in the direction of instantaneous motion undergoes length contraction and time dilation. Using a phase-matching condition, the wavelengths of the electron and laboratory inertial frames are equated, and the corrected radius is given by

$$r_n = r_n' \left[\sqrt{1 - \left(\frac{v}{c}\right)^2} \sin \left[\frac{\pi}{2} \left(1 - \left(\frac{v}{c}\right)^2 \right)^{3/2} \right] + \frac{1}{2\pi} \cos \left[\frac{\pi}{2} \left(1 - \left(\frac{v}{c}\right)^2 \right)^{3/2} \right] \right] \quad (16)$$

where the electron velocity is given by (6) (see Ref. 3, Chap. 1, Special Relativistic Correction to the Ionization Energies section). e/m_e of the electron, the electron angular momentum of \hbar , and μ_B are invariant, but the mass and charge densities increase in the laboratory frame due to the relativistically contracted electron radius. As $v \rightarrow c$, $r/r' \rightarrow 1/2\pi$ and $r = \lambda$, as shown in Fig. 4.

6.2 Nonradiation Based on Haus's Condition

The Fourier transform of the electron charge density function given by (8) is a solution of the three-dimensional wave equation in frequency space (\mathbf{k} , ω_{space}), as given in Chapter 1, Space-Time Fourier Transform of the Electron Function section, of Ref. 3. Then the corresponding Fourier transform of the current density function $K(s, \Theta, \Phi, \omega)$ is given by multiplying by the constant angular frequency:

$$K(s, \Theta, \Phi, \omega) = 4\pi\omega_n \frac{\sin(2s_n r_n)}{2s_n r_n} \otimes 2\pi \sum_{\nu=1}^{\infty} \left[\frac{(-1)^{\nu-1} (\pi \sin \Theta)^{2(\nu-1)}}{(\nu-1)!(\nu-1)!} \frac{\Gamma(1/2)\Gamma(\nu+1/2)}{(\pi \cos \Theta)^{2\nu+1}} \frac{2\nu!}{2^{\nu+1}(\nu-1)!} s^{-2\nu} \right] \otimes 2\pi \sum_{\nu=1}^{\infty} \left[\frac{(-1)^{\nu-1} (\pi \sin \Phi)^{2(\nu-1)}}{(\nu-1)!(\nu-1)!} \frac{\Gamma(1/2)\Gamma(\nu+1/2)}{(\pi \cos \Phi)^{2\nu+1}} \frac{2\nu!}{2^{\nu+1}(\nu-1)!} s^{-2\nu} \right] \frac{1}{4\pi} [\delta(\omega - \omega_n) + \delta(\omega + \omega_n)]. \quad (17)$$

$s_n \cdot v_n = s_n \cdot c = \omega_n$ implies $r_n = \lambda_n$, which is given by (16) in the case that k is the light-like k^0 . In this case, (17) vanishes. Consequently, space-time harmonics of $\omega_n/c = k$ or $(\omega_n/c)\sqrt{\epsilon/\epsilon_0} = k$ for which the Fourier transform of the current density function is nonzero do not exist. Radiation due to charge motion does not occur in any medium when this boundary condition is met. (Nonradiation is also determined from the fields based on Maxwell's equations as given in Section 6.3 below and the same section of Chapter 1, Appendix I, of Ref. 3.)

6.3 Nonradiation Based on the Electron Electromagnetic Fields and the Poynting Power Vector

A point charge undergoing periodic motion accelerates and as a consequence radiates according to the Larmor formula

$$P = \frac{1}{4\pi\epsilon_0} \frac{2e^2}{3c^3} a^2, \quad (18)$$

where e is the charge, a is its acceleration, ϵ_0 is the permittivity of free space, and c is the speed of light. Although an accelerated *point* particle radiates, an *extended distribution* modeled as a superposition of

accelerating charges does not have to radiate.^(12,16-19) An ensemble of charges, all oscillating at the same frequency, create a radiation pattern with a number of nodes. The same applies to current patterns in phased array antenna design.⁽²⁰⁾ It is possible to have an infinite number of charges oscillating in such a way as to cause destructive interference or nodes in all directions. The electromagnetic far field is determined from the current distribution in order to obtain the condition, if it exists, that the electron current distribution given by (21) must satisfy so that the electron does not radiate.

The charge density functions of the electron orbitsphere in spherical coordinates plus time are given by (14) and (15). For $\ell = 0$, the equipotential, uniform, or constant charge density function (14) further comprises a current pattern given in Section 4. It also corresponds to the nonradiative $n = 1, \ell = 0$ state of atomic hydrogen and to the spin function of the electron. The current density function is given by multiplying (14) by the constant angular velocity ω . There is acceleration without radiation. In this case, it is centripetal acceleration. A static charge distribution exists even though each point on the surface is accelerating along a great circle. Haus's condition predicts no radiation for the entire ensemble. The same result is trivially predicted from consideration of the fields and the radiated power. Since the current is not time dependent, the fields are given by

$$\nabla \times \mathbf{H} = \mathbf{J} \quad (19)$$

and

$$\nabla \times \mathbf{E} = 0, \quad (20)$$

which are the electrostatic and magnetostatic cases, respectively, *with no radiation*.

The nonradiation condition given by (17) may be confirmed by determining the fields and the current distribution condition that is nonradiative based on Maxwell's equations. For $\ell \neq 0$, the charge density functions including the time function factor are given by (15). In the cases that $m \neq 0$, (15) is a traveling charge density wave that moves on the surface of the orbitsphere about the z axis and modulates the orbitsphere corresponding to $\ell = 0$. Since the charge is moving time harmonically about the z axis with frequency ω_n and the current density function is given by the time derivative of the charge density function, the current density function is given by the normalized product of the constant angular velocity and the

charge density function. The first current term of (15) is static. Thus it is trivially nonradiative.

The current due to the time-dependent term is

$$\begin{aligned} \mathbf{J} &= A N[\delta(r-r_n)] \text{Re}\{Y_\ell^m(\theta, \phi)\} [\mathbf{u}(t) \times \mathbf{r}] \\ &= A N[\delta(r-r_n)] \text{Re}\{Y_\ell^m(\theta, \phi) e^{i\omega_n t}\} [\mathbf{u} \times \mathbf{r}] \\ &= A N'[\delta(r-r_n)] \text{Re}\{P_\ell^m(\cos \theta) e^{im\phi} e^{i\omega_n t}\} [\mathbf{u} \times \mathbf{r}] \quad (21) \\ &= A N'[\delta(r-r_n)] (P_\ell^m(\cos \theta) \cos(m\phi + \omega_n' t)) [\mathbf{u} \times \mathbf{r}] \\ &= A N'[\delta(r-r_n)] (P_\ell^m(\cos \theta) \cos(m\phi + \omega_n' t)) \sin \theta \hat{\phi}, \end{aligned}$$

where we have used the abbreviation

$$A = \frac{\omega_n}{2\pi} \frac{e}{4\pi r_n^2}$$

to save space, and, to keep the form of the spherical harmonic as a traveling wave about the z axis, $\omega_n' = m\omega_n$ and N and N' are normalization constants. The vectors are defined as

$$\hat{\phi} = \frac{\hat{\mathbf{u}} \times \hat{\mathbf{r}}}{|\hat{\mathbf{u}} \times \hat{\mathbf{r}}|} = \frac{\hat{\mathbf{u}} \times \hat{\mathbf{r}}}{\sin \theta}, \quad (22)$$

$$\hat{\mathbf{u}} = \hat{\mathbf{z}} = \text{orbital axis},$$

$$\hat{\theta} = \hat{\phi} \times \hat{\mathbf{r}}, \quad (23)$$

where $\hat{\mathbf{u}}$ denotes unit vectors (e.g., $\hat{\mathbf{u}} = \mathbf{u}/|\mathbf{u}|$), nonunit vectors are designated in bold, and the current function is normalized. For time-varying electromagnetic fields, Jackson⁽²¹⁾ gives a generalized expansion in vector spherical waves, which are convenient for electromagnetic boundary value problems possessing spherical symmetry properties and for analyzing multipole radiation from a localized source distribution. The Green function $G(\mathbf{x}', \mathbf{x})$ that is appropriate to the equation

$$(\nabla^2 + k^2)G(\mathbf{x}', \mathbf{x}) = -\delta(\mathbf{x}' - \mathbf{x}) \quad (24)$$

in the infinite domain is

$$\begin{aligned} G(\mathbf{x}', \mathbf{x}) &= \frac{e^{-ik|\mathbf{x}-\mathbf{x}'|}}{|\mathbf{x}-\mathbf{x}'|} \\ &= ik \sum_{\ell=0}^{\infty} j_\ell(kr_<) h_\ell^{(1)}(kr_>) \sum_{m=-\ell}^{\ell} Y_{\ell,m}^*(\theta', \phi') Y_{\ell,m}(\theta, \phi). \end{aligned} \quad (25)$$

where the spherical wave expansion for the outgoing wave is given. General coordinates are shown in Fig. 5. Jackson⁽²¹⁾ further gives the general multipole field solution to Maxwell's equations in a source-free region of empty space with the assumption of a time dependence $e^{i\omega_n t}$:

$$\begin{aligned} \mathbf{B} &= \sum_{\ell, m} \left[a_E(\ell, m) f_\ell(kr) \mathbf{X}_{\ell, m} \right. \\ &\quad \left. - \frac{i}{k} a_M(\ell, m) \nabla \times g_\ell(kr) \mathbf{X}_{\ell, m} \right], \\ \mathbf{E} &= \sum_{\ell, m} \left[\frac{i}{k} a_E(\ell, m) \nabla \times f_\ell(kr) \mathbf{X}_{\ell, m} \right. \\ &\quad \left. + a_M(\ell, m) g_\ell(kr) \mathbf{X}_{\ell, m} \right], \end{aligned} \quad (26)$$

where the cgs units used by Jackson are retained in this section. The radial functions $f_\ell(kr)$ and $g_\ell(kr)$ are of the form

$$g_\ell(kr) = A_\ell^{(0)} h_\ell^{(1)} + A_\ell^{(2)} h_\ell^{(2)}. \quad (27)$$

$\mathbf{X}_{\ell, m}$ is the vector spherical harmonic defined by

$$\mathbf{X}_{\ell, m}(\theta, \phi) = \frac{1}{\sqrt{\ell(\ell+1)}} \mathbf{L} Y_{\ell, m}(\theta, \phi), \quad (28)$$

where

$$\mathbf{L} = \frac{1}{i} (\mathbf{r} \times \nabla). \quad (29)$$

The coefficients $a_E(\ell, m)$ and $a_M(\ell, m)$ of (26) specify the amounts of electric (ℓ, m) multipole and magnetic (ℓ, m) multipole fields and are determined by sources and boundary conditions, as are the relative proportions in (27). Jackson gives the result of the electric and magnetic coefficients from the sources as

$$\begin{aligned} a_E(\ell, m) &= \frac{4\pi k^2}{i\sqrt{\ell(\ell+1)}} \int Y_{\ell, m}^* \left\{ \rho \frac{\delta}{\delta r} [r j_\ell(kr)] \right. \\ &\quad \left. + \frac{ik}{c} (\mathbf{r} \cdot \mathbf{J}) j_\ell(kr) - ik \nabla \cdot (\mathbf{r} \times \mathbf{M}) j_\ell(kr) \right\} d^3x \end{aligned} \quad (30)$$

and

$$\begin{aligned} a_M(\ell, m) &= \frac{-4\pi k^2}{\sqrt{\ell(\ell+1)}} \int j_\ell(kr) Y_{\ell, m}^* \mathbf{L} \cdot \left(\frac{\mathbf{J}}{c} + \nabla \times \mathbf{M} \right) d^3x, \end{aligned} \quad (31)$$

respectively, where the distribution of charge $\rho(\mathbf{x}, t)$, current $\mathbf{J}(\mathbf{x}, t)$, and intrinsic magnetization $\mathbf{M}(\mathbf{x}, t)$ are harmonically varying sources: $\rho(\mathbf{x}) e^{-i\omega_n t}$, $\mathbf{J}(\mathbf{x}) e^{-i\omega_n t}$, and $\mathbf{M}(\mathbf{x}) e^{-i\omega_n t}$. From (21) the charge and intrinsic magnetization terms are zero. Also, the current $\mathbf{J}(\mathbf{x}, t)$ is in the $\hat{\phi}$ direction; thus the $a_E(\ell, m)$ coefficient given by (30) is zero since $\mathbf{r} \cdot \mathbf{J} = 0$. Substitution of (21) into (31) gives the magnetic multipole coefficient $a_M(\ell, m)$:

$$\begin{aligned} a_M(\ell, m) &= \frac{-4\pi k^2}{\sqrt{\ell(\ell+1)}} \int j_\ell(kr) Y_{\ell, m}^* \mathbf{L} \\ &\quad \cdot \left(\frac{\frac{\omega_n}{2\pi} \frac{e}{4\pi r_n^2} N \delta(r - r_n) Y_{\ell, m}^*(\theta, \phi) \sin \theta \hat{\phi}}{c} \right) d^3x. \end{aligned} \quad (32)$$

Each mass density element of the electron moves about the z axis along a circular orbit of radius $r_n \sin \theta$ in such a way that ϕ changes at a constant rate. That is, $\phi = \omega t$ at time t , where ω_n is the constant angular frequency given in (21) and

$$\mathbf{r}(t) = i \mathbf{r}_n \sin \theta \cos \omega t + \mathbf{j} r_n \sin \theta \sin \omega t \quad (33)$$

is the parametric equation of the circular orbit. Jackson gives the operator in the xy plane corresponding to the current motion in this plane and the relations for $Y_{\ell, m}^*(\theta, \phi)$:⁽²¹⁾

$$L_+ = L_x + iL_y = e^{i\phi} \left(\frac{\partial}{\partial \theta} + i \cot \theta \frac{\partial}{\partial \phi} \right), \quad (34)$$

$$L_+ Y_{\ell, m}^*(\theta, \phi) = \sqrt{(\ell - m)(\ell + m + 1)} Y_{\ell, m+1}^*(\theta, \phi). \quad (35)$$

Using (34), $\mathbf{L} \cdot \mathbf{J}$ of (31) is

$$\begin{aligned}
& L_+(Y_\ell^m(\theta, \phi) \sin \theta) \\
&= e^{i\phi} \left(\frac{\partial}{\partial \theta} + i \cot \theta \frac{\partial}{\partial \phi} \right) Y_\ell^m(\theta, \phi) \sin \theta \\
&= e^{i\phi} Y_\ell^m(\theta, \phi) \left(\frac{\partial}{\partial \theta} + i \cot \theta \frac{\partial}{\partial \phi} \right) \sin \theta \\
&\quad + e^{i\phi} \sin \theta \left(\frac{\partial}{\partial \theta} + i \cot \theta \frac{\partial}{\partial \phi} \right) Y_\ell^m(\theta, \phi).
\end{aligned} \tag{36}$$

Using (35) in (36) gives

$$\begin{aligned}
L_+(Y_\ell^m(\theta, \phi) \sin \theta) &= e^{i\phi} Y_\ell^m(\theta, \phi) \cos \theta \\
&\quad + \sin \theta \sqrt{(\ell-m)(\ell+m+1)} Y_{\ell}^{m+1}(\theta, \phi).
\end{aligned} \tag{37}$$

The spherical harmonic is given as

$$\begin{aligned}
Y_\ell^m(\theta, \phi) &= \sqrt{\frac{2\ell+1}{4\pi} \frac{(\ell-m)!}{(\ell+m)!}} P_\ell^m(\cos \theta) e^{im\phi} \\
&= N_{\ell,m} P_\ell^m(\cos \theta) e^{im\phi}.
\end{aligned} \tag{38}$$

Thus (37) is given as

$$\begin{aligned}
L_+(Y_\ell^m(\theta, \phi) \sin \theta) &= e^{i\phi} N_{\ell,m} P_\ell^m(\cos \theta) e^{im\phi} \cos \theta \\
&\quad + \sin \theta \sqrt{(\ell-m)(\ell+m+1)} N_{\ell,m+1} P_\ell^{m+1}(\cos \theta) e^{i(m+1)\phi}.
\end{aligned} \tag{39}$$

Substitution of (39) into (32) gives

$$\begin{aligned}
a_M(\ell, m) &= \frac{-k^2}{c\sqrt{\ell(\ell+1)}} \frac{\omega_n}{2\pi} \frac{e}{r_n^2} N \\
&\quad \int j_\ell(kr) Y_\ell^{m*}(\theta, \phi) \delta(r-r_n) \\
&\quad \times [e^{i\phi} N_{\ell,m} P_\ell^m(\cos \theta) e^{im\phi} \cos \theta \\
&\quad + \sin \theta \sqrt{(\ell-m)(\ell+m+1)} \\
&\quad \times N_{\ell,m+1} P_\ell^{m+1}(\cos \theta) e^{i(m+1)\phi}] d^3x.
\end{aligned} \tag{40}$$

Substitution of $Y_\ell^{-m}(\theta, \phi) = (-1)^m Y_\ell^m(\theta, \phi)$ and (38) into (40) and integration with respect to dr gives

$$\begin{aligned}
a_M(\ell, m) &= \frac{-ek^2}{c\sqrt{\ell(\ell+1)}} \frac{\omega_n}{2\pi} N j_\ell(kr_n) \\
&\quad \int_0^{2\pi} \int_0^\pi (-1)^m N_{\ell,-m} P_\ell^{-m}(\cos \theta) e^{-im\phi} \\
&\quad \times [e^{i\phi} N_{\ell,m} P_\ell^m(\cos \theta) e^{im\phi} \cos \theta \\
&\quad + \sin \theta \sqrt{(\ell-m)(\ell+m+1)} \\
&\quad \times N_{\ell,m+1} P_\ell^{m+1}(\cos \theta) e^{i(m+1)\phi}] \sin \theta d\theta d\phi.
\end{aligned} \tag{41}$$

The integral in (41) separated in terms of $d\theta$ and $d\phi$ is

$$\begin{aligned}
a_M(\ell, m) &= \frac{-ek^2}{c\sqrt{\ell(\ell+1)}} \frac{\omega_n}{2\pi} N j_\ell(kr_n) \\
&\quad \int_0^\pi (-1)^m N_{\ell,-m} P_\ell^{-m}(\cos \theta) [N_{\ell,m} P_\ell^m(\cos \theta) \cos \theta \\
&\quad + \sin \theta \sqrt{(\ell-m)(\ell+m+1)} N_{\ell,m+1} P_\ell^{m+1}(\cos \theta)] \\
&\quad \sin \theta d\theta \int_0^{2\pi} e^{i\phi} d\phi.
\end{aligned} \tag{42}$$

Consider that the $d\theta$ integral is finite and designated by Θ . Then (42) is given as

$$a_M(\ell, m) = \frac{-ek^2}{c\sqrt{\ell(\ell+1)}} \frac{\omega_n}{2\pi} N j_\ell(kr_n) \Theta \int_0^{2\pi} e^{i\phi} d\phi. \tag{43}$$

From (26), the far fields are given by

$$\begin{aligned}
\mathbf{B} &= -\frac{i}{k} a_M(\ell, m) \nabla \times \mathbf{g}_\ell(kr) \mathbf{X}_{\ell,m}, \\
\mathbf{E} &= a_M(\ell, m) \mathbf{g}_\ell(kr) \mathbf{X}_{\ell,m},
\end{aligned} \tag{44}$$

where $a_M(\ell, m)$ is given by (43).

The power density $P(t)$ given by the Poynting power vector is

$$P(t) = \mathbf{E} \times \mathbf{H}. \tag{45}$$

For a pure multipole of order (ℓ, m) , the time-averaged power radiated per solid angle $dP(\ell, m)/d\Omega$ given by Jackson⁽²¹⁾ is

$$\frac{dP(\ell, m)}{d\Omega} = \frac{c}{8\pi k^2} |a_M(\ell, m)|^2 |\mathbf{X}_{\ell,m}|^2, \tag{46}$$

where $a_M(\ell, m)$ is given by (43).

Since the modulation function $Y_{\ell,m}(\theta, \phi)$ is a traveling charge density wave that moves time harmonically on the surface of the orbitsphere about the z axis with frequency ω_n , ϕ of the spherical harmonic function is a function of t , as shown in (33). The time dependence of the source current must also be evaluated in (43), and it can be written as

$$a_M(\ell, m) = \frac{-ek^2}{c\sqrt{\ell(\ell+1)}} \frac{\omega_n}{2\pi} Nj_\ell(kr_n) \Theta \int_0^{vT_n} \cos(mks(t)) ds, \quad (47)$$

where $s'(t)$ is the angular displacement of the rotating modulation function during one period T_n and v is the linear velocity in the $\hat{\phi}$ direction. Thus

$$\begin{aligned} a_M(\ell, m) &= \frac{-ek^2}{c\sqrt{\ell(\ell+1)}} \frac{\omega_n}{2\pi} Nj_\ell(kr_n) \Theta \sin(mkvT_n) \\ &= \frac{-ek^2}{c\sqrt{\ell(\ell+1)}} \frac{\omega_n}{2\pi} Nj_\ell(kr_n) \Theta \sin(mks). \end{aligned} \quad (48)$$

In the case that k is the light-like k^0 , then $k = \omega_n/c$, and the $\sin(mks)$ term in (48) vanishes for

$$\begin{aligned} R &= cT_n, \\ RT_n^{-1} &= c, \\ Rf &= c. \end{aligned} \quad (49)$$

Thus

$$s = vT_n = R = r_n = \lambda_n, \quad (50)$$

as given by (16), which is identical to the Haus condition for nonradiation given by (17). Then the multipole coefficient $a_M(\ell, m)$ is zero. For the condition given by (50), the time-averaged power radiated per solid angle $dP(\ell, m)/d\Omega$ given by (46) and (48) is zero. *There is no radiation.*

7. MAGNETIC FIELD EQUATIONS OF THE ELECTRON

The orbitsphere is a shell of negative charge current comprising correlated charge motion along great cir-

cles. For $\ell = 0$, the orbitsphere gives rise to a magnetic moment of one Bohr magneton.⁽²²⁾

$$\mu_B = \frac{e\hbar}{2m_e} = 9.274 \times 10^{-24} \text{ J} \cdot \text{T}^{-1}. \quad (51)$$

(The details of the derivation of the magnetic parameters including the electron g factor are given in the Appendix of this paper.) The magnetic field of the electron shown in Fig. 6 is given by

$$\mathbf{H} = \begin{cases} \frac{e\hbar}{m_e r_n^3} (\mathbf{i}_r \cos \theta - \mathbf{i}_\theta \sin \theta) & \text{for } r < r_n, \\ \frac{e\hbar}{2m_e r^3} (\mathbf{i}_r 2 \cos \theta + \mathbf{i}_\theta \sin \theta) & \text{for } r > r_n. \end{cases} \quad (52)$$

The energy stored in the magnetic field of the electron is

$$E_{mag} = \frac{1}{2} \mu_0 \int_0^{2\pi} \int_0^\pi \int_0^\infty H^2 r^2 \sin \theta dr d\theta d\Phi, \quad (53)$$

$$E_{mag, total} = \frac{\pi \mu_0 e^2 \hbar^2}{m_e^2 r_1^3}. \quad (54)$$

8. STERN-GERLACH EXPERIMENT

The Stern-Gerlach experiment implies a magnetic moment of one Bohr magneton and an associated angular momentum quantum number of $1/2$. Historically, this quantum number has been called the spin quantum number s ($s = 1/2$, $m_s = \pm 1/2$). The superposition of the vector projection of the orbitsphere angular momentum on the z axis is $\hbar/2$, with an orthogonal component of $\hbar/4$. Excitation of a resonant Larmor precession gives rise to \hbar on an axis S that precesses about the z axis called the spin axis at the Larmor frequency at an angle of $\theta = \pi/3$ to give a perpendicular projection of

$$S_\perp = \pm \sqrt{\frac{3}{4}} \hbar \quad (55)$$

and a projection onto the axis of the applied magnetic field of

$$S_0 = \pm \frac{\hbar}{2}. \quad (56)$$

The superposition of the $\hbar/2$, z axis component of the orbitsphere angular momentum and the $\hbar/2$, z axis component of S gives \hbar corresponding to the observed electron magnetic moment of a Bohr magneton, μ_B .

9. ELECTRON g FACTOR

Conservation of angular momentum of the orbitsphere permits a discrete change of its "kinetic angular momentum" ($\mathbf{r} \times m\mathbf{v}$) by the applied magnetic field of $\hbar/2$, and concomitantly the "potential angular momentum" ($\mathbf{r} \times e\mathbf{A}$) must change by $-\hbar/2$:

$$\begin{aligned} \Delta \mathbf{L} &= \frac{\hbar}{2} - \mathbf{r} \times e\mathbf{A} \\ &= \left[\frac{\hbar}{2} - \frac{e\phi}{2\pi} \right] \hat{z}. \end{aligned} \quad (57)$$

In order that the change of angular momentum $\Delta \mathbf{L}$ equal zero, ϕ must be $\Phi_0 = h/2e$, the magnetic flux quantum. The magnetic moment of the electron is parallel or antiparallel to the applied field only. During the spin-flip transition, power must be conserved. Power flow is governed by the Poynting power theorem:

$$\begin{aligned} \nabla \cdot (\mathbf{E} \times \mathbf{H}) &= -\frac{\partial}{\partial t} \left(\frac{1}{2} \mu_0 \mathbf{H} \cdot \mathbf{H} \right) \\ &\quad - \frac{\partial}{\partial t} \left(\frac{1}{2} \epsilon_0 \mathbf{E} \cdot \mathbf{E} \right) - \mathbf{J} \cdot \mathbf{E}. \end{aligned} \quad (58)$$

Equation (59) gives the total energy of the flip transition, which is the sum of the energy of reorientation of the magnetic moment (first term), the magnetic energy (second term), the electric energy (third term), and the dissipated energy of a fluxon treading the orbitsphere (fourth term), respectively:

$$\begin{aligned} \Delta E_{mag}^{spin} &= 2 \left(1 + \frac{\alpha}{2\pi} + \frac{2}{3} \alpha^2 \left(\frac{\alpha}{2\pi} \right) - \frac{4}{3} \left(\frac{\alpha}{2\pi} \right)^2 \right) \mu_B B \\ &= g \mu_B B, \end{aligned} \quad (59)$$

where the stored magnetic energy corresponding to the $\partial/\partial t[(1/2)\mu_0 \mathbf{H} \cdot \mathbf{H}]$ term increases, the stored electric energy corresponding to the $\partial/\partial t[(1/2)\epsilon_0 \mathbf{E} \cdot \mathbf{E}]$

term increases, and the $\mathbf{J} \cdot \mathbf{E}$ term is dissipative. The spin-flip transition can be considered as involving a magnetic moment of g times that of a Bohr magneton. The g factor is redesignated the fluxon g factor as opposed to the anomalous g factor. Using $\alpha^{-1} = 137.036\,03(82)$, the calculated value of $g/2$ is 1.001 159 652 137. The experimental value⁽²³⁾ of $g/2$ is 1.001 159 652 188(4). The derivation is given in the Appendix of this paper.

10. SPIN AND ORBITAL PARAMETERS

The total function that describes the spinning motion of each electron orbitsphere is composed of two functions. One function, the spin function, is spatially uniform over the orbitsphere, spins with a quantized angular velocity, and gives rise to spin angular momentum. The other function, the modulation function, can be spatially uniform — in which case there is no orbital angular momentum and the magnetic moment of the electron orbitsphere is one Bohr magneton — or not spatially uniform — in which case there is orbital angular momentum. The modulation function also rotates with a quantized angular velocity.

The spin function of the electron corresponds to the nonradiative $n = 1$, $\ell = 0$ state of atomic hydrogen, which is well known as an s state or orbital. (See Fig. 1 for the charge function and Fig. 2 for the current function.) In cases of orbitals of heavier elements and excited states of one-electron atoms and atoms or ions of heavier elements with the ℓ quantum number not equal to zero that are not constant as given by (14), the constant spin function is modulated by a time and spherical harmonic function, as given by (15) and shown in Fig. 3. The modulation or traveling charge density wave corresponds to an orbital angular momentum in addition to a spin angular momentum. These states are typically referred to as p , d , f , etc., orbitals. Application of Haus's⁽¹²⁾ condition also predicts nonradiation for a constant spin function modulated by a time and spherically harmonic orbital function. There is acceleration without radiation, as also shown in Section 6.3. (Also see Abbott and Griffiths, Goedecke, and Daboul and Jensen.^(17,18,16)) However, in the case that such a state arises as an excited state by photon absorption, it is radiative due to a radial dipole term in its current density function since it possesses space-time Fourier transform components synchronous with waves traveling at the speed of light⁽¹²⁾ (see Section 18).

10.1 Moment of Inertia and Spin and Rotational Energies

The moments of inertia and the rotational energies as a function of the ℓ quantum number for the solutions of the time-dependent electron charge density functions ((14), (15)) given in Section 5 are solved using the rigid rotor equation.⁽¹⁵⁾ The details of the derivations of the results as well as the demonstration that (14) and (15) with the results given below are solutions of the wave equation are given in Chapter 1, Rotational Parameters of the Electron (Angular Momentum, Rotational Energy, Moment of Inertia section), of Ref. 3. For $\ell = 0$,

$$I_z = I_{spin} = \frac{m_e r_n^2}{2}, \quad (60)$$

$$L_z = I\omega_z = \pm \frac{\hbar}{2}, \quad (61)$$

$$\begin{aligned} E_{rotational} &= E_{rotational, spin} \\ &= \frac{1}{2} \left[I_{spin} \left(\frac{\hbar}{m_e r_n^2} \right)^2 \right] \\ &= \frac{1}{2} \left[\frac{m_e r_n^2}{2} \left(\frac{\hbar}{m_e r_n^2} \right)^2 \right] \\ &= \frac{1}{4} \left(\frac{\hbar^2}{2I_{spin}} \right). \end{aligned} \quad (62)$$

For $\ell \neq 0$,

$$I_{orbital} = m_e r_n^2 \left[\frac{\ell(\ell+1)}{\ell^2 + 2\ell + 1} \right]^{1/2}, \quad (63)$$

$$L_z = m\hbar, \quad (64)$$

$$L_{z, total} = L_{z, spin} + L_{z, orbital}, \quad (65)$$

$$E_{rotational, orbital} = \frac{\hbar^2}{2I} \left[\frac{\ell(\ell+1)}{\ell^2 + 2\ell + 1} \right], \quad (66)$$

$$T = \frac{\hbar^2}{2m_e r_n^2}, \quad (67)$$

$$\langle E_{rotational, orbital} \rangle = 0. \quad (68)$$

From (68), the time average rotational energy is zero; thus the principal levels are degenerate except when a magnetic field is applied.

11. FORCE BALANCE EQUATION

The radius of the nonradiative ($n = 1$) state is solved using the electromagnetic force equations of Maxwell relating the charge and mass density functions, where the angular momentum of the electron is given by Planck's constant bar. The reduced mass arises naturally from an electrodynamic interaction between the electron and the proton:

$$\frac{m_e v_1^2}{4\pi r_1^2} = \frac{e}{4\pi r_1^2} \frac{Ze}{4\pi\epsilon_0 r_1^2} - \frac{1}{4\pi r_1^2} \frac{\hbar^2}{m r_n^3}, \quad (69)$$

$$r_1 = \frac{a_H}{Z}, \quad (70)$$

where a_H is the radius of the hydrogen atom.

12. ENERGY CALCULATIONS

From Maxwell's equations, the potential energy V , kinetic energy T , and electric energy or binding energy E_{ele} are

$$\begin{aligned} V &= \frac{-Ze^2}{4\pi\epsilon_0 r_1} = \frac{-Z^2 e^2}{4\pi\epsilon_0 a_H} \\ &= -Z^2 \times 4.3675 \times 10^{-18} \text{ J} = -Z^2 \times 27.2 \text{ eV}, \end{aligned} \quad (71)$$

$$T = \frac{Z^2 e^2}{8\pi\epsilon_0 a_H} = Z^2 \times 13.59 \text{ eV}, \quad (72)$$

$$T = E_{ele} = -\frac{1}{2} \epsilon_0 \int_{\infty}^r E^2 dv, \text{ where } E = -\frac{Ze}{4\pi\epsilon_0 r^2}, \quad (73)$$

$$\begin{aligned} E_{ele} &= -\frac{Z^2 e^2}{8\pi\epsilon_0 a_H} \\ &= -Z^2 \times 2.1786 \times 10^{-18} \text{ J} = -Z^2 \times 13.598 \text{ eV}. \end{aligned} \quad (74)$$

The calculated Rydberg constant is $10\,967\,758 \text{ m}^{-1}$; the experimental Rydberg constant² is $10\,967\,758 \text{ m}^{-1}$.

13. EXCITED STATES

CQM gives closed-form solutions for the resonant photons and excited state electron functions. The angular momentum of the photon given by

$$\mathbf{m} = \left| \frac{1}{8\pi} \text{Re}[\mathbf{r} \times (\mathbf{E} \times \mathbf{B}^*)] \right| = \hbar \quad (75)$$

is conserved.⁽²¹⁾ The change in angular velocity of the electron is equal to the angular frequency of the resonant photon. The energy is given by Planck's equation. The predicted energies, Lamb shift, fine structure, hyperfine structure, resonant line shape, line width, selection rules, etc., are in agreement with observation.

The orbitsphere is a dynamic spherical resonator cavity that traps photons of discrete frequencies. The relationship between an allowed radius and the "photon standing wave" wavelength is

$$2\pi r = n\lambda, \quad (76)$$

where n is an integer. The relationship between an allowed radius and the electron wavelength is

$$2\pi(nr_1) = 2\pi r_n = n\lambda_1 = \lambda_n, \quad (77)$$

where $n = 1, 2, 3, 4, \dots$. The radius of an orbitsphere increases with the absorption of electromagnetic energy. The radii of excited states are solved using the electromagnetic force equations of Maxwell relating the field from the charge of the proton, the electric field of the photon, and the charge and mass density functions of the electron, where the angular momentum of the electron is given by Planck's constant bar (69). The solutions to Maxwell's equations for modes that can be excited in the orbitsphere resonator cavity give rise to four quantum numbers, and the energies of the modes are the experimentally known hydrogen spectrum. The relationship between the electric field equation and the "trapped photon" source charge density function is given by Maxwell's equation in two dimensions:

$$\mathbf{m} \cdot (\mathbf{E}_1 - \mathbf{E}_2) = \frac{\sigma}{\epsilon_0}. \quad (78)$$

The photon standing electromagnetic wave is phase matched with the electron:

$$\begin{aligned} \mathbf{E}_{r_{\text{photon } n, j, m}} &= \frac{e(na_H)^t}{4\pi\epsilon_0} \frac{1}{r^{(\ell+2)}} \left[-Y_0^0(\theta, \phi) \right. \\ &\quad \left. + \frac{1}{n} [Y_0^0(\theta, \phi) + \text{Re}\{Y_\ell^m(\theta, \phi)e^{i\omega_n t}\}] \right] \delta(r - r_n) \hat{\mathbf{i}}_r, \\ \omega_n &= 0 \text{ for } m = 0, \\ \ell &= 1, 2, \dots, n-1, \\ m &= -\ell, -\ell+1, \dots, 0, \dots, +\ell, \end{aligned} \quad (79)$$

$$\begin{aligned} \mathbf{E}_{r_{\text{total}}} &= \frac{e}{4\pi\epsilon_0 r^2} + \frac{e(na_H)^t}{4\pi\epsilon_0} \frac{1}{r^{(\ell+2)}} \left[-Y_0^0(\theta, \phi) \right. \\ &\quad \left. + \frac{1}{n} [Y_0^0(\theta, \phi) + \text{Re}\{Y_\ell^m(\theta, \phi)e^{i\omega_n t}\}] \right] \delta(r - r_n) \hat{\mathbf{i}}_r, \quad (80) \\ \omega_n &= 0 \text{ for } m = 0. \end{aligned}$$

For $r = na_H$ and $m = 0$, the total radial electric field is

$$\mathbf{E}_{r_{\text{total}}} = \frac{1}{n} \frac{e}{4\pi\epsilon_0 (na_H)^2} \hat{\mathbf{i}}_r. \quad (81)$$

The energy of the photon that excites a mode in the electron spherical resonator cavity from radius a_H to radius na_H is

$$E_{\text{photon}} = \frac{e^2}{8\pi\epsilon_0 a_H} \left(1 - \frac{1}{n^2} \right) = h\nu = \hbar\omega. \quad (82)$$

The change in angular velocity of the orbitsphere for an excitation from $n = 1$ to $n = n$ is

$$\Delta\omega = \frac{\hbar}{m_e(a_H)^2} - \frac{\hbar}{m_e(na_H)^2} = \frac{\hbar}{m_e(a_H)^2} \left(1 - \frac{1}{n^2} \right). \quad (83)$$

The kinetic energy change of the transition is

$$\frac{1}{2} m_e (\Delta v)^2 = \frac{e^2}{8\pi\epsilon_0 a_H} \left(1 - \frac{1}{n^2} \right) = \hbar\omega. \quad (84)$$

The change in angular velocity of the electron orbitsphere is identical to the angular velocity of the photon necessary for the excitation, ω_{photon} . The *correspondence principle holds*. It can be demonstrated that the resonance condition between these frequencies is to be satisfied in order to have a net change of the energy field.⁽²⁴⁾

14. ORBITAL AND SPIN SPLITTING

The ratio of the square of the angular momentum, M^2 , to the square of the energy, U^2 , for a pure (ℓ, m) multipole is⁽²⁵⁾

$$\frac{M^2}{U^2} = \frac{m^2}{\omega^2}. \quad (85)$$

The magnetic moment is defined as

$$\mu = \frac{\text{charge} \times \text{angular momentum}}{2 \times \text{mass}}. \quad (86)$$

The radiation of a multipole of order (ℓ, m) carries $m\hbar$ units of the z component of angular momentum per photon of energy $\hbar\omega$. Thus the z component of the angular momentum of the corresponding excited state electron orbitsphere is

$$L_z = m\hbar. \quad (87)$$

Therefore

$$\mu_z = \frac{em\hbar}{2m_e} = m\mu_B, \quad (88)$$

where μ_B is the Bohr magneton. The orbital splitting energy is

$$E_{mag}^{orb} = m\mu_B B. \quad (89)$$

The spin and orbital splitting energies superimpose; thus the principal excited state energy levels of the hydrogen atom are split by the energy $E_{mag}^{spin/orb}$:

$$E_{mag}^{spin/orb} = m \frac{e\hbar}{2m_e} B + m_s g \frac{e\hbar}{m_e} B, \text{ where} \quad (90)$$

$$n = 2, 3, 4, \dots,$$

$$\ell = 1, 2, \dots, n-1,$$

$$m = -\ell, -\ell+1, \dots, 0, \dots, +\ell,$$

$$m_s = \pm \frac{1}{2}.$$

For the electric dipole transition the selection rules are

$$\begin{aligned} \Delta m &= 0, \pm 1, \\ \Delta m_s &= 0. \end{aligned} \quad (91)$$

15. RESONANT LINE SHAPE AND LAMB SHIFT

The spectroscopic line width shown in Fig. 7 arises from the classical rise-time bandwidth relationship, and the Lamb shift is due to conservation of energy and linear momentum and arises from the radiation reaction force between the electron and the photon. It follows from the Poynting power theorem with spherical radiation that the transition probabilities are given by the ratio of the power to the energy of the transition.⁽²⁶⁾ The transition probability in the case of the electric multipole moment is

$$\begin{aligned} \frac{1}{\tau} &= \frac{\text{power}}{\text{energy}} \\ &= \frac{\left[\frac{2\pi c}{[(2\ell+1)!!]^2} \left(\frac{\ell+1}{\ell} \right) k^{2\ell+1} |Q_{\ell m} + Q'_{\ell m}|^2 \right]}{\hbar\omega} \end{aligned} \quad (92)$$

$$= 2\pi \left(\frac{e^2}{h} \right) \sqrt{\frac{\mu_0}{\epsilon_0}} \frac{2\pi}{[(2\ell+1)!!]^2} \times \left(\frac{\ell+1}{\ell} \right) \left(\frac{3}{\ell+3} \right)^2 (k r_n)^{2\ell} \omega,$$

$$|E(\omega)| \propto \int_0^\infty e^{-\alpha t} e^{-i\omega t} dt = \frac{1}{\alpha - i\omega}. \quad (93)$$

The relationship between the rise time and the bandwidth for exponential decay is

$$\tau\Gamma = \frac{1}{\pi}. \quad (94)$$

The energy radiated per unit frequency interval is

$$\frac{dI(\omega)}{d\omega} = I_0 \frac{\Gamma}{2\pi} \frac{1}{(\omega - \omega_0 - \Delta\omega)^2 + (\Gamma/2)^2}. \quad (95)$$

16. LAMB SHIFT

The Lamb shift of the $^2P_{1/2}$ state of the hydrogen atom is due to conservation of linear momentum of

the electron, atom, and photon. The electron component is

$$\Delta f = \frac{\Delta\omega}{2\pi} = \frac{E_{hv}}{h} = \frac{(E_{hv})^2}{2h\mu_e c^2} = 1052.48 \text{ MHz}, \quad (96)$$

where

$$E_{hv} = 13.5983 \text{ eV} \left(1 - \frac{1}{n^2}\right) \frac{3}{4\pi} \sqrt{\frac{3}{4}} - h\Delta f, \quad (97)$$

$$h\Delta f \ll 10 \text{ eV}. \quad (98)$$

Therefore

$$E_{hv} = 13.5983 \text{ eV} \left(1 - \frac{1}{n^2}\right) \frac{3}{4\pi} \sqrt{\frac{3}{4}}. \quad (99)$$

The atom component is

$$\begin{aligned} \Delta f &= \frac{\Delta\omega}{2\pi} = \frac{E_{hv}}{h} = \frac{(E_{hv})^2}{2hm_H c^2} \\ &= \frac{\left(13.5983 \text{ eV} \left(1 - \frac{1}{n^2}\right) \left(1 + \frac{1}{2} - \sqrt{\frac{3}{4}}\right)\right)^2}{2hm_H c^2} \quad (100) \\ &= 5.3839 \text{ MHz}. \end{aligned}$$

The sum of the components is

$$\begin{aligned} \Delta f &= 1052.48 \text{ MHz} + 5.3839 \text{ MHz} \\ &= 1057.87 \text{ MHz}. \end{aligned} \quad (101)$$

The experimental Lamb shift is

$$\Delta f = 1057.862 \text{ MHz}. \quad (102)$$

17. SPIN-ORBITAL COUPLING

The electron's motion in the hydrogen atom is always perpendicular to its radius; consequently, as shown by (7), the electron's angular momentum of \hbar is invariant. The angular momentum of the photon given in Section 19 is $|\mathbf{m}| = |(1/8\pi)\text{Re}[\mathbf{r} \times (\mathbf{E} \times \mathbf{B}^*)]| = \hbar$. It is conserved for the solutions for the resonant photons and excited state electron functions given in Sections 13 and 19. Thus the electrodynamic angular

momentum and the inertial angular momentum are matched such that the correspondence principle holds. It follows from the principle of conservation of angular momentum that e/m_e of (51) is invariant, given in Section 6.1 and shown previously.⁽³⁾ In the case of spin-orbital coupling, the invariants \hbar of spin angular momentum and orbital angular momentum each give rise to a corresponding invariant magnetic moment of a Bohr magneton, and their corresponding energies superimpose, as given in Section 14. The interaction of the two magnetic moments gives rise to a relativistic spin-orbital coupling energy. The vector orientations of the momenta must be considered as well as the condition that flux must be linked by the electron in units of the magnetic flux quantum in order to conserve the invariant electron angular momentum of \hbar . The energy may be calculated with the additional conditions of the invariance of the electron's charge and mass-to-charge ratio e/m_e .

As shown in Section 9 ((57) to (59)), flux must be linked by the electron orbitsphere in units of the magnetic flux quantum. The maximum projection of the rotating spin angular momentum of the electron onto an axis given by (55) is $\sqrt{3}/4 \hbar$. Then, using the magnetic energy term of (59), the spin-orbital coupling energy $E_{s/o}$ is given by

$$\begin{aligned} E_{s/o} &= 2 \frac{\alpha}{2\pi} \left(\frac{e\hbar}{2m_e} \right) \frac{\mu_0 e\hbar}{2(2\pi m_e) \left(\frac{r}{2\pi} \right)^3} \sqrt{\frac{3}{4}} \\ &= \frac{\alpha\pi\mu_0 e^2 \hbar^2}{m_e^2 r^3} \sqrt{\frac{3}{4}}. \end{aligned} \quad (103)$$

In the case that $n = 2$, the radius given by (77) is $r = 2a_0$. The predicted energy difference between the $^2P_{3/2}$ and $^2P_{1/2}$ levels of the hydrogen atom, $E_{s/o}$, given by (103), is

$$E_{s/o} = \frac{\alpha\pi\mu_0 e^2 \hbar^2}{8m_e^2 a_0^3} \sqrt{\frac{3}{4}}. \quad (104)$$

As in the case of the $^2P_{1/2} \rightarrow ^2S_{1/2}$ transition, the photon-momentum transfer for the $^2P_{3/2} \rightarrow ^2P_{1/2}$ transition gives rise to a frequency shift derived after that of the Lamb shift with $\Delta m_l = -1$ included. The energy E_{FS} for the $^2P_{3/2} \rightarrow ^2P_{1/2}$ transition, called the fine-structure splitting, is given by

$$\begin{aligned}
 E_{FS} &= \frac{\alpha^5 (2\pi)^2}{8} m_e c^2 \sqrt{\frac{3}{4}} \\
 &\quad + \left(13.5983 \text{ eV} \left(1 - \frac{1}{2^2} \right) \right)^2 \\
 &\quad \times \left[\frac{\left(\frac{3}{4\pi} \left(1 - \sqrt{\frac{3}{4}} \right) \right)^2}{2\hbar\mu_e c^2} + \frac{\left(1 + \left(1 - \sqrt{\frac{3}{4}} \right) \right)^2}{2\hbar m_H c^2} \right] \quad (105) \\
 &= 4.5190 \times 10^{-5} \text{ eV} + 1.75407 \times 10^{-7} \text{ eV} \\
 &= 4.53659 \times 10^{-5} \text{ eV},
 \end{aligned}$$

where the first term corresponds to E_{slo} given by (104), expressed in terms of the mass energy of the electron using (176) and (177), and the second and third terms correspond to the electron recoil and atom recoil, respectively. The energy of $4.53659 \times 10^{-5} \text{ eV}$ corresponds to a frequency of 10 969.4 MHz or a wavelength of 2.73298 cm. The experimental value of the $^2P_{3/2} \rightarrow ^2P_{1/2}$ transition frequency is 10 969.1 MHz. The large natural widths of the hydrogen 2p levels limit the experimental accuracy; yet, given this limitation, the agreement between the theoretical and experimental fine structure is excellent.

18. INSTABILITY OF EXCITED STATES

For the excited energy states of the hydrogen atom, σ_{photon} , the two-dimensional surface charge due to the "trapped photons" at the electron orbitsphere, given by (78) and (79), is

$$\begin{aligned}
 \sigma_{photon} &= \frac{e}{4\pi(r_n)^2} \left[Y_0^0(\theta, \phi) - \frac{1}{n} [Y_0^0(\theta, \phi) \right. \\
 &\quad \left. + \text{Re}\{Y_l^m(\theta, \phi)e^{i\omega_n t}\}] \right] \delta(r - r_n), \quad (106)
 \end{aligned}$$

where $n = 2, 3, 4, \dots$, whereas $\sigma_{electron}$, the two-dimensional surface charge of the electron orbitsphere given by (15), is

$$\begin{aligned}
 \sigma_{electron} &= \frac{-e}{4\pi(r_n)^2} \{ Y_0^0(\theta, \phi) \\
 &\quad + \text{Re}[Y_l^m(\theta, \phi)e^{i\omega_n t}] \} \delta(r - r_n). \quad (107)
 \end{aligned}$$

The superposition of σ_{photon} (106) and $\sigma_{electron}$ is equivalent to the sum of a radial electric dipole repre-

sented by a doublet function and a radial electric monopole represented by a delta function:

$$\begin{aligned}
 \sigma_{photon} + \sigma_{electron} &= \\
 &\frac{e}{4\pi(r_n)^2} \left[Y_0^0(\theta, \phi) \delta(r - r_n) - \frac{1}{n} [Y_0^0(\theta, \phi) \delta(r - r_n) \right. \\
 &\quad \left. - \left(1 + \frac{1}{n} \right) [\text{Re}\{Y_l^m(\theta, \phi)e^{i\omega_n t}\}] \delta(r - r_n) \right], \quad (108)
 \end{aligned}$$

where $n = 2, 3, 4, \dots$. Due to the radial doublet, excited states are radiative since space-time harmonics of $\omega_n/c = k$ or $(\omega_n/c)\sqrt{\epsilon/\epsilon_0} = k$ do exist for which the space-time Fourier transform of the current density function is nonzero.

19. PHOTON EQUATIONS

The time-averaged angular momentum density \mathbf{m} of an emitted photon is

$$\mathbf{m} = \int \frac{1}{8\pi c} \text{Re}[\mathbf{r} \times (\mathbf{E} \times \mathbf{B}^*)] dx^4 = \hbar. \quad (109)$$

By reiterations of (110) and (111), a photon orbitsphere is generated from two orthogonal great circle field lines, as shown in Fig. 8, rather than two great circle current loops, as in the case of the electron spin function. The output given by the nonprimed coordinates is the input of the next iteration corresponding to each successive nested rotation by the infinitesimal angle $\Delta\alpha$, where the summation of the rotation about the x' axis and the y' axis in each case is $(\sqrt{2}/4)\pi$. The right-handed circularly polarized photon orbitsphere shown in Fig. 9 corresponds to the case where the $\Delta\alpha$'s for the x' and y' rotations are of the same sign, and the mirror image left-handed circularly polarized photon orbitsphere corresponds to the case where they are of opposite signs. A linearly polarized photon orbitsphere is the superposition of the right- and left-handed circularly polarized photon orbitspheres.

19.1 Nested Set of Great Circle Field Lines Generates the Photon Function

Note the abbreviations c for cosine and s for sine.

H Field:

$$\begin{bmatrix} x_1 \\ y_1 \\ z_1 \end{bmatrix} = \begin{bmatrix} c(\Delta\alpha) & -s^2(\Delta\alpha) & -s(\Delta\alpha)c(\Delta\alpha) \\ 0 & c(\Delta\alpha) & s(\Delta\alpha) \\ s(\Delta\alpha) & -c(\Delta\alpha)s(\Delta\alpha) & c^2(\Delta\alpha) \end{bmatrix} \begin{bmatrix} x'_1 \\ y'_1 \\ z'_1 \end{bmatrix} \quad (110)$$

E Field:

$$\begin{bmatrix} x_1 \\ y_1 \\ z_1 \end{bmatrix} = \begin{bmatrix} c(\Delta\alpha) & -s^2(\Delta\alpha) & -s(\Delta\alpha)c(\Delta\alpha) \\ 0 & c(\Delta\alpha) & s(\Delta\alpha) \\ s(\Delta\alpha) & -c(\Delta\alpha)s(\Delta\alpha) & c^2(\Delta\alpha) \end{bmatrix} \begin{bmatrix} x'_1 \\ y'_1 \\ z'_1 \end{bmatrix} \quad (111)$$

The angular sum in (110) and (111) is

$$\lim_{\Delta\alpha \rightarrow 0} \sum_{n=1}^{\frac{\sqrt{2}}{4}\pi} |\Delta\alpha_{r,j}| = \frac{\sqrt{2}}{4}\pi.$$

The field lines in the lab frame follow from the relativistic invariance of charge, as given by Purcell.⁽²⁷⁾ The relationship between the relativistic velocity and the electric field of a moving charge is shown schematically in Fig. 10. From (110) and (111) corresponding to the rotations over $\Delta\alpha$, the photon equation in the lab frame of a right-handed circularly polarized photon orbitsphere is

$$\mathbf{E} = \mathbf{E}_0 [\mathbf{x} + i\mathbf{y}] e^{-jk_z z} e^{-j\omega t}, \quad (112)$$

$$\begin{aligned} \mathbf{H} &= \left(\frac{\mathbf{E}_0}{\eta} \right) [\mathbf{y} - i\mathbf{x}] e^{-jk_z z} e^{-j\omega t} \\ &= \mathbf{E}_0 \sqrt{\frac{\epsilon}{\mu}} [\mathbf{y} - i\mathbf{x}] e^{-jk_z z} e^{-j\omega t}, \end{aligned} \quad (113)$$

with a wavelength of

$$\lambda = 2\pi \frac{c}{\omega}. \quad (114)$$

The relationship between the photon orbitsphere radius and wavelength is

$$2\pi r_0 = \lambda_0. \quad (115)$$

The electric field lines of a right-handed circularly polarized photon orbitsphere as seen along the axis of propagation in the lab inertial reference frame as it passes a fixed point is shown in Fig. 11.

19.2 Spherical Wave

Photons superimpose, and the amplitude due to N photons is

$$E_{total} = \sum_{n=1}^N \frac{e^{-ik_r |r-r'|}}{4\pi |r-r'|} f(\theta, \phi). \quad (116)$$

In the far field the emitted wave is a spherical wave:

$$E_{total} = E_0 \frac{e^{-ikr}}{r}. \quad (117)$$

The Green function is given as the solution of the wave equation. Thus the superposition of photons gives the classical result. As r goes to infinity, the spherical wave becomes a plane wave. The double-slit interference pattern is predicted. From the equation of a photon the wave-particle duality arises naturally. The energy is always given by Planck's equation; yet an interference pattern is observed when photons add over time or space. The results also predict those of the Aspect experiment involving Bell's inequalities.⁽³⁾

20. EQUATIONS OF THE FREE ELECTRON

20.1 Charge Density Function

The radius of an electron orbitsphere increases with the absorption of electromagnetic energy.⁽²⁸⁾ With the absorption of a photon of energy exactly equal to the ionization energy, the electron becomes ionized and is a plane wave (spherical wave in the limit) with the de Broglie wavelength. The ionized electron traveling at constant velocity is nonradiative and is a two-dimensional surface with a total charge of e and a total mass of m_e . The solution of the boundary value problem of the free electron is given by the projection of the orbitsphere into a plane that linearly propagates along an axis perpendicular to the plane, where the velocity of the plane and the orbitsphere is given by

$$v = \frac{\hbar}{m_e \rho_0} \quad (118)$$

and the radius of the orbitsphere in spherical coordinates is equal to the radius of the free electron in cylindrical coordinates ($\rho_0 = r_0$). The mass density function of a free electron, as shown in Fig. 12, is a two-dimensional disk with mass density distribution in the $xy(\rho)$ plane

$$\rho_m(\rho, \phi, z) = \frac{m_e}{\frac{2}{3}\pi\rho_0^3} \sqrt{\rho_0^2 - \rho^2} \delta(z) \quad (119)$$

and charge density distribution $\rho_e(\rho, \phi, z)$ in the xy plane given by replacing m_e with e . The charge density distribution of the free electron has recently been confirmed experimentally.⁽²⁹⁻³⁰⁾ Researchers working at the Japanese National Laboratory for High Energy Physics (KEK) demonstrated that the charge of the free electron increases toward the particle's core and is symmetrical as a function of ϕ . In addition, the wave-particle duality arises naturally, and the result is consistent with scattering experiments from helium and the double-slit experiment.⁽³⁾

20.2 Current Density Function

Consider an electron initially bound as an orbitsphere of radius $r = r_n = r_0$ ionized from a hydrogen atom with the magnitude of the angular velocity of the orbitsphere given by

$$\omega = \frac{\hbar}{m_e r^2}. \quad (120)$$

The current density function of the free electron propagating with velocity v_z along the z axis in the inertial frame of the proton is given by the vector projection of the current into the xy plane as the radius increases from $r = r_0$ to $r = \infty$. The current density function of the free electron is

$$\mathbf{J}(\rho, \phi, z, t) = \left[\frac{e}{\frac{2}{3}\pi\rho_0^3} \sqrt{\rho_0^2 - \rho^2} \frac{5}{2} \frac{\hbar}{m_e \rho_0^2} \mathbf{i}_\phi \right]. \quad (121)$$

The angular momentum \mathbf{L} is given by

$$\mathbf{L} \mathbf{i}_z = m_e r^2 \omega. \quad (122)$$

Substitution of m_e for e in (121) followed by substitution into (122) gives the angular momentum density function \mathbf{L} :

$$\mathbf{L} \mathbf{i}_z = \frac{m_e}{\frac{2}{3}\pi\rho_0^3} \sqrt{\rho_0^2 - \rho^2} \frac{5}{2} \frac{\hbar}{m_e \rho_0^2} \rho^2. \quad (123)$$

The total angular momentum of the free electron is given by integration over the two-dimensional disk with angular momentum density given by (123):

$$\begin{aligned} \mathbf{L} \mathbf{i}_z &= \int_0^{2\pi} \int_0^{\rho_0} \frac{m_e}{\frac{2}{3}\pi\rho_0^3} \sqrt{\rho_0^2 - \rho^2} \frac{5}{2} \frac{\hbar}{m_e \rho_0^2} \rho^2 \rho d\rho d\phi \\ &= \hbar \mathbf{i}_z. \end{aligned} \quad (124)$$

The four-dimensional space-time current density function of the free electron that propagates along the z axis with velocity given by (118) corresponding to $r = r_0 = \rho_0$ is given by substitution of (118) into (121):

$$\begin{aligned} \mathbf{J}(\rho, \phi, z, t) &= \left[\frac{e}{\frac{2}{3}\pi\rho_0^3} \sqrt{\rho_0^2 - \rho^2} \frac{5}{2} \frac{\hbar}{m_e \rho_0^2} \mathbf{i}_\phi \right] \\ &\quad + \frac{e\hbar}{m_e \rho_0} \delta\left(z - \frac{\hbar}{m_e \rho_0} t\right) \mathbf{i}_z. \end{aligned} \quad (125)$$

The space-time Fourier transform of (125) is

$$\begin{aligned} &\frac{e}{\frac{4}{3}\pi\rho_0^3} \frac{\hbar}{m_e} \text{sinc}(2\pi s \rho_0) \\ &\quad + 2\pi e \frac{\hbar}{m_e \rho_0} \delta(\omega - \mathbf{k}_z \cdot \mathbf{v}_z). \end{aligned} \quad (126)$$

The boundary condition is that the space-time harmonics of $\omega_n/c = k$ or $(\omega_n/c) \sqrt{\epsilon/\epsilon_0} = k$ do not exist. Radiation due to charge motion does not occur in any medium when this boundary condition is met. Thus no Fourier components that are synchronous with light velocity with the propagation constant $|\mathbf{k}_z| = \omega/c$ exist, and radiation due to charge motion of the free electron does not occur when this boundary condition is met. It follows from (118) and the relationship

$2\pi\rho_0 = \lambda_0$ that the wavelength of the free electron is the de Broglie wavelength:

$$\lambda_0 = \frac{h}{m_e v_z} = 2\pi\rho_0. \quad (127)$$

The Stern–Gerlach experiment implies a magnetic moment of one Bohr magneton and an associated angular momentum quantum number of $1/2$ ($s = 1/2$, $m_s = \pm 1/2$). The superposition of the vector projection of the angular momentum of the free electron onto the z axis is \hbar corresponding to the observed electron magnetic moment of a Bohr magneton, μ_B . Excitation of the Larmor precession by a photon carrying \hbar of angular momentum causes the angular momentum of the free electron to rotate about both an axis in the transverse plane and the z axis such that each of the photon and electron angular momentum projections onto the z axis is $\hbar/2$. In order to conserve angular momentum, which is distributed equivalently to $Y_0^0(\theta, \phi)$ during the spin-flip transition, a magnetic flux quantum $\Phi_0 = h/2e$ must be linked by the electron, and the electron magnetic moment can only be parallel or antiparallel to an applied field, as observed with the Stern–Gerlach experiment. The energy ΔE_{mag}^{spin} of the spin-flip transition corresponding to the $m_s = 1/2$ quantum number is given by (59):

$$\Delta E_{mag}^{spin} = g\mu_B B. \quad (128)$$

(See Chap. 3 of Ref. 3 for details of the derivations.)

21. TWO-ELECTRON ATOMS

Two-electron atoms may be solved from a central force balance equation with the nonradiation condition. The force balance equation using (6) is

$$\begin{aligned} \frac{m_e v_z^2}{4\pi r_2^2 r_2} &= \frac{m_e}{4\pi r_2^2} \frac{\hbar^2}{m_e r_2^3} \\ &= \frac{e}{4\pi r_2^2} \frac{(Z-1)e}{4\pi\epsilon_0 r_2^2} \\ &\quad + \frac{1}{4\pi r_2^2} \frac{\hbar^2}{Zm_e r_2^3} \sqrt{s(s+1)}, \end{aligned} \quad (129)$$

which gives the radius of both electrons as

$$r_2 = r_1 = a_0 \left(\frac{1}{Z-1} - \frac{\sqrt{s(s+1)}}{Z(Z-1)} \right), \quad s = \frac{1}{2}. \quad (130)$$

21.1 Ionization Energies Calculated Using the Poynting Power Theorem

For helium, which has no electric field beyond r_1 ,

$$\begin{aligned} \text{Ionization Energy(He)} \\ = -E(\text{electric}) + E(\text{magnetic}), \end{aligned} \quad (131)$$

where

$$E(\text{electric}) = -\frac{(Z-1)e^2}{8\pi\epsilon_0 r_1}, \quad (132)$$

$$E(\text{magnetic}) = \frac{2\pi\mu_0 e^2 \hbar^2}{m_e^2 r_1^3}. \quad (133)$$

For $3 \leq Z$,

$$\begin{aligned} \text{Ionization energy} \\ = -\text{Electric energy} - \frac{1}{Z} \text{Magnetic energy}. \end{aligned} \quad (134)$$

The energies of several two-electron atoms are given in Table I. The exact solutions for one- through twenty-electron atoms are given in Ref. 3.

22. ELASTIC ELECTRON SCATTERING FROM HELIUM ATOMS

The aperture distribution function $a(\rho, \phi, z)$ for the elastic scattering of an incident electron plane wave, represented by $\pi(z)$, by a helium atom, represented by

$$\frac{2}{4\pi(0.567a_0)^2} [\delta(r - 0.567a_0)], \quad (135)$$

is given by the convolution of the plane wave $\pi(z)$ with the helium atom function:

$$\begin{aligned} a(\rho, \phi, z) \\ = \pi(z) \otimes \frac{2}{4\pi(0.567a_0)^2} [\delta(r - 0.567a_0)]. \end{aligned} \quad (136)$$

The aperture function is

$$a(\rho, \phi, z) = \frac{2}{4\pi(0.567a_0)^2} \sqrt{(0.567a_0)^2 - z^2} \quad (137)$$

$$\times \delta\left(r - \sqrt{(0.567a_0)^2 - z^2}\right).$$

22.1 Far Field Scattering (Circular Symmetry)

Applying Huygens's principle to a disturbance caused by the plane wave electron over the helium atom as an aperture gives the amplitude of the far field or Fraunhofer diffraction pattern $F(s)$ as the Fourier transform of the aperture distribution:

$$F(s) = \frac{2}{4\pi(0.567a_0)^2} 2\pi \int_0^\infty \int_{-\infty}^\infty \sqrt{(0.567a_0)^2 - z^2} \quad (138)$$

$$\times \delta\left(\rho - \sqrt{(0.567a_0)^2 - z^2}\right) J_0(s\rho) e^{-i\omega z} \rho d\rho dz.$$

The intensity I_1^{ed} is the square of the amplitude:

$$I_1^{ed} = F(s)^2 = I_e \left[\left[\frac{2\pi}{(z_0 w)^2 + (z_0 s)^2} \right]^{1/2} \right.$$

$$\times \left(2 \left[\frac{z_0 s}{(z_0 w)^2 + (z_0 s)^2} \right] J_{3/2} [((z_0 w)^2 + (z_0 s)^2)^{1/2}] \right. \quad (139)$$

$$\left. \left. \left(- \left[\frac{z_0 s}{(z_0 w)^2 + (z_0 s)^2} \right] J_{5/2} [((z_0 w)^2 + (z_0 s)^2)^{1/2}] \right) \right) \right]^2,$$

$$s = \frac{4\pi}{\lambda} \sin \frac{\theta}{2}, \quad w = 0 \text{ (units of } C^{-1}). \quad (140)$$

The experimental results of Bromberg⁽³³⁾ the extrapolated experimental data of Hughes⁽³³⁾ the small angle data of Geiger⁽³⁴⁾ and the semi-experimental results of Lassette⁽³³⁾ for the elastic differential cross-section for the elastic scattering of electrons by helium atoms is shown graphically in Fig. 13. The elastic differential cross-section as a function of the angle numerically calculated by Khare⁽³³⁾ using the first Born approximation and first-order exchange approximation also appears in Fig. 13. These results, which are based on a quantum-mechanical model, are compared with experiment.^(33,34) The closed-form function ((139) and (140)) for the elastic differential cross-section for the elastic scattering of electrons by helium atoms is

shown graphically in Fig. 14. The scattering amplitude function $F(s)$ (138) is shown as an inset. It is apparent from Fig. 13 that the quantum-mechanical calculations fail completely at predicting the experimental results at small scattering angles; but there is good agreement between (139) and the experimental results.

23. THE NATURE OF THE CHEMICAL BOND OF HYDROGEN

The hydrogen molecule charge and current density functions, bond distance, and energies are solved from the Laplacian in ellipsoidal coordinates with the constraint of nonradiation:

$$(\eta - \zeta) R_\xi \frac{\partial}{\partial \xi} \left(R_\xi \frac{\partial \phi}{\partial \xi} \right)$$

$$+ (\zeta - \xi) R_\eta \frac{\partial}{\partial \eta} \left(R_\eta \frac{\partial \phi}{\partial \eta} \right) \quad (141)$$

$$+ (\xi - \eta) R_\zeta \frac{\partial}{\partial \zeta} \left(R_\zeta \frac{\partial \phi}{\partial \zeta} \right) = 0.$$

The force balance equation for the hydrogen molecule is

$$\frac{\hbar^2}{m_e a^2 b^2} 2ab^2 X = \frac{e^2}{4\pi\epsilon_0} X + \frac{\hbar^2}{2m_e a^2 b^2} 2ab^2 X, \quad (142)$$

where

$$X = \frac{1}{\sqrt{\xi + a^2}} \frac{1}{\sqrt{\xi + b^2}} \frac{1}{c} \sqrt{\frac{\xi^2 - 1}{\xi^2 - \eta^2}}. \quad (143)$$

Equation (142) has the parametric solution

$$r(t) = ia \cos \omega t + jb \sin \omega t \quad (144)$$

when the semimajor axis a is

$$a = a_0. \quad (145)$$

The internuclear distance $2c'$, which is the distance between the foci, is

$$2c' = \sqrt{2}a_0. \quad (146)$$

The experimental internuclear distance is $\sqrt{2} a_0$. The semiminor axis is

$$b = \frac{1}{\sqrt{2}} a_0. \quad (147)$$

The eccentricity e is

$$e = \frac{1}{\sqrt{2}}. \quad (148)$$

23.1 The Energies of the Hydrogen Molecule

The potential energy of the two electrons in the central field of the protons at the foci is

$$V_e = \frac{-2e^2}{8\pi\epsilon_0\sqrt{a^2-b^2}} \ln \frac{a+\sqrt{a^2-b^2}}{a-\sqrt{a^2-b^2}} \quad (149)$$

$$= -67.8358 \text{ eV}.$$

The potential energy of the two protons is

$$V_p = \frac{e^2}{8\pi\epsilon_0\sqrt{a^2-b^2}} = 19.2415 \text{ eV}. \quad (150)$$

The kinetic energy of the electrons is

$$T = \frac{\hbar^2}{2m_e a \sqrt{a^2-b^2}} \ln \frac{a+\sqrt{a^2-b^2}}{a-\sqrt{a^2-b^2}} \quad (151)$$

$$= 33.9179 \text{ eV}.$$

The energy V_m of the magnetic force between the electrons is

$$V_m = \frac{-\hbar^2}{4m_e a \sqrt{a^2-b^2}} \ln \frac{a+\sqrt{a^2-b^2}}{a-\sqrt{a^2-b^2}} \quad (152)$$

$$= -16.959 \text{ eV}.$$

During bond formation, the electrons undergo a reentrant oscillatory orbit with vibration of the protons. The corresponding energy \bar{E}_{osc} is the sum of the Doppler and average vibrational kinetic energies:

$$\bar{E}_{osc} = \bar{E}_D + \bar{E}_{Kvib}$$

$$= (V_e + T + V_m + V_p) \sqrt{\frac{2\bar{E}_K}{Mc^2}} + \frac{1}{2} \hbar \sqrt{\frac{k}{\mu}}. \quad (153)$$

The total energy is

$$E_T = V_e + T + V_m + V_p + \bar{E}_{osc}$$

$$= -\frac{e^2}{8\pi\epsilon_0 a_0}$$

$$\times \left[\left(2\sqrt{2} - \sqrt{2} + \frac{\sqrt{2}}{2} \right) \ln \frac{\sqrt{2}+1}{\sqrt{2}-1} - \sqrt{2} \right] \quad (154)$$

$$\times \left[1 + \sqrt{\frac{2\hbar\sqrt{e^2/(4\pi\epsilon_0 a_0^3/m_e)}}{m_e c^2}} \right] - \frac{1}{2} \hbar \sqrt{\frac{k}{\mu}}$$

$$= -31.689 \text{ eV}.$$

The energy of two hydrogen atoms is

$$E(2H[a_H]) = -27.21 \text{ eV}. \quad (155)$$

The bond dissociation energy E_D is the difference between the total energy of the corresponding hydrogen atoms (155) and E_T (154):

$$E_D = E(2H[a_H]) - E_T = 4.478 \text{ eV}. \quad (156)$$

The experimental energy is $E_D = 4.478 \text{ eV}$. The calculated and experimental parameters of H_2 , D_2 , H_2^+ , and D_2^+ from Chapter 12 of Ref. 3 are given in Table II.

24. COSMOLOGICAL THEORY BASED ON MAXWELL'S EQUATIONS

Maxwell's equations and special relativity are based on the law of propagation of a electromagnetic wavefront in the form

$$\frac{1}{c^2} \left(\frac{\partial \omega}{\partial t} \right)^2 - \left[\left(\frac{\partial \omega}{\partial x} \right)^2 + \left(\frac{\partial \omega}{\partial y} \right)^2 + \left(\frac{\partial \omega}{\partial z} \right)^2 \right] = 0. \quad (157)$$

For any kind of wave advancing with limiting velocity and capable of transmitting signals, the equation of front propagation is the same as the equation for the front of a light wave. Thus the equation

$$\frac{1}{c^2} \left(\frac{\partial \omega}{\partial t} \right)^2 - (\text{grad } \omega)^2 = 0 \quad (158)$$

acquires a general character; it is more general than Maxwell's equations, from which Maxwell originally derived it.

A discovery of the present work shown in this section with the results of the previous sections regarding the bound electron is that the classical wave equation governs (1) the motion of bound electrons, (2) the propagation of any form of energy, (3) measurements between inertial frames of reference such as time, mass, momentum, and length (Minkowski tensor), (4) fundamental particle production and the conversion of space-matter to energy, (5) a relativistic correction of space-time due to particle production or annihilation (SM), (6) the expansion and contraction of the universe, and (7) the basis of the relationship between Maxwell's equations, Planck's equation, the de Broglie equation, Newton's laws, and special and general relativity.

The relationship between the time interval between ticks t of a clock in motion with velocity v relative to an observer and the time interval t_0 between ticks on a clock at rest relative to an observer is⁽³⁵⁾

$$(ct)^2 = (ct_0)^2 + (vt)^2. \quad (159)$$

Thus the time dilation relationship based on the constant maximum speed of light c in any inertial frame is

$$t = \frac{t_0}{\sqrt{1 - v^2/c^2}}. \quad (160)$$

The metric $g_{\mu\nu}$ for Euclidean space is the Minkowski tensor $\eta_{\mu\nu}$. In this case, the separation of proper time between two events x^μ and $x^\mu + dx^\mu$ is $d\tau^2 = -\eta_{\mu\nu} dx^\mu dx^\nu$.

25. THE EQUIVALENCE OF THE GRAVITATIONAL MASS AND THE INERTIAL MASS

Mass also experimentally causes time dilation (i.e., clocks run slower in the presence of a gravitational field). The equivalence of the gravitational mass and the inertial mass, $m_g/m_i = \text{universal constant}$, which is predicted by Newton's law of mechanics and gravitation, is experimentally confirmed to less than 1×10^{-11} .⁽³⁶⁾ In physics, the discovery of a universal constant often leads to the development of an entirely

new theory. From the universal constancy of the velocity of light c the special theory of relativity was derived; from Planck's constant h the quantum theory was deduced. Therefore the universal constant m_g/m_i should be the key to the gravitational problem. The energy equation of Newtonian gravitation is

$$E = \frac{1}{2}mv^2 - \frac{GMm}{r} \quad (161)$$

$$= \frac{1}{2}mv_0^2 - \frac{GMm}{r_0} = \text{constant}.$$

Since h , the angular momentum per unit mass, is

$$h = \frac{L}{m} = |\mathbf{r} \times \mathbf{v}| = r_0 v_0 \sin \phi,$$

the eccentricity e may be written as

$$e = \left[1 + \left(v_0^2 - \frac{2GM}{r_0} \right) \frac{r_0^2 v_0^2 \sin^2 \phi}{G^2 M^2} \right]^{1/2}, \quad (162)$$

where m is the inertial mass of a particle, v_0 is the speed of the particle, r_0 is the distance of the particle from a massive object, ϕ is the angle between the direction of motion of the particle and the radius vector from the object, and M is the total mass of the object (including a particle). The eccentricity e given by Newton's differential equations of motion in the case of the central field permits the classification of the orbits according to the total energy $E^{(37)}$ (column 1 of (163)) and the orbital velocity squared, v_0^2 relative to the gravitational velocity squared, $2GM/r_0$ ⁽³⁷⁾ (column 2 of (163)):

$E < 0$	$v_0^2 < \frac{2GM}{r_0}$	$e < 1$	ellipse
$E < 0$	$v_0^2 < \frac{2GM}{r_0}$	$e = 0$	circle (special case of ellipse)
$E = 0$	$v_0^2 = \frac{2GM}{r_0}$	$e = 1$	parabolic orbit
$E > 0$	$v_0^2 > \frac{2GM}{r_0}$	$e > 1$	hyperbolic orbit

(163)

26. CONTINUITY CONDITIONS FOR THE

PRODUCTION OF A PARTICLE FROM A PHOTON TRAVELING AT LIGHT SPEED

A photon traveling at the speed of light gives rise to a particle with an initial radius equal to its Compton wavelength bar:

$$r = \lambda_c = \frac{\hbar}{mc} = r_a^* \quad (164)$$

The particle must have an orbital velocity equal to the Newtonian gravitational escape velocity v_g of the antiparticle:

$$v_g = \sqrt{\frac{2Gm}{r}} = \sqrt{\frac{2Gm_0}{\lambda_c}} \quad (165)$$

The eccentricity is one. The orbital energy is zero, corresponding to conservation of energy. The particle production trajectory is a parabola relative to the center of mass of the antiparticle.

26.1 A Gravitational Field as a Front Equivalent to a Light-Wave Front

A particle with a finite gravitational mass gives rise to a gravitational field that travels out as a front equivalent to a light-wave front. The form of the outgoing gravitational field front traveling at the speed of light is $f(t - r/c)$, and $d\tau^2$ is given by

$$d\tau^2 = f(r)dt^2 - \frac{1}{c^2} [f(r)^{-1} dr^2 + r^2 d\theta^2 + r^2 \sin^2 \theta d\phi^2] \quad (166)$$

The speed of light as a constant maximum as well as the phase-matching and continuity conditions of the electromagnetic and gravitational waves require the following form of the squared displacements:

$$(c\tau)^2 + (v_g t)^2 = (ct)^2, \quad (167)$$

$$f(r) = \left(1 - \left(\frac{v_g}{c} \right)^2 \right). \quad (168)$$

In order that the wave-front velocity not exceed c in any frame, space-time must undergo time dilation and length contraction due to the particle production event. *The derivation and result of space-time time dilation are analogous to the derivation and result of*

special relativistic time dilation, where the relative velocity of two inertial frames replaces the gravitational velocity.

The general form of the metric due to the relativistic effect on space-time due to mass m_0 with v_g given by (165) is

$$d\tau^2 = \left(1 - \left(\frac{v_g}{c} \right)^2 \right) dt^2 - \frac{1}{c^2} \left[\left(1 - \left(\frac{v_g}{c} \right)^2 \right)^{-1} dr^2 + r^2 d\theta^2 + r^2 \sin^2 \theta d\phi^2 \right] \quad (169)$$

The gravitational radius r_g of each orbitsphere of the particle production event, each of mass m_0 , and the corresponding general form of the metric are, respectively,

$$r_g = \frac{2Gm_0}{c^2}, \quad (170)$$

and

$$d\tau^2 = \left(1 - \frac{r_g}{r} \right) dt^2 - \frac{1}{c^2} \left[\left(1 - \frac{r_g}{r} \right)^{-1} dr^2 + r^2 d\theta^2 + r^2 \sin^2 \theta d\phi^2 \right] \quad (171)$$

The metric $g_{\mu\nu}$ for non-Euclidean space due to the relativistic effect on space-time due to mass m_0 is

$$g_{\mu\nu} = \begin{pmatrix} -(1-B) & 0 & 0 & 0 \\ 0 & \frac{1}{c^2}(1-B)^{-1} & 0 & 0 \\ 0 & 0 & \frac{1}{c^2}r^2 & 0 \\ 0 & 0 & 0 & \frac{1}{c^2}r^2 \sin^2 \theta \end{pmatrix}, \quad (172)$$

where $B = 2Gm_0/c^2 r$ has been used to save space. Masses and their effects on space-time *superimpose*.

The separation of proper time between two events x^μ and $x^\mu + dx^\mu$ is

$$d\tau^2 = \left(1 - \frac{2GM}{c^2 r}\right) dt^2 - \frac{1}{c^2} \left[\left(1 - \frac{2GM}{c^2 r}\right)^{-1} dr^2 + r^2 d\theta^2 + r^2 \sin^2 \theta d\phi^2 \right] \quad (173)$$

The SM (173) gives the relationship whereby matter causes relativistic corrections to space-time that determines the curvature of space-time and is the origin of gravity.

26.2 Particle Production Continuity Conditions from Maxwell's Equations, and the SM

The photon-to-particle event requires a transition state that is continuous, where the velocity of a transition state orbitsphere is the speed of light. The radius r is the Compton wavelength bar λ_c given by (164). At production the Planck equation energy, the electric potential energy, and the magnetic energy are equal to $m_0 c^2$.

The SM gives the relationship whereby matter causes relativistic corrections to space-time that determines the masses of fundamental particles. Substitution of $r = \lambda_c$, $dr = 0$, $d\theta = 0$, and $\sin^2 \theta = 1$ into the SM gives

$$d\tau = dt \left(1 - \frac{2Gm_0}{c^2 r_a} - \frac{v^2}{c^2} \right)^{1/2}, \quad (174)$$

with $v^2 = c^2$; the relationship between the proper time and the coordinate time is

$$\tau = ti \sqrt{\frac{2GM}{c^2 r_a}} = ti \sqrt{\frac{2GM}{c^2 \lambda_c}} = ti \frac{v_g}{c}. \quad (175)$$

When the orbitsphere velocity is the speed of light, continuity conditions based on the constant maximum speed of light given by Maxwell's equations are mass energy = Planck equation energy = electric potential energy = magnetic energy = mass/space-time metric energy. Therefore

$$m_0 c^2 = \hbar \omega^* = V = E_{mag} = E_{space-time}, \quad (176)$$

$$\begin{aligned} m_0 c^2 &= \hbar \omega^* = \frac{\hbar^2}{m_0 \lambda_c^2} = \alpha^{-1} \frac{e^2}{4\pi \epsilon_0 \lambda_c} \\ &= \alpha^{-1} \frac{\pi \mu_0 e^2 \hbar^2}{(2\pi m_0)^2 \lambda_c^3} = \frac{\alpha \hbar}{1 \text{ sec}} \sqrt{\frac{\lambda_c c^2}{2Gm}}, \end{aligned} \quad (177)$$

where sec is the symbol for time defined in End-note 3. The continuity conditions based on the constant maximum speed of light given by the SM are

$$\begin{aligned} &\frac{\text{proper time}}{\text{coordinate time}} \\ &= \frac{\text{gravitational wave condition}}{\text{electromagnetic wave condition}} \\ &= \frac{\text{gravitational mass phase matching}}{\text{charge/inertial mass phase matching}} \\ &= i \frac{\sqrt{2Gm/c^2 \lambda_c}}{\alpha} = i \frac{v_g}{\alpha c}. \end{aligned} \quad (178)$$

27. MASSES OF FUNDAMENTAL PARTICLES

Each of the Planck equation energy, electric energy, and magnetic energy corresponds to a particle given by the relationship between the proper time and the coordinate time.⁽³⁾ The electron and down-down-up neutron correspond to the Planck equation energy. The muon and strange-strange-charmed neutron correspond to the electric energy. The tau and bottom-bottom-top neutron correspond to the magnetic energy. The particle must possess the escape velocity v_g relative to the antiparticle, where $v_g < c$. According to Newton's law of gravitation, the eccentricity is one and the particle production trajectory is a parabola relative to the center of mass of the antiparticle.

27.1 Electron and Muon Production

A clock is defined in terms of a self-consistent system of units used to measure the particle mass.³ The proper time of the particle is equated with the coordinate time according to the SM corresponding to light speed. The special relativistic condition corresponding to the Planck energy (177) gives the mass of the electron.⁽³⁾

$$2\pi \frac{\hbar}{mc^2} = 1 \text{ sec} \sqrt{\frac{2GM}{\alpha^2 \hbar}}, \quad (179)$$

$$m_e = \left(\frac{h\alpha}{1 \text{ sec } c^2} \right)^{1/2} \left(\frac{c\hbar}{2G} \right)^{1/4} = 9.0998 \times 10^{-31} \text{ kg}, \quad (180)$$

where $m_{e,\text{experimental}} = 9.109 454 55 \times 10^{-31} \text{ kg}$.

The special relativistic condition corresponding to the electric energy (177) gives the mass of the muon.⁽³⁾

$$m_\mu = \frac{\hbar}{c} \left(\frac{1}{2Gm_e(\alpha \text{ sec})^2} \right)^{1/3} \quad (181)$$

$$= 1.8874 \times 10^{-28} \text{ kg},$$

where $m_{\mu,\text{experimental}} = 1.883 55 \times 10^{-28} \text{ kg}$. The differences between the calculated and experimental values of the electron and muon masses are due to the slight difference between the present MKS second and the corresponding time unit defined by (179). The relation between the muon and electron masses, which is independent of the definition of the imaginary time ruler ti given by (179), including the contribution of the neutrinos given in Chapter 27, the Leptons section, of Ref. 3, is

$$\frac{m_\mu}{m_e} = \left(\frac{\alpha^{-2}}{2\pi} \right)^{2/3} \frac{1+2\pi(\alpha^2/2)}{1+\alpha/2} \quad (182)$$

$$= 206.768 28 \quad (206.768 27).$$

The experimental lepton mass ratio according to the 1998 CODATA and the Particle Data Group is given in parentheses.^(38,39)

27.2 Down-Down-Up Neutron

The corresponding equations for production of the members of the neutron family are derived from the corresponding energies too.⁽³⁾ For example, the mass of the neutron comprising down-down-up quarks given by the Planck energy is

$$\frac{2\pi \frac{2\pi\hbar}{m_N \left(\frac{1}{2\pi} - \frac{\alpha}{2\pi} \right) c^2}}{3 \left(\frac{1}{2\pi} - \frac{\alpha}{2\pi} \right) c^2} \quad (183)$$

$$= 1 \text{ sec} \sqrt{\frac{2G \left[\frac{m_N \left(\frac{1}{2\pi} - \frac{\alpha}{2\pi} \right) \right]^2}{3c(2\pi)^2 \hbar}},$$

$$m_{N,\text{calculated}} = (3)(2\pi) \left(\frac{1}{1-\alpha} \right) \left(\frac{2\pi\hbar}{1 \text{ sec } c^2} \right)^{1/2} \left(\frac{2\pi(3)c\hbar}{2G} \right)^{1/4} \quad (184)$$

$$= 1.6726 \times 10^{-27} \text{ kg},$$

where $m_{N,\text{experimental}} = 1.6749 \times 10^{-27} \text{ kg}$. The relation between the neutron and electron masses, which is independent of the definition of the imaginary time ruler ti given by (179), including the contribution of the neutrinos given in Chapter 30, the Quarks section, of Ref. 3, is

$$\frac{m_N}{m_e} = \frac{12\pi^2}{1-\alpha} \sqrt{\frac{\sqrt{3}}{\alpha} \frac{1+2\pi(\alpha^2/2)}{1-2\pi(\alpha^2/2)}} \quad (185)$$

$$= 1838.67 \quad (1838.68).$$

The parameters of the nucleons and the beta decay energy of the neutron are given in the Weak Nuclear Force: Beta Decay of the Neutron section and the Proton and Neutron section of Ref. 3, respectively.

28. GRAVITATIONAL POTENTIAL ENERGY

Three families of quarks are given by (183), with the corresponding energies given by (177).⁽³⁾ The gravitational potential energy gives the possibility of a fourth family. The gravitational radius, α_G or r_G , of an orbitsphere of mass m_0 is defined as

$$\alpha_G = r_G = \frac{Gm_0}{c^2}. \quad (186)$$

When $r_G = r_\alpha^* = \lambda_C$, the gravitational potential energy equals $m_0 c^2$:

$$r_G = \frac{Gm_0}{c^2} = \lambda_C = \frac{\hbar}{m_0 c}, \quad (187)$$

$$E_{\text{grav}} = \frac{Gm_0^2}{r} = \frac{Gm_0^2}{\lambda_C} = \frac{Gm_0^2}{r_\alpha^*} = \hbar\omega^* = m_0 c^2. \quad (188)$$

The mass m_0 is the Planck mass, m_u :

$$m_u = m_0 = \sqrt{\frac{\hbar c}{G}}. \quad (189)$$

The corresponding gravitational velocity v_G is defined as

$$v_G = \sqrt{\frac{Gm_0}{r}} = \sqrt{\frac{Gm_0}{\lambda_c}} = \sqrt{\frac{Gm_u}{\lambda_c}} \quad (190)$$

28.1 Relationship of the Equivalent Planck Mass Particle Production Energies

For the Planck mass particle, the relationships corresponding to (177) are (mass energy = Planck equation energy = electric potential energy = magnetic energy = gravitational potential energy = mass/space-time metric energy)

$$m_0 c^2 = \hbar \omega^* = V = E_{mag} = E_{grav} = E_{space-time} \quad (191)$$

$$\begin{aligned} m_0 c^2 = \hbar \omega^* &= \frac{\hbar^2}{m_0 \lambda_c} = \alpha^{-1} \frac{e^2}{4\pi\epsilon_0 \lambda_c} \\ &= \alpha^{-1} \frac{\pi\mu_0 e^2 \hbar^2}{(2\pi m_0)^2 \lambda_c^3} = \alpha^{-1} \frac{\mu_0 e^2 c^2}{2h} \sqrt{\frac{Gm_0}{\lambda_c}} \sqrt{\frac{\hbar c}{G}} \quad (192) \\ &= \frac{\alpha h}{1} \sqrt{\frac{\lambda_c c^2}{2Gm}} \end{aligned}$$

These equivalent energies give the particle masses in terms of the gravitational velocity v_G and the Planck mass m_u :

$$\begin{aligned} m_0 &= \alpha^{-1} \frac{\mu_0 e^2 c}{2h} \sqrt{\frac{Gm_0}{\lambda_c}} m_u \\ &= \alpha^{-1} \frac{\mu_0 e^2 c}{2h} \sqrt{\frac{Gm_0}{c^2 \lambda_c}} m_u = \alpha^{-1} \frac{\mu_0 e^2 c}{2h} \frac{v_G}{c} m_u \quad (193) \\ &= \frac{v_G}{c} m_u. \end{aligned}$$

28.2 Planck Mass Particles

A pair of particles each of the Planck mass corresponding to the gravitational potential energy is not observed since the velocity of each transition state orbitsphere is the gravitational velocity v_G that in this case is the speed of light; but the Newtonian gravitational escape velocity v_g is $\sqrt{2}$ times the speed of light. In this case, an electromagnetic wave of mass energy equivalent to the Planck mass travels in a circular orbit about the center of mass of another elec-

tromagnetic wave of mass energy equivalent to the Planck mass, where the eccentricity is equal to zero and the escape velocity can never be reached. The Planck mass is a "measuring stick." The extraordinarily high Planck mass ($\sqrt{\hbar c / G} = 2.18 \times 10^{-8}$ kg) is the unobtainable mass bound imposed by the angular momentum and speed of the photon relative to the gravitational constant. It is analogous to the unattainable bound of the speed of light for a particle possessing finite rest mass imposed by the Minkowski tensor.

28.3 Astrophysical Implications of Planck Mass Particles

The limiting speed of light eliminates the singularity problem of Einstein's equation that arises as the radius of a black hole equals the Schwarzschild radius. General relativity with the singularity eliminated resolves the paradox of the infinite propagation velocity required for the gravitational force in order to explain why the angular momentum of objects orbiting a gravitating body does not increase due to the finite propagation delay of the gravitational force, according to special relativity.⁽⁴⁰⁾ When the gravitational potential energy density of a massive body such as a black hole equals that of a particle with Planck mass, the matter may transition to photons of the Planck mass. Even light from a black hole will escape when the decay rate of the trapped matter with the concomitant space-time expansion is greater than the effects of gravity that oppose this expansion. Gamma-ray bursts are the most energetic phenomenon known, and can release an explosion of gamma rays packing 100 times more energy than a supernova explosion.⁽⁴¹⁾ The annihilation of a black hole may be the source of *gamma-ray bursts*. The source may be conversion of matter to photons of the Planck mass/energy, which may also give rise to cosmic rays, which are the most energetic particles known (their origin is also a mystery⁽⁴²⁾). According to the GZK cutoff, the cosmic spectrum cannot extend beyond 5×10^{19} eV, but AGASA, the world's largest air shower array, has shown that the spectrum is extending beyond 10^{20} eV without any clear sign of cutoff.⁽⁴³⁾ Photons, each of the Planck mass, may be the source of these inexplicably energetic cosmic rays.

29. RELATIONSHIP OF MATTER TO ENERGY AND SPACE-TIME EXPANSION

The SM gives the relationship whereby matter causes relativistic corrections to space-time. The limiting velocity c results in the contraction of space-time due to particle production, which is given by

$2\pi r_g$, where r_g is the gravitational radius of the particle. This has implications for the expansion of space-time when matter converts to energy. Q is the mass/energy to expansion/contraction quotient of space-time and is given by the ratio of the mass of a particle at production to T , the period of production:

$$Q = \frac{m_0}{T} = \frac{m_0}{2\pi r_g / c} = \frac{m_0}{2\pi(2Gm_0/c^2)/c} \quad (194)$$

$$= \frac{c^3}{4\pi G} = 3.22 \times 10^{34} \text{ kg/s.}$$

The gravitational equations with the equivalence of the particle production energies (177) permit the conservation of mass/energy ($E = mc^2$) and space-time ($c^3/4\pi G = 3.22 \times 10^{34} \text{ kg/s}$). With the conversion of $3.22 \times 10^{34} \text{ kg}$ of matter to energy, space-time expands by 1 s. The photon has inertial mass and angular momentum, but due to Maxwell's equations and the implicit special relativity it does not have a gravitational mass. The observed gravitational deflection of light is predicted.⁽³⁾

29.1 Cosmological Consequences

The universe is closed (it is finite but with no boundary). It is a 3-sphere universe—Riemannian three-dimensional hyperspace plus time of constant positive curvature at each r-sphere. *The universe is oscillatory in matter/energy and space-time* with a finite minimum radius, the gravitational radius. Space-time expands as mass is released as energy, which provides the basis of the atomic, thermodynamic, and cosmological arrows of time. Different regions of space are isothermal even though they are separated by greater distances than that over which light could travel during the time of the expansion of the universe.⁽⁴⁴⁾ Stars and large-scale structures now exist that are older than the elapsed time of the present expansion because stellar, galaxy, and supercluster evolution occurred during the contraction phase.⁽⁴⁵⁻⁵¹⁾ The maximum power radiated by the universe, which occurs at the beginning of the expansion phase, is $P_U = c^5/4\pi G = 2.89 \times 10^{51} \text{ W}$. Observations beyond the beginning of the expansion phase are not possible since the universe was entirely matter filled.

29.2 The Period of Oscillation of the Universe Based on Closed Propagation of Light

Mass/energy is conserved during harmonic expansion and contraction. The gravitational potential energy E_{grav} given by (188) with $m_0 = m_U$ is equal to $m_U c^2$ when the radius of the universe r is the gravita-

tional radius r_G . The gravitational velocity v_G ((190) with $r = r_G$ and $m_0 = m_U$) is the speed of light in a circular orbit, where the eccentricity is equal to zero and the escape velocity from the universe can never be reached. The period of the oscillation of the universe and the period for light to traverse the universe corresponding to the gravitational radius r_G must be equal. The harmonic oscillation period T is

$$T = \frac{2\pi r_G}{c} = \frac{2\pi G m_U}{c^3} = \frac{2\pi G (2 \times 10^{54} \text{ kg})}{c^3} \quad (195)$$

$$= 3.10 \times 10^{19} \text{ s} = 9.83 \times 10^{11} \text{ years,}$$

where the mass of the universe m_U is approximately $2 \times 10^{54} \text{ kg}$. (The initial mass of the universe of $2 \times 10^{54} \text{ kg}$ is based on internal consistency with the size, age, Hubble constant, temperature, density of matter, and power spectrum.) Thus the observed universe will expand as mass is released as photons for 4.92×10^{11} years. At this point in its world-line, the universe will obtain its maximum size and begin to contract.

30. THE DIFFERENTIAL EQUATION OF THE RADIUS OF THE UNIVERSE

Based on conservation of mass/energy ($E = mc^2$) and space-time ($c^3/4\pi G = 3.22 \times 10^{34} \text{ kg/s}$), the universe behaves as a simple harmonic oscillator with a restoring force F proportional to the radius. The proportionality constant k is given in terms of the potential energy E gained as the radius decreases from the maximum expansion to the minimum contraction:

$$\frac{E}{\aleph^2} = k. \quad (196)$$

Since the gravitational potential energy E_{grav} is equal to $m_U c^2$ when the radius of the universe r is the gravitational radius r_G ,

$$F = -k\aleph = -\frac{m_U c^2}{r_G^2} \aleph = -\frac{m_U c^2}{(Gm_U/c^2)^2} \aleph. \quad (197)$$

And, considering the oscillation, the differential equation of the radius \aleph of the universe is

$$m_U \ddot{\aleph} + \frac{m_U c^2}{r_G^2} \aleph = m_U \ddot{\aleph} + \frac{m_U c^2}{(Gm_U/c^2)^2} \aleph = 0. \quad (198)$$

The *maximum radius of the universe*, the amplitude r_0 of the time harmonic variation in the radius of the universe, is given by the quotient of the total mass of the universe and Q (194), the mass/energy to expansion/contraction quotient:

$$r_0 = \frac{m_U}{Q} = \frac{m_U}{c^3/4\pi G} = \frac{2 \times 10^{54} \text{ kg}}{c^3/4\pi G} \quad (199)$$

$$= 1.97 \times 10^{12} \text{ light-years.}$$

The *minimum radius* corresponding to the gravitational radius r_g given by (170) with $m_0 = m_U$ is

$$r_g = \frac{2Gm_U}{c^2} = 2.96 \times 10^{27} \text{ m} \quad (200)$$

$$= 3.12 \times 10^{11} \text{ light-years.}$$

When the radius of the universe is the gravitational radius r_g , the proper time is equal to the coordinate time by (175), and the gravitational escape velocity v_g of the universe is the speed of light. The radius of the universe as a function of time, as shown in Fig. 15, is

$$\begin{aligned} \dot{\kappa} &= \left(r_g + \frac{cm_U}{Q} \right) - \frac{cm_U}{Q} \cos \left(\frac{2\pi t}{2\pi r_g/c} \right) \\ &= \left(\frac{2Gm_U}{c^2} + \frac{cm_U}{c^3/4\pi G} \right) \\ &\quad - \frac{cm_U}{c^3/4\pi G} \cos \left(\frac{2\pi t}{2\pi Gm_U/c^3} \right). \end{aligned} \quad (201)$$

The expansion/contraction rate $\dot{\kappa}$, as shown in Fig. 16, is given by the time derivative of (201):

$$\dot{\kappa} = 4\pi c \times 10^{-3} \sin \left(\frac{2\pi t}{2\pi Gm_U/c^3} \right) \text{ km/s.} \quad (202)$$

31. THE HUBBLE CONSTANT

The *Hubble constant* is given by the ratio of the expansion rate given in units of kilometers per second divided by the radius of the expansion in megaparsecs (Mpc). The radius of expansion is equivalent to the radius of the light sphere with an origin at the time point when the universe stopped contracting and started to expand:

$$H = \frac{\dot{\kappa}}{ct \text{ (Mpc)}} \quad (203)$$

$$= \frac{4\pi c \times 10^{-3} \sin(2\pi t/(2\pi Gm_U/c^3)) \text{ km/s}}{ct \text{ (Mpc)}}$$

For $t = 10^{10}$ light-years corresponding to 3.069×10^3 Mpc, the Hubble constant H_0 is

$$H_0 = 78.6 \text{ km/s/Mpc.} \quad (204)$$

The experimental value⁽⁵²⁾ as shown in Fig. 17 is

$$H_0 = 80 \pm 17 \text{ km/s/Mpc.} \quad (205)$$

32. THE DENSITY OF THE UNIVERSE AS A FUNCTION OF TIME

The density of the universe as a function of time $\rho_U(t)$ given by the ratio of the mass as a function of time and the volume as a function of time, as shown in Fig. 18, is

$$\begin{aligned} \rho_U(t) &= \frac{m_u(t)}{V(t)} = \frac{m_u(t)}{\frac{4}{3}\pi \dot{\kappa}(t)^3} \\ &= \frac{\frac{m_U}{2} \left(1 + \cos \left(\frac{2\pi t}{\frac{2\pi Gm_U}{c^3}} \right) \right)}{\frac{4}{3}\pi \left(\left(\frac{2Gm_U}{c^2} + \frac{cm_U}{c^3/4\pi G} \right) - \frac{cm_U}{c^3/4\pi G} \cos \left(\frac{2\pi t}{\frac{2\pi Gm_U}{c^3}} \right) \right)^3}. \end{aligned} \quad (206)$$

For $t = 10^{10}$ light-years, $\rho_U = 1.7 \times 10^{-32} \text{ g/cm}^3$. The density of luminous matter of the stars and gas of galaxies is about $\rho_U = 2 \times 10^{-31} \text{ g/cm}^3$.^(53,54)

33. THE POWER OF THE UNIVERSE AS A FUNCTION OF TIME, $P_U(t)$

From $E = mc^2$ and (194),

$$P_U(t) = \frac{c^5}{8\pi G} \left(1 + \cos \frac{2\pi t}{2\pi r_g/c} \right). \quad (207)$$

For $t = 10^{10}$ light-years, $P_U(t) = 2.88 \times 10^{51}$ W. The observed power is consistent with that predicted. The power of the universe as a function of time is shown in Fig. 19.

34. THE TEMPERATURE OF THE UNIVERSE AS A FUNCTION OF TIME

The temperature of the universe as a function of time $T_U(t)$, as shown in Fig. 20, follows from the Stefan-Boltzmann law:

$$T_U(t) = \left(\frac{1}{1 + Gm_U(t)/c^2 \aleph(t)} \right) \left[\frac{R_U(t)}{e\sigma} \right]^{1/4} \quad (208)$$

$$= \left(\frac{1}{1 + Gm_U(t)/c^2 \aleph(t)} \right) \left[\frac{P_U(t)/4\pi \aleph(t)^2}{e\sigma} \right]^{1/4}.$$

The calculated uniform temperature is about 2.7 K, which is in agreement with the observed microwave background temperature.⁽⁴⁴⁾

35. POWER SPECTRUM OF THE COSMOS

The power spectrum of the cosmos, as measured by the Las Campanas survey, generally follows the prediction of cold dark matter on the scale of 200 million to 600 million light-years. However, the power increases dramatically on a scale of 600 million to 900 million light-years.⁽⁵¹⁾ This discrepancy means that the universe is much more structured on those scales than current theories can explain.

The universe is oscillatory in matter/energy and space-time with a finite minimum radius. The *minimum radius* corresponding to the gravitational radius r_g given by (200) is 3.12×10^{11} light-years. The minimum radius is larger than that provided by the current expansion, approximately 10^{10} light-years.⁽⁵²⁾ The universe is a four-dimensional hyperspace of constant positive curvature at each r -sphere. The coordinates are spherical, and the space can be described as a series of spheres, each of constant radius r , whose centers coincide at the origin. The existence of the mass m_U causes the area of the spheres to be less than $4\pi r^2$ and causes the clock of each r -sphere to run so that it is no longer observed from other r -spheres to be at the same rate. The SM given by (173) is the general form of the metric that allows for these effects. Consider the present observable universe, which has undergone expansion for 10^{10} years. The radius of the universe as a function of time from the coordinate r -sphere is of the same form as (201). The average size of the universe r_U is given as the sum of

the gravitational radius r_g and the observed radius, 10^{10} light-years:

$$r_U = r_g + 10^{10} \text{ light-years}$$

$$= 3.12 \times 10^{11} \text{ light-years} + 10^{10} \text{ light-years} \quad (209)$$

$$= 3.22 \times 10^{11} \text{ light-years}.$$

The frequency of (201) is one half the amplitude of space-time expansion from the conversion of the mass of the universe into energy according to (194). Thus, keeping the same relationships, the frequency of the current expansion function is the reciprocal of one half the current age. Substitution of the average size of the universe, the frequency of expansion, and the amplitude of expansion, 10^{10} light-years, into (201) gives the radius of the universe as a function of time for the coordinate r -sphere:

$$\aleph = 3.22 \times 10^{11} - 1 \times 10^{10}$$

$$\times \cos \left(\frac{2\pi t}{5 \times 10^9 \text{ light-years}} \right) \text{ light-years}. \quad (210)$$

The SM gives the relationship between the proper time and the coordinate time. The infinitesimal temporal displacement $d\tau^2$ is given by (173). In the case that $dr^2 = d\theta^2 = d\phi^2 = 0$, the relationship between the proper time and the coordinate time is

$$d\tau^2 = \left(1 - \frac{2Gm_U}{c^2 r} \right) dt^2, \quad (211)$$

$$\tau = t \sqrt{1 - \frac{r_g}{r}}. \quad (212)$$

The maximum power radiated by the universe is given by (207) and occurs when the proper radius, the coordinate radius, and the gravitational radius r_g are equal. For the present universe the coordinate radius is given by (209). The gravitational radius is given by (200). The maximum of the power spectrum of a trigonometric function occurs at its frequency.⁽⁵⁵⁾ Thus the coordinate maximum power according to (210) occurs at 5×10^9 light-years. The maximum power corresponding to the proper time is given by the substitution of the coordinate radius, the gravitational radius r_g , and the coordinate power maximum into (212). The power maximum in the proper frame occurs at

$$\tau = 5 \times 10^9 \text{ light-years} \sqrt{1 - \frac{3.12 \times 10^{11} \text{ light-years}}{3.22 \times 10^{11} \text{ light-years}}} \quad (213)$$

$$= 880 \times 10^6 \text{ light-years}$$

The power maximum of the current observable universe is predicted to occur on the scale of 880×10^6 light-years. There is excellent agreement between the predicted value and the experimental value of 600 to 900×10^6 light-years.⁽⁵¹⁾

36. THE EXPANSION/CONTRACTION ACCELERATION \ddot{R}

The expansion/contraction acceleration rate \ddot{R} , as shown in Fig. 21, is given by the time derivative of (202):

$$\ddot{R} = 2\pi \frac{c^4}{Gm_U} \cos\left(\frac{2\pi t}{2\pi Gm_U / c^3}\right). \quad (214)$$

The differential in the radius of the universe, ΔR , due to its acceleration is given by $\Delta R = 1/2 \ddot{R} t^2$. The differential in expanded radius for the elapsed time of expansion, $t = 10^{10}$ light-years, corresponds to a decrease in brightness of a supernova standard candle of about an order of magnitude of that expected, where the distance is taken as ΔR . This result, based on the predicted rate of acceleration of the expansion, is consistent with the experimental observation.⁽⁵⁶⁻⁵⁸⁾

Furthermore, the microwave background radiation image obtained by the Boomerang telescope⁽⁵⁹⁾ is consistent with a universe of nearly flat geometry since the commencement of its expansion. The data are consistent with a large offset radius of the universe with a fractional increase in size since the commencement of expansion about 10^{10} years ago. More details on these results are given in the Differential Equation of the Radius of the Universe section of Ref. 3.

37. POWER SPECTRUM OF THE COSMIC MICROWAVE BACKGROUND

When the universe reaches the maximum radius corresponding to the maximum contribution of the amplitude r_0 of the time harmonic variation in the radius of the universe, (199), it is entirely radiation filled. Since the photon has no gravitational mass, the radiation is uniform. As energy converts into matter,

the power of the universe may be considered negative for the first quarter cycle, starting from the point of maximum expansion, as given by (220), and space-time contracts according to (194). The gravitational field from particle production travels as a light-wave front. As the universe contracts to a minimum radius, the gravitational radius given by (200), constructive interference of the gravitational fields occurs for distances that are integers of the amplitude r_0 of the time harmonic variation in the radius of the universe for the times when the power is negative according to (220). The resulting slight variations in the density of matter are observed from our present r -sphere. The observed radius of expansion is equivalent to the radius of the light sphere with an origin at the time point when the universe stopped contracting and started to expand. The spherical harmonic parameter ℓ is given by the ratio of the amplitude r_0 of the time harmonic variation in the radius of the universe (199) divided by the present radius of the light sphere, where the universe is a 3-sphere universe — Riemannian three-dimensional hyperspace plus time of constant positive curvature at each r -sphere. For $t = 10^{10}$ light-years the fundamental ℓ is given by

$$\ell = \frac{r_0}{t} = \frac{2 \times 10^{54} \text{ kg} / (c^3 / 4\pi G)}{t} \quad (215)$$

$$= \frac{1.97 \times 10^{12} \text{ light-years}}{10^{10} \text{ light-years}} = 197.$$

The number of constructive interferences is given by the maximum integer of the ratio of the amplitude r_0 of the time harmonic variation in the radius of the universe (199) to the minimum radius, the gravitational radius (200). The number of peaks is

$$\frac{r_0}{r_g} = \frac{2 \times 10^{54} \text{ kg} / (c^3 / 4\pi G)}{2Gm_U / c^2} \quad (216)$$

$$= \frac{1.97 \times 10^{12} \text{ light-years}}{3.12 \times 10^{10} \text{ light-years}} = 6.3 \rightarrow 6.$$

The peaks are predicted to occur at the fundamental plus harmonics of the fundamental — integer multiples, $n = 2, 3, 4, 5$, and 6, of the fundamental $\ell = 197$:

$$\ell = 197 \text{ (fundamental),} \quad (217)$$

$$\ell = 197 + n197, \quad n = 2, 3, 4, 5, \text{ and } 6 \text{ (harmonics).}$$

From (217), the predicted harmonic parameters ℓ are given in Table III.

The harmonic peaks correspond to the condition that the amplitude of the harmonic term of the radius of the universe $r_0(n)$ is a reciprocal integer to that of the maximum amplitude r_0 . Thus $r_0(n)$ is given by

$$r_0(n) = \frac{r_0}{n} = \frac{2 \times 10^{54} \text{ kg} / (c^3 / 4\pi G)}{n} = \frac{1.97 \times 10^{12} \text{ light-years}}{n} \quad (218)$$

The power flow of radiant energy into mass decreases as the radius contracts, and the relative intensities of the peaks follow from the power flow. The relative intensities are given by the normalized power as a function of $t(n)$; the time at which the magnitude of the amplitude of the harmonic term of the radius of the universe $r_0(n)$ is given by (218) corresponding to each contracted radius at which constructive interference occurs. Starting the clock at the point of the maximum expansion where the universe is entirely radiation filled and the cosmic microwave background is uniform, the fact that the time at which the magnitude of the amplitude of the harmonic term of the radius of the universe $r_0(n)$ is given by (218) follows from (201):

$$\begin{aligned} r_0(n) &= \frac{r_0}{n} = \frac{1.97 \times 10^{12}}{n} \\ &= 1.97 \times 10^{12} \cos\left(\frac{2\pi t(n)}{9.83 \times 10^{11} \text{ years}}\right) \text{ light-years}, \\ t(n) &= \frac{9.83 \times 10^{11}}{2\pi} \cos^{-1}\left(\frac{1}{n}\right) \text{ years} \\ &= 1.564 \times 10^{11} \cos^{-1}\left(\frac{1}{n}\right) \text{ years}. \end{aligned} \quad (219)$$

The power of the universe as a function of time is given by (207) and is shown in Fig. 19. To express the negative power flow relative to the radiant energy of the universe corresponding to the conversion of energy into matter, the power of the universe as a function of time may be expressed as

$$\begin{aligned} P_U(t) &= -\frac{c^5}{4\pi G} \cos\left(\frac{2\pi t}{9.83 \times 10^{11} \text{ years}}\right) W, \\ &= -2.9 \times 10^{51} \cos\left(\frac{2\pi t}{9.83 \times 10^{11} \text{ years}}\right) W, \end{aligned} \quad (220)$$

where $t = 0$ corresponds to the time when the universe reaches the maximum radius corresponding to the maximum contribution of the amplitude r_0 of the time harmonic variation to the radius of the universe (199). At $t = 0$ as defined, the universe is entirely radiation filled, and the power into particle production is a maximum. At $t = (\pi/2)/[2\pi/(9.83 \times 10^{11} \text{ years})]$, according to (220), particle production is in balance with matter-to-energy conversion, and the latter dominates for the following half cycle.

The relative intensities are given by substitution of (219) into (220), which is normalized by the magnitude of the maximum power, which occurs at the maximum radius. Thus the relative intensities are given by

$$\begin{aligned} I(n) &= \cos\left(\frac{2\pi(1.564 \times 10^{11} \cos^{-1}(1/n) \text{ years})}{9.83 \times 10^{11} \text{ years}}\right) \\ &= \frac{1}{n}. \end{aligned} \quad (221)$$

The relative intensities $I(n)$ as a function of peak n are given in Table III.

The cosmic microwave background radiation is an average temperature of 2.7 K, with deviations of 30 or so microkelvins in different parts of the sky representing slight variations in the density of matter. The measurements of the anisotropy in the cosmic microwave background have been measured with the DASI.⁽⁶⁰⁾ The angular power spectrum was measured in the range $100 < \ell < 900$, and peaks in the power spectrum from the temperature fluctuations of the cosmic microwave background radiation appear at certain values of ℓ of spherical harmonics. Peaks were observed at $\ell \approx 200$, $\ell \approx 550$, and $\ell \approx 800$ with relative intensities of 1, 0.5, and 0.3, respectively (Fig. 1 of Ref. 60). There is excellent agreement between the predicted parameters given in Table III and the observed peaks.

38. THE PERIODS OF SPACE-TIME EXPANSION/CONTRACTION AND PARTICLE DECAY/PRODUCTION FOR THE UNIVERSE ARE EQUAL

The period of the expansion/contraction cycle of the radius of the universe T is given by (195). It follows from the Poynting power theorem with spherical radiation that the transition lifetimes are given by the ratio of energy and the power of the transition (92). Exponential decay applies to electromagnetic energy decay:

$$h(t) = e^{-at} u(t) = e^{-\frac{2\pi}{T}t} u(t). \quad (222)$$

The coordinate time is imaginary because energy transitions are space-like due to space-time expansion from matter-to-energy conversion. For example, the mass of the electron (a fundamental particle) is given by

$$\frac{2\pi\lambda_c}{\sqrt{2Gm_e/\lambda_c}} = \frac{2\pi\lambda_c}{v_g} = i\alpha^{-1} \text{ sec}, \quad (223)$$

where v_g is Newtonian gravitational velocity (165). When the gravitational radius r_g is the radius of the universe, the proper time is equal to the coordinate time by (175), and the gravitational escape velocity v_g of the universe is the speed of light. Replacement of the coordinate time t with the space-like time it gives

$$h(t) = \text{Re}[e^{-i(2\pi/T)t}] = \cos\left[\left(\frac{2\pi}{T}\right)t\right], \quad (224)$$

where the period is T (195). The continuity conditions based on the constant maximum speed of light (Maxwell's equations) are given by (176) and (177). The continuity conditions based on the constant maximum speed of light (SM) are given by (178). The periods of space-time expansion/contraction and particle decay/production for the universe are equal because only the particles that satisfy Maxwell's equations and the relationship between proper time and coordinate time imposed by the SM may exist.

39. WAVE EQUATION

The general form of the light-wave front equation is given by (157) and (158). The equation of the radius of the universe \aleph may be written as

$$\aleph = \left(\frac{2Gm_U}{c^2} + \frac{cm_U}{c^3/4\pi G} \right) - \frac{cm_U}{c^3/4\pi G} \cos\left(\frac{2\pi}{2\pi Gm_U/c^3} \left(t - \frac{\aleph}{c} \right) \right), \quad (225)$$

which is a solution of the wave equation for a light-wave front.

40. CONCLUSION

Maxwell's equations, Planck's equation, the de Broglie equation, Newton's laws, and special and general relativity are unified. Classical physical laws apply on all scales.

APPENDIX A: DERIVATION OF THE SPIN FUNCTION

A.1 The Orbitsphere Equation of Motion for $\ell = 0$

A.1.1 Stern–Gerlach Experiment Boundary Condition

It is known from the Stern–Gerlach experiment that a beam of silver atoms splits into two components when passed through an inhomogeneous magnetic field. This implies that the electron is a spin-1/2 particle with an intrinsic angular momentum of $\pm\hbar/2$ in the direction of the applied field (spin axis), and the magnitude of the angular momentum vector that precesses about the spin axis is $\sqrt{3/4}\hbar$. Furthermore, the magnitude of the splitting implies a magnetic moment of μ_B , a full Bohr magneton, given by (51), corresponding to the \hbar of total angular momentum on the axis of the applied field.

The algorithm to generate the $Y_0^0(\theta, \phi)$ orbitsphere equation of motion of the electron ((14) and (15)) is developed in this section. It was shown in Section 5 that the integral of the magnitude of the angular momentum over the orbitsphere must be constant. The constant is \hbar , as given by (7). It is shown in this section that the projection of the intrinsic orbitsphere angular momentum onto the spin axis is $\pm\hbar/2$, and the projection onto S , the axis that precesses about the spin axis, is \hbar , with a precessing component in the perpendicular plane of $\sqrt{3/4}\hbar$ and a component on the spin axis of $\pm\hbar/2$. Thus the mystery of an intrinsic angular momentum of $\pm\hbar/2$ and a total angular momentum in a resonant rotating frame (RF) experiment of $L_z = \hbar$ is resolved since the sum of the intrinsic and spin axis projections of the precessing component is \hbar . The Stern–Gerlach experiment implies a magnetic moment of one Bohr magneton and an associated angular momentum quantum number of 1/2. Histori-

cally, this quantum number has been called the spin quantum number s ($s = 1/2$, $m_s = \pm 1/2$), and that designation is maintained here.

The electron has a measured magnetic field and corresponding magnetic moment of a Bohr magneton and behaves as a spin-1/2 particle or fermion. For any magnetic field, the solution for the corresponding current from Maxwell's equations is unique. Thus the electron field requires a unique current according to Maxwell's equations. Several boundary conditions must be satisfied, and the orbitsphere equation of motion for $\ell = 0$ is solved as a boundary value problem. The boundary conditions are as follows:

1. Each infinitesimal point (position) on the orbitsphere comprising a charge (mass) density element must have the same angular and linear velocities given by (6) and (9), respectively.
2. According to condition 1, every such infinitesimal point must move along a great circle, and the current density distribution must be uniform.
3. The electron magnetic moment must be completely parallel or antiparallel to an applied magnetic field, in agreement with the Stern-Gerlach experiment.
4. According to condition 3, the projection of the intrinsic angular momentum of the orbitsphere onto the z axis must be $\pm \hbar/2$, and the projection into the transverse plane must be $\pm \hbar/4$ to achieve the spin-1/2 aspect.
5. The Larmor excitation of the electron in the applied magnetic field must give rise to a component of electron spin angular momentum that precesses about the applied magnetic field such that the contribution along the z axis is $\pm \hbar/2$ and the projection onto the orthogonal axis, which precesses about the z axis, must be $\pm \sqrt{3}/4 \hbar$.
6. Due to conditions 4 and 5, the angular momentum components corresponding to the current of the orbitsphere and to the Larmor precession must rise to a total angular momentum on the applied field axis of $\pm \hbar$.
7. Due to condition 6, the precessing electron has a magnetic moment of one Bohr magneton.
8. The energy of the transition of the alignment of the magnetic moment with an applied magnetic field must be given by (59), corresponding to the extended electron having a total angular momentum on the applied field axis of $\pm \hbar$.

Consider the derivation of (1.58) and (1.59) of Ref.

3. The moment of inertia of a point particle is mr^2 , and that of a globe spinning about some axis is $I = (2/3)mr^2$. For $\ell = 0$, the electron mass and charge are

uniformly distributed over the orbitsphere, a two-dimensional, spherical shell, but the orbitsphere is *not* analogous to a globe. The velocity of a point mass on a spinning globe is a function of θ , but the magnitude of the velocity at each point of the orbitsphere is not a function of θ . To picture the distinction, it is a useful concept to consider that the orbitsphere comprises an infinite number of point elements that move on the spherical surface. Then each point on the sphere with mass m_i has the same angular velocity (ω_n), the same magnitude of linear velocity (v_n), and the same moment of inertia ($m_i r_n^2$). The motion of each point of the orbitsphere is along a great circle, and the motion along each great circle is correlated with the motion on all other great circles such that the sum of all the contributions of the corresponding angular momenta is different from that of a point or globe. The orbitsphere angular momentum is uniquely directed disproportionately along two orthogonal axes.

The current density function of the orbitsphere is generated from a basis set current vector field defined as the orbitsphere-cvf. This in turn is generated from orthogonal great circle current loops that serve as basis elements. Due to the symmetry properties of the angular momentum components and the corresponding current of the orbitsphere-cvf, a uniform current distribution with the same angular momentum components as that of the orbitsphere-cvf is obtained by using an autocorrelation-type convolution operator on the orbitsphere-cvf. This uniform current density function comprises $Y_0^0(\theta, \phi)$, the orbitsphere equation of motion of the electron ((14) and (15)). Then the uniform, equipotential charge density function of the orbitsphere with only a radial discontinuous field at the surface according to (1) of Appendix IV of Ref. 3 is constant in time due to the motion of the current along great circles. The current flowing into any given point of the orbitsphere equals the current flowing out to satisfy the current continuity condition $\nabla \cdot J = 0$.

The current vector field pattern of the orbitsphere-cvf is not spatially uniform. There is no coincidence or nonuniqueness of elements of the current vector field. But there are many crossings among elements at single points on the two-dimensional surface of the electron, and the density of the crossings is nonuniform over the surface. *Thus each element of the basis set to generate the current pattern, a great circle current loop, must be one-dimensional so that the crossings are zero-dimensional with no element interaction at their crossing.* (This is a logical and necessary geometric progression for the construction of a fundamental two-dimensional particle.) In the limit the

basis set generates a continuous two-dimensional current density with a constant charge (mass) density, where the crossings have no effect on the vector fields. Each one-dimensional element is independent of the others, and its contribution to the angular momentum and magnetic field independently superimposes with that of the others.

This unique aspect of a fundamental particle has the same properties of superposition as the electric and magnetic fields of a photon. As shown in the Excited States of the One-Electron Atom (Quantization), the Creation of Matter from Energy, the Pair Production, and the Leptons sections of Ref. 3, the angular momentum in the electric and magnetic fields is conserved in excited states and in the creation of an electron from a photon, in agreement with Maxwell's equations. It is useful to regard an electron as a photon frozen in time. The particle production conditions are given in Sections 26 and 27.

The equation of motion for each charge density element (and correspondingly for each mass density element) that gives the current pattern of the orbitsphere-cvf is generated in two steps as follows:

A procedure is used to generate the current pattern of the orbitsphere-cvf from which the physical properties are derived in Section A.2 and are shown to match the boundary conditions.

The current density of the orbitsphere-cvf is *continuous*, but it may be modeled as a current pattern comprising a superposition of an infinite series of correlated orthogonal great circle current loops. The *time-independent* current pattern is obtained by defining a basis set for generating the current distribution over the surface of a spherical shell of zero thickness. As such a basis set, consider that the electron current is first evenly distributed within two orthogonally linked great circle current loops. These loops will be further divided into two sets of linked orthogonal pairs, where each pair undergoes independent transformations over the surface, where the electron current is correspondingly divided by the number of basis loops, four, and then by the angular span of the transformations, to form a normalized current density in each case. The *continuous* uniform electron current density function $Y_0^0(\theta, \phi)$ ((14) and (15)) is then exactly generated from this orbitsphere-cvf as a basis element by a convolution operator comprising an autocorrelation-type function.

The stationary or laboratory Cartesian coordinate system for the first step, Step 1, of the algorithm to

generate the orbitsphere-cvf is shown in Fig. 22 as the xyz system. It is also designated the orbitsphere-cvf reference frame. The primed coordinate system is the stationary frame for the basis elements, where the first current loop always lies in the $y'z'$ plane and the second current loop always lies in the $x'z'$ plane. The primed coordinates are only coincident with the corresponding xyz coordinates for the initial positions, as shown in Fig. 22, since the current density pattern is generated by a series of transformations of the primed coordinates relative to the unprimed coordinates. Each successive transformation of the primed system defines an orientation of the basis set in the $x'y'z'$ frame relative to the xyz frame that comprises a current element of the current density pattern.

Rotations and reflections are the transformations on the surface of a sphere that may be used to generate the orbitsphere-cvf. The orbitsphere-cvf is simply generated by two steps, each comprising an infinite series of nested rotations of the two orthogonal great circle current loops each by an infinitesimal angle $\pm\Delta\alpha_i$ and $\pm\Delta\alpha_j$ about the new i' axis and new j' axis, respectively, which result from the preceding such rotation. Each orientation following the conjugate i' and j' rotations of the two orthogonal great circle current loops, where the first current loop lies in the $j'k'$ plane and the second current loop lies in the $i'k'$ plane, is an element of the infinite series, where for Step 1 $i' = x', j' = y',$ and $k' = z',$ and for Step 2 $i' = z', j' = x',$ and $k' = y'.$

For Step 1 the first such pair of orthogonal great circle current loops is shown in Fig. 22. The second element of the series is generated by rotation of the first element by an infinitesimal angle $\pm\Delta\alpha_x$ about the first x' axis followed by a rotation by the infinitesimal angle $\pm\Delta\alpha_y$ about the new (second) y' axis to form a second x' axis. The third element of the series is generated by the rotation of the second element by the same infinitesimal angle $\pm\Delta\alpha_x$ about the second x' axis followed by the rotation by the same infinitesimal angle $\pm\Delta\alpha_y$ about the new (third) y' axis. In general, the $(n + 1)$ th element of the series is generated by the rotation of the n th basis coordinate system by the infinitesimal angle $\pm\Delta\alpha_x$ about the n th x' axis followed by the rotation of the n th orbitsphere-cvf coordinate system by the infinitesimal angle $\pm\Delta\alpha_y$ about the $(n + 1)$ th new y' axis.

The sign of the corresponding angle is maintained throughout the rotations, and the summation of the reiterative rotations about the i' axis and the j' axis is

$$\lim_{\Delta\alpha \rightarrow 0} \sum_{n=1}^{\frac{\sqrt{2}}{2}\pi} |\Delta\alpha_{i,j}| = \frac{\sqrt{2}}{2}\pi$$

when the k' axis rotates from the k axis to the $-k$ axis. (The total angle $(\sqrt{2}/2)\pi$ is the hypotenuse of the triangle with sides of $\pi/2$ radians corresponding to i' axis rotations and $\pi/2$ radians corresponding to j' axis rotations.) Step 1 and Step 2 comprise the use of $\Delta\alpha_i$ and $\Delta\alpha_j$ as given in Table IV.

Next, consider two infinitesimal charge (mass) density elements at two separate positions or points, 1 and 2, of the two orthogonal great circle current loops that serve as the basis set, as shown in Figs. 22 and 23. The vector projection of the corresponding angular momentum at each point of each current element is integrated over the entire orbitsphere-cvf surface to give the electron angular momentum. The correct current pattern is confirmed by achieving the condition that the magnitude of the velocity at any point on the surface is given by (6) and by obtaining the required angular momentum projections of $\hbar/2$ and $\hbar/4$ along the z axis and along an axis in the xy plane, respectively, as given in Section A.2.

Thus the orbitsphere-cvf is generated from two orthogonal great circle current loops that are rotated about the n th i' axis and then about the $(n+1)$ th j' axis in two steps. For Step 1, consider two charge (mass) density elements, point 1 and point 2, in the basis set reference frame at time zero. Element 1 is at $x' = 0$, $y' = 0$, and $z' = r_n$, and element 2 is at $x' = r_n$, $y' = 0$, and $z' = 0$. Let element 1 move on a great circle counterclockwise toward the $-y'$ axis, as shown in Fig. 22, and let element 2 move clockwise on a great circle toward the z' axis, as shown in Fig. 22. The equations of motion, in the sub-basis set reference frame, are given as follows.

For point 1,

$$x'_1 = 0, y'_1 = -r_n \sin(\omega_n t), z'_1 = r_n \cos(\omega_n t). \quad (\text{A-1a})$$

For point 2,

$$x'_2 = r_n \cos(\omega_n t), y'_2 = 0, z'_2 = r_n \sin(\omega_n t). \quad (\text{A-1b})$$

For Step 2, consider two charge (mass) density elements, point 1 and point 2, in the basis set reference frame at time zero. Element 1 is at $x' = 0$, $y' = r_n$, and $z' = 0$, and element 2 is at $x' = r_n$, $y' = 0$, and $z' = 0$. Let element 1 move clockwise on a great circle to-

ward the $-z'$ axis, as shown in Fig. 23, and let element 2 move counterclockwise on a great circle toward the y' axis, as shown in Fig. 23. The equations of motion in the basis set reference frame are given as follows.

For point 1,

$$x'_1 = 0, y'_1 = r_n \cos(\omega_n t), z'_1 = -r_n \sin(\omega_n t). \quad (\text{A-2a})$$

For point 2,

$$x'_2 = r_n \cos(\omega_n t), y'_2 = r_n \sin(\omega_n t), z'_2 = 0. \quad (\text{A-2b})$$

The great circles are rotated by an infinitesimal angle $\pm\Delta\alpha_i$ (rotations around the x' axis and z' axis for Steps 1 and 2, respectively) and then by $\pm\Delta\alpha_j$ (rotations around the new y' axis and x' axis for Steps 1 and 2, respectively), where the positive directions are shown in Figs. 22 and 23. The coordinates of each point on each rotated great circle (x' , y' , z') are expressed in terms of the first (x , y , z) coordinates by the following transforms, where clockwise rotations are defined as positive. To save space, c and s have been used as abbreviations for cosine and sine, respectively.

Step 1:

$$\begin{aligned} \begin{bmatrix} x \\ y \\ z \end{bmatrix} &= \begin{bmatrix} c(\Delta\alpha_y) & 0 & -s(\Delta\alpha_y) \\ 0 & 1 & 0 \\ s(\Delta\alpha_y) & 0 & c(\Delta\alpha_y) \end{bmatrix} \\ &\quad \times \begin{bmatrix} 1 & 0 & 0 \\ 0 & c(\Delta\alpha_x) & s(\Delta\alpha_x) \\ 0 & -s(\Delta\alpha_x) & c(\Delta\alpha_x) \end{bmatrix} \begin{bmatrix} x' \\ y' \\ z' \end{bmatrix} \\ &= \begin{bmatrix} c(\Delta\alpha_y) & s(\Delta\alpha_y)s(\Delta\alpha_x) & -s(\Delta\alpha_y)c(\Delta\alpha_x) \\ 0 & c(\Delta\alpha_x) & s(\Delta\alpha_x) \\ s(\Delta\alpha_y) & -c(\Delta\alpha_y)s(\Delta\alpha_x) & c(\Delta\alpha_y)c(\Delta\alpha_x) \end{bmatrix} \begin{bmatrix} x' \\ y' \\ z' \end{bmatrix}. \end{aligned} \quad (\text{A-3a})$$

Step 2:

$$\begin{aligned}
 \begin{bmatrix} x \\ y \\ z \end{bmatrix} &= \begin{bmatrix} 1 & 0 & 0 \\ 0 & c(\Delta\alpha_x) & s(\Delta\alpha_x) \\ 0 & -s(\Delta\alpha_x) & c(\Delta\alpha_x) \end{bmatrix} \begin{bmatrix} c(\Delta\alpha_z) & s(\Delta\alpha_z) & 0 \\ -s(\Delta\alpha_z) & c(\Delta\alpha_z) & 0 \\ 0 & 0 & 1 \end{bmatrix} \begin{bmatrix} x' \\ y' \\ z' \end{bmatrix} \\
 &= \begin{bmatrix} c(\Delta\alpha_z) & s(\Delta\alpha_z) & 0 \\ -c(\Delta\alpha_x)s(\Delta\alpha_z) & c(\Delta\alpha_x)c(\Delta\alpha_z) & s(\Delta\alpha_x)s(\Delta\alpha_z) \\ s(\Delta\alpha_x)s(\Delta\alpha_z) & -s(\Delta\alpha_x)c(\Delta\alpha_z) & c(\Delta\alpha_x)c(\Delta\alpha_z) \end{bmatrix} \begin{bmatrix} x' \\ y' \\ z' \end{bmatrix}. \quad (\text{A-3b})
 \end{aligned}$$

The angular sum in (A-3a) and (A-3b) is

$$\lim_{\Delta\alpha \rightarrow 0} \sum_{n=1}^{\frac{\sqrt{2}}{2}\pi} |\Delta\alpha_{i',j'}| = \frac{\sqrt{2}}{2}\pi.$$

The orbitsphere-cvf is given by n reiterations of (A-3a) and (A-3b) for each point on each of the two orthogonal great circles during each of Steps 1 and 2, where the sign of $\pm\Delta\alpha_{i'}$ and $\pm\Delta\alpha_{j'}$ for each step is given in Table IV. The output given by the nonprimed coordinates is the input of the next iteration corresponding to each successive nested rotation by the infinitesimal angle $\pm\Delta\alpha_{i'}$ or $\pm\Delta\alpha_{j'}$, where the magnitude of the angular sum of the n rotations about the i' axis and the j' axis is $(\sqrt{2}/2)\pi$. Half of the orbitsphere-cvf is generated during each of Steps 1 and 2.

Thus, in the limit as the number of nested conjugate rotations n goes to infinity and the incremental rotation angles $\pm\Delta\alpha_{i'}$ and $\pm\Delta\alpha_{j'}$ each go to zero, the orbitsphere-cvf is generated from two orthogonal great circle current loops that are rotated about the n th i' axis and then about the $(n+1)$ th j' axis until the k' axis coincides with the $-k$ axis in two separate implementations of the algorithm comprising the two steps. Each step involves a unique combination of the initial direction of the angular momentum vectors and orientation of the incremental rotation angles, as summarized in Table IV. In the case of the n th element of Step 1, the intersection of the two orthogonal great circle current loops occurs at the n th z' axis, which is along a great circle in a half plane that is parallel to the z axis and bisects the $(-x)(+y)$ quadrant of Fig. 22. The nested rotations are also equivalent to rotating the orthogonal great circle basis set about the axis $(\hat{i}_x, \hat{i}_y, 0\hat{i}_z)$ by an angle π .⁽³⁾ In the case of the n th element of Step 2, the intersection of the two orthogonal great circle current loops occurs at the n th y' axis, which is along a great circle in a half plane that

is parallel to the y axis and bisects the $(-x)(-z)$ quadrant of Fig. 23. The nested rotations are also equivalent to rotating the orthogonal great circle basis set about the axis $(-\hat{i}_x, 0\hat{i}_y, \hat{i}_z)$ by an angle $-\pi$.⁽³⁾

Following Step 2, in order to match the boundary condition that the magnitude of the velocity at any given point on the surface is given by (6), the output half of the orbitsphere-cvf is rotated clockwise by an angle of $\pi/4$ about the z axis. Using (A-3b) with $\Delta\alpha_z = \pi/4$ and $\Delta\alpha_x = 0$ gives the rotation. Then the one half of the orbitsphere-cvf generated from Step 1 is superimposed with the complementary half obtained from Step 2 following its rotation about the z axis of $\pi/4$ to give the orbitsphere-cvf.

The current pattern of the orbitsphere-cvf generated by the nested rotations of the orthogonal great circle current loops is a continuous and total coverage of the spherical surface, but it is shown as a visual representation using 6° increments of the infinitesimal angular variable $\pm\Delta\alpha_{i'}$ and $\pm\Delta\alpha_{j'}$ of (A-3a) and (A-3b) from the z axis perspective in Fig. 2. The complete orbitsphere-cvf current pattern corresponds to all the correlated points, points 1 and 2, of the orthogonal great circles shown in Figs. 22 and 23, which are rotated according to (A-3a) and (A-3b), where $\pm\Delta\alpha_{i'}$ and $\pm\Delta\alpha_{j'}$ approach zero and the summation of the infinitesimal angular rotations of $\pm\Delta\alpha_{i'}$ and $\pm\Delta\alpha_{j'}$ about the successive i' axes and j' axes is $(\sqrt{2}/2)\pi$ for each step. The pattern also represents the momentum vector field, which is not equivalent to the mass (charge) density, which for $Y_0^0(\theta, \phi)$ is uniform. Thus the patterns represent the directions of the nonuniform flow of the uniform and constant mass and charge distribution of $Y_0^0(\theta, \phi)$. The orbitsphere-cvf serves as a basis element to exactly generate $Y_0^0(\theta, \phi)$, as given in Appendix III of Ref. 3.

A.2 Spin Angular Momentum of the Orbitsphere with $\ell = 0$

As demonstrated in Figs. 2, 22, and 23, the orbitsphere-cvf is generated from two orthogonal great circle current loops that are rotated about the n th i' axis and then about the $(n+1)$ th j' axis in two steps of the series of n nested conjugate rotations. Next, consider two infinitesimal charge (mass) density elements at two separate positions or points, 1 and 2, of the two orthogonal great circle current loops that serve as the sub-basis set, as shown in each of Figs. 22 and 23. The vector projection of the corresponding angular momentum at each point of each current element is integrated over the entire orbitsphere-cvf surface to give the corresponding electron angular momentum. The correct current pattern is confirmed by

achieving the condition that the magnitude of the velocity at any point on the surface is given by (6) and by obtaining the required angular momentum projections of $\hbar/2$ and $\hbar/4$ along the z axis and along an axis in the xy plane, respectively, to satisfy the Stern-Gerlach experimental boundary condition.

The mass density $m_e/4\pi r_1^2$ of the orbitsphere of radius r_1 is uniform; however, the projections of the angular momenta of the great circle current loops of the orbitsphere onto the z axis and onto the xy plane are not. The resultant vectors can be derived by considering the contributions of the momenta corresponding to the two orthogonal great circle current loops of Figs. 22 and 23 as each basis set generates the current pattern of the orbitsphere-cvf in the two steps. The electron current, and thus the momentum, is first evenly distributed within the two orthogonally linked great circle current loops each with mass $m_e/2$. The total sum of the magnitude of the angular momentum from the contributions of all of the infinitesimal points on the orbitsphere is \hbar (7). Thus the angular momentum of each great circle at this point is $\hbar/2$. The planes of the great circles are oriented at an angle of $\pi/2$ with respect to each other, and the resultant angular momentum is $\hbar/\sqrt{2}$ in the plane transverse to the axis on which they intersect. These loops are further divided into two sets of linked orthogonal pairs that undergo the independent transformations over the surface during Steps 1 and 2, where the electron momentum and mass are correspondingly divided again by two. Thus the angular momentum of each great circle of each algorithmic step is $\hbar/4$ and the resultant angular momentum is $\hbar/(2\sqrt{2})$ in the transverse plane. In cases where the angular momentum vectors are rotated relative to the xyz coordinate system during the algorithm, the angular momenta are then divided by the angular span of the rotation to form normalized momentum densities corresponding to the normalized current densities. Half of the angular momentum is distributed over the orbitsphere-cvf in Step 1 and the other half is distributed in Step 2.

Consider the vector current directions shown in Fig. 22. During Step 1, $\Delta\alpha_x'$ and $\Delta\alpha_y'$ are both positive, and the resultant angular momentum vector of magnitude $\hbar/(2\sqrt{2})$ moves along half a great circle in the plane that is parallel to the z axis and bisects the $(+x)(-y)$ quadrant and the $(-x)(+y)$ quadrant. The trajectory of the resultant angular momentum vector from the xy plane to the z axis and back to the xy plane is shown in Fig. 24, where the angle θ of the resultant angular momentum vector from the initial xy plane position varies from $\theta = 0$ to $\theta = \pi$. Here it can be appreciated that the vector projections onto the z

axis all add positively and the vector projections into the xy plane sum to zero. With the initial direction defined as positive, the projection in the xy plane varies from a maximum of $\hbar/(2\sqrt{2})$ to zero to $\hbar/(2\sqrt{2})$. The projection onto the z axis varies from zero to a maximum of $\hbar/(2\sqrt{2})$ to zero again. In each case, the projection of the angular momentum is periodic over the angular range of θ . The total of each projection, \mathbb{L}_{xy} and \mathbb{L}_z , is the integral as a function of θ of the magnitude of the resultant vector of the two orthogonal angular momentum component vectors corresponding to the two orthogonal great circles. For Step 1, the vector projection of the angular momentum onto the xy plane is given by the sum of the vector contributions from each great circle:

$$\begin{aligned}\mathbb{L}_{xy} &= \sqrt{\frac{2}{\pi} \int_0^{\pi/2} \left[\frac{\hbar}{4} \cos \theta \right]^2 + \left[\frac{\hbar}{4} \cos \theta \right]^2 d\theta} \\ &\quad - \sqrt{\frac{2}{\pi} \int_{\pi/2}^{\pi} \left[\frac{\hbar}{4} \cos \theta \right]^2 + \left[\frac{\hbar}{4} \cos \theta \right]^2 d\theta} \quad (\text{A-4a}) \\ &= \frac{\hbar}{2\sqrt{2}} \frac{1}{\sqrt{2}} - \frac{\hbar}{2\sqrt{2}} \frac{1}{\sqrt{2}} = 0,\end{aligned}$$

where each angular integral is normalized by $\pi/2$, the angular range of θ . Similarly, the vector projection of the angular momentum onto the z axis as shown in Fig. 24 is

$$\begin{aligned}\mathbb{L}_z &= \sqrt{\frac{1}{\pi} \int_0^{\pi} \left[\frac{\hbar}{4} \sin \theta \right]^2 + \left[\frac{\hbar}{4} \sin \theta \right]^2 d\theta} \quad (\text{A-4b}) \\ &= \frac{\hbar}{2\sqrt{2}} \frac{1}{\sqrt{2}} = \frac{\hbar}{4},\end{aligned}$$

where each angular integral is normalized by π , the angular range of θ . Thus, from the initial $\hbar/4$ of angular momentum along each of the x and y axes, $\hbar/4$ canceled in the xy plane and $\hbar/4$ was projected onto the z axis as the angular momentum was spread over one half of the surface of the sphere with Step 1.

Consider the vector current directions shown in Fig. 23. During Step 2, $\Delta\alpha_z$ is negative, $\Delta\alpha_x$ is positive, and the nested rotations cause the orthogonal great-circle basis set to rotate about the vector $(-\hbar i_x/4, 0 i_y, \hbar i_z/4)$. Thus the resultant angular momentum vector of magnitude $\hbar/(2\sqrt{2})$ is stationary throughout the nested rotations that transform the axes, as given in

Table IV. Then the $\pi/4$ rotation about the z axis following Step 2 only rotates L_x by the same angle in the xy plane such that the component is oriented along the bisector of the $(-x)(+y)$ quadrant, as shown in Fig. 23. Thus the resultant angular momentum component of Step 2 that is transverse to the z axis, L_{xy} , is in the direction of $(-i_x, i_y, 0i_z)$, which is also the direction of the trajectory of the angular momentum component vectors of Step 1, as shown in Fig. 24. The resultant angular momentum projections are as given in Fig. 23:

$$L_{xy} = \frac{\hbar}{4}, \quad (A-5a)$$

$$L_z = \frac{\hbar}{4}. \quad (A-5b)$$

The total vector projection of the angular momentum onto the xy plane given by the sum of (A-4a) and (A-5a) is

$$L_{xy} = 0 + \frac{\hbar}{4} = \frac{\hbar}{4}. \quad (A-6a)$$

The total vector projection of the angular momentum into the z axis given by the sum of (A-4b) and (A-5b) is

$$L_z = \frac{\hbar}{4} + \frac{\hbar}{4} = \frac{\hbar}{2}. \quad (A-6b)$$

The trajectories of the angular momenta and the resultant projections, L_{xy} and L_z , given in Table IV have been confirmed by computer simulations.⁽⁶¹⁾ These results meet the boundary condition for the unique current with an angular velocity magnitude at each point on the surface given by (6) and give rise to the Stern-Gerlach experiment, as shown below in Sections A.3 and A.5. The further constraint that the current density is uniform such that the charge density is uniform, corresponding to an equipotential, minimum-energy surface, is satisfied by using the orbitsphere-cvf as a basis element to generate $Y_0^0(\theta, \phi)$.

A convolution operator comprising an autocorrelation-type function gives rise to the spherically symmetric current density $Y_0^0(\theta, \phi)$. The operator comprises the convolution of each great circle current loop of the orbitsphere-cvf designated as the primary orbitsphere-cvf with a second orbitsphere-cvf designa-

ted as the secondary orbitsphere-cvf. The orbitsphere-cvf comprises two components corresponding to Steps 1 and 2, respectively. As shown in Appendix III of Ref. 3, Step 2 can also be generated by a 2π rotation of a single basis element current loop about the $(-i_x/\sqrt{2}, i_y/\sqrt{2}, i_z)$ axis or a π rotation of two orthogonal current loops such that the angular momentum vector is stationary on the $(-i_x/\sqrt{2}, i_y/\sqrt{2}, i_z)$ axis as the component orbitsphere-cvf is generated. In the general case that the resultant angular momentum of each pair of orthogonal great circle current loops of the component orbitsphere-cvf is along the π rotational axis (defined as the rotational axis that generates the component orbitsphere-cvf from a basis element great circle), a secondary n th-component orbitsphere-cvf can serve as a basis element to match the angular momentum of any given n th great circle of a primary component orbitsphere-cvf. The replacement of each great circle of the primary orbitsphere-cvf with a secondary orbitsphere-cvf of matching angular momentum, orientation, and phase comprises an autocorrelation-type function that exactly gives rise to the spherically symmetric current density $Y_0^0(\theta, \phi)$.

The orbitsphere-cvf comprises the superposition or sum of the components corresponding to Steps 1 and 2. Thus the convolution is performed on each component designated a primary component. The convolution of a secondary component orbitsphere-cvf element with each great circle current loop of each primary orbitsphere-cvf is designated as the convolution operator, $A(\theta, \phi)$, given by

$$\begin{aligned} A(\theta, \phi) &= \frac{1}{2r_n^2} \lim_{\Delta\theta_2 \rightarrow 0} \sum_{m'=1}^{m'=\frac{2\pi}{|\Delta\theta_2|}} \lim_{\Delta\phi \rightarrow 0} \sum_{m=1}^{m=\frac{2\pi}{|\Delta\phi|}} 2^\circ O(\theta, \phi) \\ &\otimes (1^\circ_1 O(\theta, \phi) \delta(\theta - m\Delta\theta_1, \phi - \phi') \\ &+ 1^\circ_2 O(\theta, \phi) \delta(\theta - m'\Delta\theta_2, \phi - \phi'')) \quad (A-6c) \\ &= \frac{1}{2r_n^2} \lim_{\Delta\theta_2 \rightarrow 0} \sum_{m'=1}^{m'=\frac{2\pi}{|\Delta\theta_2|}} \lim_{\Delta\phi \rightarrow 0} \sum_{m=1}^{m=\frac{2\pi}{|\Delta\phi|}} 2^\circ O(\theta, \phi) \\ &\otimes (GC_{\text{Step 1}}(m\Delta\theta_1, \phi') + GC_{\text{Step 2}}(m'\Delta\theta_2, \phi'')), \end{aligned}$$

where (1) the secondary component orbitsphere-cvf that is matched to the basis element of the primary is defined by the symbol $2^\circ O(\theta, \phi)$; (2) the primary component orbitsphere-cvf of Step M is defined by the symbol $1^\circ_M O(\theta, \phi)$; (3) each rotated great circle of the primary component orbitsphere-cvf of Step M is selected by the Dirac delta function $\delta(\theta - m\Delta\theta_M, \phi - \phi')$; the product $1^\circ_M O(\theta, \phi) \delta(\theta - m\Delta\theta_M, \phi - \phi')$ is

zero except for the great circle at the angle $\theta = m\Delta\theta_M$ about the 2π rotational axis; each selected great circle having $0 \leq \phi \leq 2\pi$ is defined by $GC_{\text{Step } M}(m\Delta\theta_M, \phi)$; and (4) $1/2r_n^2$ is the normalization constant. In (A-6c), the angular momentum of each secondary component orbitsphere-cvf is equal in magnitude and direction to that of the current loop with which it is convolved. With the magnitude of the angular momentum of the secondary component orbitsphere-cvf matching that of the current loop that it replaces during the convolution and the loop then serving as a unit vector, the angular momentum resulting from the convolution operation is inherently normalized to that of the primary component orbitsphere-cvf.

The convolution of a sum is the sum of the convolutions. Thus the convolution operation may be performed on each of Steps 1 and 2 separately, and the result may be superposed in terms of the current densities and angular momenta. Factoring out the secondary component orbitsphere-cvf, which is a constant at each position of $GC_{\text{Step } M}(m\Delta\theta_M, \phi)$, gives

$$A(\theta, \phi) = \frac{1}{2r_n^2} 2^\circ O(\theta, \phi) \left(\lim_{\Delta\theta_2 \rightarrow 0} \sum_{m'=1}^{m'=\frac{2\pi}{|\Delta\theta_2|}} GC_{\text{Step } 1}(m'\Delta\theta_1, \phi') \right. \\ \left. + \lim_{\Delta\theta_1 \rightarrow 0} \sum_{m=1}^{m=\frac{2\pi}{|\Delta\theta_1|}} GC_{\text{Step } 2}(m'\Delta\theta_2, \phi'') \right). \quad (\text{A-6d})$$

The summation is the operator that generates the primary component orbitsphere-cvf of Step M , $1^\circ_M O(\theta, \phi)$. Thus the current density function is given by the dot product of each primary orbitsphere-cvf with itself. The result is the scalar sum of the square of the Step 1 and 2 primary component orbitsphere-cvfs:

$$A(\theta, \phi) = \frac{1}{2r_n^2} ((1^\circ_1 O(\theta, \phi))^2 + (1^\circ_2 O(\theta, \phi))^2), \quad (\text{A-6e})$$

where the dot-product scalar is valid over the entire spherical surface. The orbitsphere-cvf squared given in (A-6e) is the equation of a uniform sphere. The superposition of the uniform distributions from Steps 1 and 2 is the exact uniform current density function $Y_0^0(\theta, \phi)$ that is an equipotential, minimum energy surface, as shown in Fig. 1. The angular momentum is identically that of the superposition of the component orbitsphere-cvfs of the primary orbitsphere-cvf, $\mathbb{L}_{xy} = \hbar/4$ and $\mathbb{L}_z = \hbar/2$, given by (A-6a) and (A-6b).

The Stern–Gerlach experiment described below demonstrates that the magnetic moment of the electron can only be parallel or antiparallel to an applied magnetic field. In spherical coordinates this implies a spin quantum number of $1/2$ corresponding to an angular momentum on the z axis of $\hbar/2$. However, the Zeeman splitting energy corresponds to a magnetic moment of μ_B and implies an electron angular momentum on the z axis of \hbar — twice that given by (A-1) to (A-6). Consider the case of a magnetic field applied to the orbitsphere. The magnetic moment corresponding to the angular momentum along the z axis results in the alignment of the z axis of the orbitsphere with the magnetic field, while the $\hbar/4$ resultant vector in the xy plane causes precession about the applied field. The precession frequency is the Larmor frequency given by the product of the gyromagnetic ratio of the electron, $e/2m$, and the magnetic flux B .⁽⁶²⁾ The precessing electron can interact with a resonant photon that gives rise to Zeeman splitting — energy levels corresponding to parallel or antiparallel alignment of the electron magnetic moment with the magnetic field. The energy of the transition between these states is that of the resonant photon. The angular momentum of the precessing orbitsphere comprises the initial $\hbar/2$ projection on the z axis and the initial $\hbar/4$ vector component in the xy plane that then precesses about the z axis. As shown in the Excited States of the One-Electron Atom (Quantization) section of Ref. 3, conservation of the angular momentum of the photon of \hbar gives rise to the \hbar of electron angular momentum. The parameters of the photon standing wave for the Zeeman effect are given in Sections A.3 and A.4.

The angular momentum of the orbitsphere in a magnetic field comprises the static $\hbar/2$ projection on the z axis (A-6b) and the $\hbar/4$ vector component in the xy plane (A-6a) that precesses about the z axis at the Larmor frequency. A resonant excitation of the Larmor precession frequency gives rise to a trapped photon with the \hbar of angular momentum along a precessing S axis. In the coordinate system rotating at the Larmor frequency (denoted by the axes labeled X_R , Y_R , and Z_R in Fig. 25), the X_R component of magnitude $\hbar/4$ and the S of magnitude \hbar are stationary. The $\hbar/4$ angular momentum along X_R with a corresponding magnetic moment of $\mu_B/4$ (A-55) causes S to rotate in the $Y_R Z_R$ plane to an angle of $\theta = \pi/3$ such that the torques due to the Z_R component of $\hbar/2$ and the orthogonal X_R component of $\hbar/4$ are balanced. Then the Z_R component due to S is $\pm\hbar \cos(\pi/3) = \pm\hbar/2$. The reduction of the magnitude of S along Z_R from \hbar to $\hbar/2$ corresponds to the ratio of the X_R component and the static Z_R component of $(\hbar/4)/(\hbar/2) = 1/2$.⁴ Since

the X_R component is $\hbar/4$, the Z_R component of S is $\hbar/2$, which adds to the initial $\hbar/2$ component to give a total Z_R component of \hbar .

In summary, since the vector S precesses about the z axis at an angle of $\theta = \pi/3$ and an angle of $\phi = \pi/2$ with respect to L_{xy} given by (A-6a) and has a magnitude of \hbar , the S projections in the $X_R Y_R$ plane and along the Z_R axis are

$$S_{\perp} = \hbar \sin \frac{\pi}{3} = \pm \sqrt{\frac{3}{4}} \hbar i_{Y_R}, \quad (\text{A-7a})$$

$$S_{\parallel} = \pm \hbar \cos \frac{\pi}{3} = \pm \frac{\hbar}{2} i_{Z_R}. \quad (\text{A-7b})$$

The plus or minus sign of (A-7a) and (A-7b) corresponds to the two possible vector orientations observed with the Stern–Gerlach experiment described below. The sum of the torques in the external magnetic field is balanced unless an RF field is applied to cause a Stern–Gerlach transition, as discussed in Section A.4.

As shown in Fig. 26, S forms a cone in time in the nonrotating laboratory frame with an angular momentum of \hbar that is the source of the known magnetic moment of a Bohr magneton (A-55), as shown in Section A.3. The projection of this angular momentum of $\hbar/2$ onto the z axis adds to the z axis component before the magnetic field was applied to give a total of \hbar . Thus, in the absence of a resonant precession, the z component of the angular momentum is $\hbar/2$, but the excitation of the precessing S component gives \hbar — twice the angular momentum on the z axis. In addition, rather than a continuum of orientations with corresponding energies, the orientation of the magnetic moment must be only parallel or antiparallel to the magnetic field. This arises from conservation of angular momentum between the “static” and “dynamic” z axis projections of the angular momentum with the additional constraint that the angular momentum has a “kinetic” as well as a “potential” or vector potential component. To conserve angular momentum, flux linkage by the electron is quantized in units of the magnetic flux quantum $\Phi_0 = h/2e$, as shown in Sections A.4 and A.5. Thus the spin quantum number is $s = 1/2$, $m_s = \pm 1/2$, but the observed Zeeman splitting corresponds to a full Bohr magneton due to the \hbar of angular momentum. This aspect was historically felt to be inexplicable in terms of classical physics and was merely postulated in the past.

The demonstration that the boundary conditions of the electron in a magnetic field are met appears in Section A.4. The observed electron parameters are explained physically. Classical laws give (1) a gyro-magnetic ratio of $e/2m$, (2) a Larmor precession frequency of $eB/2m$, (3) the Stern–Gerlach experimental result of quantization of the angular momentum that implies a spin quantum number of $1/2$ corresponding to an angular momentum of $\hbar/2$ on the z axis, and (4) the observed Zeeman splitting due to a magnetic moment of a Bohr magneton $\mu_B = e\hbar/2m_e$ corresponding to an angular momentum of \hbar on the z axis. Furthermore, the solution is relativistically invariant, as shown in the Special Relativistic Correction to the Ionization Energies section of Ref. 3. Dirac originally attempted to solve the bound electron physically with stability with respect to radiation according to Maxwell’s equations with the further constraints that it was relativistically invariant and gave rise to electron spin.⁽¹⁹⁾ He was unsuccessful and resorted to the current mathematical probability wave model, which has many problems, as discussed previously (Refs. 5 and 63 and Chapter 1, Appendix II, of Ref. 3).

A.3 Magnetic Parameters of the Electron (Bohr Magnetron)

A.3.1 The Magnetic Field of an Orbitsphere from Spin

The orbitsphere with $\ell = 0$ is a shell of negative charge current comprising correlated charge motion along great circles. The superposition of the vector projection of the orbitsphere angular momentum on the z axis is $\hbar/2$, with an orthogonal component of $\hbar/4$. As shown in Section A.1, the application of a magnetic field to the orbitsphere gives rise to a precessing angular momentum vector S directed from the origin of the orbitsphere at an angle of $\theta = \pi/3$ relative to the applied magnetic field. The precession of S with an angular momentum of \hbar forms a cone in the nonrotating laboratory frame to give a perpendicular projection of $S_{\perp} = \pm \sqrt{3/4} \hbar$ (A-7a) and a projection onto the axis of the applied magnetic field of $S_{\parallel} = \pm \hbar/2$ (A-7b). The superposition of the $\hbar/2$, z axis component of the orbitsphere angular momentum and the $\hbar/2$, z axis component of S gives \hbar corresponding to the observed magnetostatic electron magnetic moment of a Bohr magneton. The \hbar of angular momentum along S has a corresponding precessing magnetic moment of one Bohr magneton.⁽⁶⁴⁾

$$\mu_B = \frac{e\hbar}{2m_e} = 9.274 \times 10^{-24} \text{ J} \cdot \text{T}^{-1}. \quad (\text{A-8})$$

The rotating magnetic field of S is discussed in Section A.4. The magnetostatic magnetic field corresponding to μ_B derived below is given by

$$\mathbf{H} = \begin{cases} \frac{e\hbar}{m_e r_n^3} (\mathbf{i}_r \cos \theta - \mathbf{i}_\theta \sin \theta) & \text{for } r < r_n, \\ \frac{e\hbar}{2m_e r^3} (\mathbf{i}_r 2 \cos \theta + \mathbf{i}_\theta \sin \theta) & \text{for } r > r_n. \end{cases} \quad (\text{A-9})$$

It follows from (A-8), the relationship for the Bohr magneton, and the relationship between the magnetic dipole field and the magnetic moment \mathbf{m} ,⁽⁶⁵⁾ that (A-9) is the equation for the magnetic field due to a magnetic moment of one Bohr magneton, $\mathbf{m} = \mu_B \mathbf{i}_z$, where $\mathbf{i}_z = \mathbf{i}_r \cos \theta - \mathbf{i}_\theta \sin \theta$. Note that the magnetic field is a constant for $r < r_n$ (see Fig. 6). It is shown in Section 7 that the energy stored in the magnetic field of the electron orbitsphere is

$$E_{\text{mag, total}} = \frac{\pi \mu_0 e^2 \hbar^2}{m_e^2 r_n^3}. \quad (\text{A-10})$$

A.3.2 Derivation of the Magnetic Field

For convenience the angular momentum vector with a magnitude in the stationary frame of \hbar will be defined as the z axis, as shown in Fig. 6.⁵ The magnetic field must satisfy the following relationships:

$$\nabla \cdot \mathbf{H} = 0 \text{ in free space,} \quad (\text{A-11})$$

$$\mathbf{n} \times (\mathbf{H}_a - \mathbf{H}_b) = \mathbf{K}, \quad (\text{A-12})$$

$$\mathbf{n} \cdot (\mathbf{H}_a - \mathbf{H}_b) = 0, \quad (\text{A-13})$$

$$\mathbf{H} = -\nabla \psi. \quad (\text{A-14})$$

Since the field is magnetostatic, the current is equivalent to current loops along the z axis. Then the z component of the current $|\mathbf{i}|$ for a current loop of total charge e , oriented at an angle θ with respect to the z axis, is given by the product of the charge, the angular velocity given by (9), and $\sin \theta$, where the projection of the current of the orbitsphere perpendicular to the z axis that carries the incremental current i_ϕ is a function of $\sin \theta$:

$$|\mathbf{i}| = \frac{e\hbar}{m_e r_n^2} \sin \theta. \quad (\text{A-15})$$

The angular function of the current density of the orbitsphere is normalized by the geometrical factor N ⁽⁶⁶⁾ given by

$$N = \frac{4\pi r_n^3}{2\pi \int_{-r_n}^{r_n} (r_n^2 - z^2) dz} = \frac{3}{2}, \quad (\text{A-16})$$

corresponding to the angular momentum of \hbar . (Equation (A-16) can also be expressed in spherical coordinates for the density of a uniform shell divided by the integral in θ and ϕ of that of a spherical dipole squared.⁽⁶⁷⁾ The integration gives $8\pi/3$, which, normalized by the uniform mass density factor of 4π , gives the geometrical factor of $(2/3)^{-1}$.) The current density $K i_\phi$ along the z axis with vector orientation perpendicular to the angular momentum vector is given by dividing the magnitude of i_ϕ (A-15) by the length r_n . The current density of the orbitsphere in the incremental length dz is

$$\mathbf{K}(\rho, \phi, z) = \mathbf{i}_\phi N \frac{e\hbar}{m_e r_n^3} = \mathbf{i}_\phi \frac{3}{2} \frac{e\hbar}{m_e r_n^3}. \quad (\text{A-17})$$

Because

$$z = r \cos \theta, \quad (\text{A-18})$$

the differential length is given by

$$dz = -\sin \theta r_n d\theta, \quad (\text{A-19})$$

and so the current density in the differential length $r_n d\theta$ as measured along the periphery of the orbitsphere is a function of $\sin \theta$, as given in (A-15). From (A-17), the surface current density function of the orbitsphere about the z axis (S axis) is given by

$$\mathbf{K}(r, \theta, \phi) = \mathbf{i}_\phi \frac{3}{2} \frac{e\hbar}{m_e r_n^3} \sin \theta. \quad (\text{A-20})$$

Substitution of (A-20) into (A-12) gives

$$H_\theta^a - H_\theta^b = \mathbf{i}_\phi \frac{3}{2} \frac{e\hbar}{m_e r_n^3} \sin \theta. \quad (\text{A-21})$$

To obtain H_θ , the derivative of Ψ with respect to θ must be taken, and this suggests that the θ dependence of Ψ be taken as $\cos \theta$. The field is finite at the origin and zero at infinity, so solutions of Laplace's equation in spherical coordinates are selected because they are consistent with these conditions:⁽⁶⁸⁾

$$\Psi = \begin{cases} C \left(\frac{r}{r_n} \right) \cos \theta, & r < r_n, \\ A \left(\frac{r_n}{r} \right)^2 \cos \theta, & r > r_n. \end{cases} \quad (\text{A-22})$$

The negative gradients of these potentials are

$$\mathbf{H} = \begin{cases} \frac{-C}{r_n} (\mathbf{i}_r \cos \theta - \mathbf{i}_\theta \sin \theta) & \text{for } r < r_n, \\ \frac{A}{r_n} \left(\frac{r_n}{r} \right)^3 (\mathbf{i}_r 2 \cos \theta + \mathbf{i}_\theta \sin \theta) & \text{for } r > r_n. \end{cases} \quad (\text{A-23})$$

The continuity conditions of (A-12), (A-13), (A-20), and (A-21) are applied to obtain the following relationships among the variables:

$$\frac{-C}{r_n} = \frac{2A}{r_n}, \quad (\text{A-24})$$

$$\frac{A}{r_n} - \frac{C}{r_n} = \frac{3}{2} \frac{e\hbar}{m_e r_n^3}. \quad (\text{A-25})$$

Solving the variables algebraically gives the magnetic fields of an electron:

$$\mathbf{H} = \begin{cases} \frac{e\hbar}{m_e r_n^3} (\mathbf{i}_r \cos \theta - \mathbf{i}_\theta \sin \theta) & \text{for } r < r_n, \\ \frac{e\hbar}{2m_e r^3} (\mathbf{i}_r 2 \cos \theta + \mathbf{i}_\theta \sin \theta) & \text{for } r > r_n. \end{cases} \quad (\text{A-26})$$

The field is that of a Bohr magneton, which matches the observed boundary conditions given in Section A.1, including the required spherical symmetry. The demonstration that the boundary conditions of the

electron in a magnetic field are met appears in Section A.4.

A.3.3 Derivation of the Energy

The energy stored in the magnetic field of the electron is

$$E_{\text{mag}} = \frac{1}{2} \mu_0 \int_0^{2\pi} \int_0^\pi \int_0^\infty H^2 r^2 \sin \theta dr d\theta d\Phi, \quad (\text{A-27})$$

$$E_{\text{mag, total}} = E_{\text{mag, external}} + E_{\text{mag, internal}}, \quad (\text{A-28})$$

$$\begin{aligned} E_{\text{mag, internal}} &= \frac{1}{2} \mu_0 \\ &\times \int_0^{2\pi} \int_0^\pi \int_0^{r_1} \left[\left(\frac{e\hbar}{m_e r_1^3} \right)^2 [c^2(\theta) + s^2(\theta)] \right] r^2 s(\theta) dr d\theta d\Phi \quad (\text{A-29}) \\ &= \frac{2\pi \mu_0 e^2 \hbar^2}{3m_e^2 r_1^3}, \end{aligned}$$

$$\begin{aligned} E_{\text{mag, external}} &= \frac{1}{2} \mu_0 \\ &\times \int_0^{2\pi} \int_0^\pi \int_{r_1}^\infty \left[\left(\frac{e\hbar}{2m_e r^3} \right)^2 [4c^2(\theta) + s^2(\theta)] \right] r^2 s(\theta) dr d\theta d\Phi \\ &= \frac{\pi \mu_0 e^2 \hbar^2}{3m_e^2 r_1^3}, \end{aligned} \quad (\text{A-30})$$

$$\begin{aligned} E_{\text{mag, total}} &= \frac{2\pi \mu_0 e^2 \hbar^2}{3m_e^2 r_1^3} + \frac{\pi \mu_0 e^2 \hbar^2}{3m_e^2 r_1^3} \\ &= \frac{\pi \mu_0 e^2 \hbar^2}{m_e^2 r_1^3} = \frac{4\pi \mu_0 \mu_B^2}{r_1^3}, \end{aligned} \quad (\text{A-31})$$

where the abbreviations c for cosine and s for sine have been used where necessary to save space.

A.4 Boundary Conditions of the Electron in a Magnetic Field Are Met

As shown in Section A.5, when a magnetic field with flux \mathbf{B} is applied to an electron in a central field comprising current loops, the orbital radius of each

does not change due to the Lorentzian force provided by \mathbb{B} , but the velocity changes as follows:⁽⁶⁹⁾

$$\Delta v = \frac{e r B}{2 m_e}, \quad (\text{A-32}) \quad \text{and}$$

corresponding to a precession frequency of

$$\omega = \frac{\Delta v}{r} = \frac{e B}{2 m_e} = \gamma_e B, \quad (\text{A-33})$$

where γ_e is the electron gyromagnetic ratio and ω is the Larmor frequency. Equation (A-32) applies to the current perpendicular to the magnetic flux. In this case the moment of inertia I of the orbitsphere that is independent of and superimposes the spin moment of inertia is

$$I = \frac{2}{3} m_e r_1^2, \quad (\text{A-34})$$

since the charge (mass) is uniformly distributed on a spherical surface.⁽⁶⁶⁾ From (A-33) and (A-34) the angular momentum L and rotational energy E_{rot} are

$$L = I \omega = \frac{2}{3} m_e r_1^2 \gamma_e B \quad (\text{A-35})$$

and

$$E_{rot} = \frac{1}{2} I \omega^2 = \frac{1}{3} m_e r_1^2 (\gamma_e B)^2, \quad (\text{A-36})$$

respectively. The change in the magnetic moment corresponding to (A-32) is⁽⁶⁹⁾

$$\Delta m = -\frac{e^2 r_1^2}{4 m_e} \mathbb{B}. \quad (\text{A-37})$$

Using (A-33) to (A-37), in the case of a very strong magnetic flux of 10 T applied to atomic hydrogen,

$$\omega = 8.794 \times 10^{11} \text{ rad} \cdot \text{s}^{-1}, \quad (\text{A-38})$$

$$I = 1.701 \times 10^{-51} \text{ kg} \cdot \text{m}^2, \quad (\text{A-39})$$

$$L = 1.496 \times 10^{-39} \text{ J} \cdot \text{s}, \quad (\text{A-40})$$

$$E_{rot} = 6.576 \times 10^{-38} \text{ J} = 4.104 \times 10^{-9} \text{ eV}, \quad (\text{A-41})$$

$$\Delta m = 1.315 \times 10^{-28} \text{ J} \cdot \text{T}^{-1}, \quad (\text{A-42})$$

where the radius is given by (70), and $2/3$, the geometrical factor of a uniformly charged sphere,⁽⁶⁶⁾ was used in the case of (A-42). Thus these effects of the magnetic field are very small when they are compared to the intrinsic angular momentum of the electron of

$$L = \hbar = 1.055 \times 10^{-34} \text{ J} \cdot \text{s}. \quad (\text{A-43})$$

The electronic angular frequency of hydrogen given by (9) and (70) is

$$\omega_1 = \frac{\hbar}{m_3 r_1^2} = 4.134 \times 10^{16} \text{ rad} \cdot \text{s}^{-1}. \quad (\text{A-44})$$

The total kinetic energy given by (72) is

$$T = 13.606 \text{ eV}. \quad (\text{A-45})$$

The magnetic moment of a Bohr magneton given by (A-8) is

$$\mu_B = \frac{e \hbar}{2 m_e} = 9.274 \times 10^{-24} \text{ J} \cdot \text{T}^{-1}. \quad (\text{A-46})$$

E_{rot} is the energy that arises due to the application of the external flux \mathbb{B} . Thus the external work required to apply the field is also given by (A-41). Since the orbitsphere is uniformly charged and is superconducting, this energy is conserved when the field is removed. It is also independent of the direction of the magnetic moment due to the intrinsic angular momentum \hbar of the orbitsphere. The corresponding magnetic moment given by (A-37) does not change when the intrinsic magnetic moment of the electron changes orientation. Thus it does not contribute to the energy of a spin-flip transition observed by the Stern-Gerlach experiment. It always opposes the applied field and gives rise to the phenomenon of the diamagnetic susceptibility of materials, which (A-37) predicts with very good agreement with observations.⁽⁶⁹⁾ Equation (A-37) also predicts the absolute chemical shifts of hydride ions that match experimental obser-

vations, as shown in the Hydrino Hydride Ion Nuclear Magnetic Resonance Shift section of Ref. 3.

As shown in Section A.2, the angular momentum of the orbitsphere in a magnetic field comprises the initial $\hbar/2$ projection on the z axis and the initial $\hbar/4$ vector component in the xy plane that precesses about the z axis. A resonant excitation of the Larmor precession frequency gives rise to an additional component of angular momentum, which is consistent with Maxwell's equations. As shown in the Excited States of the One-Electron Atom (Quantization) section of Ref. 3, conservation of the \hbar of angular momentum of a trapped photon can give rise to the \hbar of electron angular momentum along the S axis. The photon standing waves of excited states are spherical harmonic functions that satisfy Laplace's equation in spherical coordinates and provide the force balance for the corresponding charge (mass) density waves. Consider the photon in the case of the precessing electron with a Bohr magneton of magnetic moment along the S axis. The radius of the orbitsphere is unchanged, and the photon gives rise to current on the surface that satisfies the condition

$$\nabla \cdot J = 0, \quad (A-47)$$

corresponding to a rotating spherical harmonic dipole⁽⁷⁰⁾ that phase-matches the current (mass) density of (A-20). Thus the electrostatic energy is constant, and only the magnetic energy need be considered, as given by (A-50) to (A-52). The corresponding central field at the orbitsphere surface given by the superposition of the central field of the proton and that of the photon follows from (2.10) to (2.17) of Ref 3:

$$E = \frac{e}{4\pi\epsilon_0 r^2} [Y_0^0(\theta, \phi) \mathbf{i}_r + \text{Re}\{Y_l^m(\theta, \phi) e^{i\omega t}\} \mathbf{i}_l \delta(r - r_l)], \quad (A-48)$$

where the spherical harmonic dipole $Y_l^m(\theta, \phi) = \sin \theta$ is with respect to the S axis. The dipole spins about the S axis at the angular velocity given by (9). The resulting current is nonradiative, as shown in Section 6 and in Chapter 1, Appendix I, of Ref. 3. Thus the field in the RF rotating frame is magnetostatic, as shown in Fig. 6, but directed along the S axis. However, the precessing dipole results in magnetic dipole radiation or absorption during a Stern-Gerlach transition. The application of a magnetic field causes alignment of the intrinsic electron magnetic moment

of atoms of a material such that the population of parallel versus antiparallel electrons is a Boltzmann distribution that depends on the temperature of the material. Following the removal of the field, the original random orientation distribution is restored, as is the original temperature. The distribution may be altered by the application of an RF pulse at the Larmor frequency.

The application of a magnetic field with a resonant Larmor excitation gives rise to a precessing angular momentum vector S of magnitude \hbar directed from the origin of the orbitsphere at an angle of $\theta = \pi/3$ relative to the applied magnetic field. S rotates about the axis of the applied field at the Larmor frequency. The magnitude of the components of S that are parallel and orthogonal to the applied field (A-7b) and (A-7a) are $\hbar/2$ and $\sqrt{3}/4 \hbar$, respectively. Since both the RF field and the orthogonal components shown in Fig. 25 rotate at the Larmor frequency, the RF field that causes a Stern-Gerlach transition produces a stationary magnetic field with respect to these components, as described by Patz.⁽⁷¹⁾

The component of (A-7b) adds to the initial $\hbar/2$ parallel component to give a total of \hbar in the stationary frame corresponding to a Bohr magneton, μ_B , of magnetic moment. Equations (A-33) and (A-37) also hold in the case of the Stern-Gerlach experiment. Superposition holds for Maxwell's equations, and only the angular momentum given by (A-1) to (A-6) and the source current corresponding to (A-48) need be considered. Since it does not change, the diamagnetic component given by (A-32) does not contribute to the spin-flip transition, as discussed below. The potential energy of a magnetic moment \mathbf{m} in the presence of flux \mathbf{B} ⁽⁶⁴⁾ is

$$E = \mathbf{m} \cdot \mathbf{B}. \quad (A-49)$$

The angular momentum of the electron gives rise to a magnetic moment of μ_B . Thus the energy ΔE_{mag}^{spin} to switch from parallel to antiparallel to the field is given by (A-66):

$$\Delta E_{mag}^{spin} = 2\mu_B \mathbf{i}_z \cdot \mathbf{B} = 2\mu_B B \cos \theta = 2\mu_B B. \quad (A-50)$$

In the case of an applied flux of 10 T, (A-50) gives

$$\Delta E_{mag}^{spin} = 1.855 \times 10^{-22} \text{ J} = 1.158 \times 10^{-3} \text{ eV}. \quad (A-51)$$

ΔE_{mag}^{spin} is also given by Planck's equation. It can be shown from conservation of angular momentum con-

siderations ((A-53) to (A-59)) that the Zeeman splitting is given by Planck's equation and the Larmor frequency based on the gyromagnetic ratio (A-33). The electron's magnetic moment may only be parallel or antiparallel to the magnetic field rather than at a continuum of angles, including perpendicular, according to (A-49). No continuum of energies predicted by (A-49) for a pure magnetic dipole are possible. The energy difference for the magnetic moment to flip from parallel to antiparallel to the applied field is

$$\Delta E_{mag}^{spin} = 2\hbar\omega \quad (A-52)$$

$$= 1.855 \times 10^{-22} \text{ J} = 1.158 \times 10^{-3} \text{ eV},$$

corresponding to magnetic dipole radiation.

As demonstrated in Section A.1, $\hbar/2$ of the orbitsphere angular momentum designated the static component is initially parallel to the field. An additional $\hbar/2$ parallel component designated the dynamic component comes from the \hbar of angular momentum along S. The angular momentum in the presence of an applied magnetic field is⁽⁷²⁾

$$\mathbb{L} = \mathbf{r} \times (m_e \mathbf{v} + e\mathbf{A}), \quad (A-53)$$

where A is the vector potential evaluated at the location of the orbitsphere. The circular integral of A is the flux linked by the electron. During a Stern-Gerlach transition, a resonant RF photon is absorbed or emitted, and the \hbar component along S reverses direction. It is shown by (A-56) to (A-59) that the dynamic parallel component of angular momentum corresponding to the vector potential due to the light-like transition is equal to the "kinetic angular momentum" ($\mathbf{r} \times m\mathbf{v}$) of $\hbar/2$. Conservation of angular momentum of the orbitsphere requires that the static angular momentum component concomitantly flip. The static component of angular momentum undergoes a spin-flip, and concomitantly the "potential angular momentum" ($\mathbf{r} \times e\mathbf{A}$) of the dynamic component must change by $-\hbar/2$ due to the linkage of flux by the electron such that the total angular momentum is conserved.

In spherical coordinates the relationship between the vector potential A and the flux B is

$$2\pi r A = \pi r^2 B. \quad (A-54)$$

Equation (A-54) can be substituted into (A-53) since the magnetic moment m is given⁽⁶⁴⁾ as

$$m = \frac{\text{charge} \cdot \text{angular momentum}}{2 \cdot \text{mass}} \quad (A-55)$$

and the corresponding energy is consistent with (A-50) and (A-52) in this case as follows:

$$\Delta m = -\frac{e(\mathbf{r} \times e\mathbf{A})}{2m_e} = \frac{e\hbar/2}{2m_e} = \frac{\mu_B}{2}. \quad (A-56)$$

The boundary condition that the angular momentum is conserved is shown by (A-65) to (A-67). It can be shown that (A-56) is also consistent with the vector potential along the axis of the applied field⁽⁷²⁾ given by

$$\begin{aligned} A &= \cos \frac{\pi}{3} \mu_0 \frac{e\hbar}{2m_e r^2} \sin \theta \mathbf{i}_\phi \\ &= \mu_0 \frac{1}{2} \frac{e\hbar}{2m_e r^2} \sin \theta \mathbf{i}_\phi. \end{aligned} \quad (A-57)$$

Substitution of (A-57) into (A-56) gives

$$\begin{aligned} \Delta m &= -\frac{e \left(\mathbf{r} \times e \mu_0 \frac{1}{2} \frac{e\hbar}{2m_e r^2} \sin \theta \mathbf{i}_\phi \right)}{2m_e} \\ &= -\frac{1}{2} \left(\frac{\mu_0 e^2}{2m_e r} \right) \frac{e\hbar}{2m_e}, \end{aligned} \quad (A-58)$$

with the geometrical factor of $2/3$ ⁽⁶⁶⁾ and the current given by (A-20). Since k is the light-like k^0 , then $k = \omega_n/c$, corresponding to the RF photon field. The relativistic corrections of (A-58) are given by (1.218) and (1.219) of Ref. 3 and the relativistic radius $r = \lambda_C$ is given by (1.217) of Ref. 3. The relativistically corrected (A-58) is

$$\Delta m = -\frac{1}{2} (2\pi\alpha)^{-1} \left(\frac{\mu_0 e^2}{2m_e \alpha a_0} \right) \frac{e\hbar}{2m_e} = \frac{\mu_B}{2}. \quad (A-59)$$

The magnetic flux of the electron is given by

$$\nabla \times \mathbf{A} = \mathbf{B}. \quad (A-60)$$

Substitution of (A-57) into (A-60) gives half the flux of the $r > r_n$ part of (A-26).

From (A-55), the $\hbar/2$ of angular momentum before and after the field is applied corresponds to an initial magnetic moment on the applied field axis of $\mu_B/2$. After the field is applied, the contribution of $\mu_B/2$ from (A-56) with (A-54) gives a total magnetic moment along the applied field axis of μ_B , a Bohr magneton, where the additional contribution (A-55) arises from the angular momentum of \hbar on the S axis. Thus, even though the magnitude of the vector projection of the angular momentum of the electron in the direction of the magnetic field is $\hbar/2$, the magnetic moment corresponds to \hbar due to the $\hbar/2$ contribution from the dynamic component, and the quantized transition is due to the requirement of angular momentum conservation as given by (A-55).

Equation (A-49) implies a continuum of energies; whereas (A-56) shows that the static-kinetic and dynamic vector potential components of the angular momentum are quantized at $\hbar/2$. Consequently, as shown in Section A.5, the flux linked during a spin transition is quantized as the magnetic flux quantum:

$$\Phi_0 = \frac{h}{2e} \quad (\text{A-61})$$

Only the states corresponding to

$$m_s = \pm \frac{1}{2} \quad (\text{A-62})$$

are possible due to conservation of angular momentum. It is further shown using the Poynting power vector, with the requirement that flux be linked in units of the magnetic flux quantum, that the factor 2 of (A-50) and (A-52) is replaced with the electron g factor.

A.5 Electron g Factor

As demonstrated by Purcell,⁽⁶²⁾ when a magnetic field is applied to an electron in a central field that comprises a current loop, the orbital radius does not change, but the velocity changes as follows:

$$\Delta v = \frac{e r B}{2 m_e} \quad (\text{A-63})$$

This corresponds to diamagnetism and gives rise to precession with a corresponding resonance, as shown in Section A.4. The angular momentum in the presence of an applied magnetic field is⁽⁶²⁾

$$\mathbf{L} = \mathbf{r} \times (m_e \mathbf{v} + e \mathbf{A}), \quad (\text{A-64})$$

where \mathbf{A} is the vector potential evaluated at the location of the orbitsphere. Conservation of angular momentum of the orbitsphere permits a discrete change of its kinetic angular momentum ($\mathbf{r} \times m\mathbf{v}$) with respect to the field of $\hbar/2$, and concomitantly the potential angular momentum ($\mathbf{r} \times e\mathbf{A}$) must change by $-\hbar/2$. The flux change ϕ of the orbitsphere for $r < r_n$ is determined as follows:⁽⁶²⁾

$$\begin{aligned} \Delta \mathbf{L} &= \frac{\hbar}{2} - \mathbf{r} \times e \mathbf{A} \\ &= \left(\frac{\hbar}{2} - \frac{e 2 \pi r A}{2 \pi} \right) \hat{z} \\ &= \left(\frac{\hbar}{2} - \frac{e \phi}{2 \pi} \right) \hat{z}. \end{aligned} \quad (\text{A-65})$$

In order that the change in angular momentum $\Delta \mathbf{L}$ be equal to zero, ϕ must be $\Phi_0 = h/2e$, the magnetic flux quantum. Thus, to conserve angular momentum in the presence of an applied magnetic field, the orbitsphere magnetic moment can be parallel or antiparallel to an applied field, as observed with the Stern-Gerlach experiment, and the flip between orientations is accompanied by the "capture" of the magnetic flux quantum by the orbitsphere "coils" comprising infinitesimal loops of charge moving along great circles. A superconducting loop with a weak link also demonstrates this effect.⁽⁷³⁾

The energy to flip the orientation of the orbitsphere due to its magnetic moment of a Bohr magneton μ_B is

$$\Delta E_{\text{mag}}^{\text{spin}} = 2 \mu_B B, \quad (\text{A-66})$$

where

$$\mu_B = \frac{e \hbar}{2 m_e}. \quad (\text{A-67})$$

During the spin-flip transition, power must be conserved. Power flow is governed by the Poynting power theorem,

$$\begin{aligned} \nabla \cdot (\mathbf{E} \times \mathbf{H}) &= -\frac{\partial}{\partial t} \left(\frac{1}{2} \mu_0 \mathbf{H} \cdot \mathbf{H} \right) \\ &\quad - \frac{\partial}{\partial t} \left(\frac{1}{2} \epsilon_0 \mathbf{E} \cdot \mathbf{E} \right) - \mathbf{J} \cdot \mathbf{E}. \end{aligned} \quad (\text{A-68})$$

A.5.1 Stored Magnetic Energy

Energy superimposes; thus the calculation of the spin-flip energy is determined as a sum of contributions. The energy change corresponding to the “capture” of the magnetic flux quantum is derived below. From (A-31) for one electron,

$$\frac{1}{2} \mu_0 \mathbf{H} \cdot \mathbf{H} = E_{mag}^{fluxon} = \frac{\pi \mu_0 e^2 \hbar^2}{(m_e)^2 r_n^3} \quad (\text{A-69})$$

is the energy stored in the magnetic field of the electron. The orbitsphere is equivalent to a Josephson junction that can trap integer numbers of fluxons, where the quantum of magnetic flux is $\Phi_0 = h/2e$. Consider (A-69). During the flip transition, a fluxon treads the orbitsphere at the speed of light; therefore the radius of the orbitsphere in the lab frame is 2π times the relativistic radius in the fluxon frame, as shown in the Special Relativistic Correction to the Ionization Energies section of Ref. 3. Thus the energy of the transition corresponding to the “capture” of a fluxon by the orbitsphere, E_{mag}^{fluxon} , is

$$\begin{aligned} E_{mag}^{fluxon} &= \frac{\pi \mu_0 e^2 \hbar^2}{(m_e)^2 (2\pi r_n)^3} \\ &= \frac{\mu_0 e^2}{4\pi^2 m_e r_n} \left(\frac{e\hbar}{2m_e} \right) \left(\frac{h}{2e\pi r_n^2} \right) \quad (\text{A-70}) \\ &= \frac{\mu_0 e^2}{4\pi^2 m_e r_n} \mu_B \left(\frac{\Phi_0}{A} \right), \end{aligned}$$

where A is the area and Φ_0 is the magnetic flux quantum. We have

$$E_{mag}^{fluxon} = 2 \left(\frac{e^2 \mu_0}{2m_e r_n} \right) \frac{1}{4\pi^2} \mu_B B, \quad (\text{A-71})$$

where the n th fluxon treading through the area of the orbitsphere is equivalent to the applied magnetic flux. Furthermore, the term in brackets can be expressed in terms of the fine-structure constant α as follows:

$$\frac{e^2 \mu_0}{2m_e r_n} = \frac{e^2 \mu_0 c v}{2m_e v r_n c}. \quad (\text{A-72})$$

Substitution of (6) gives

$$\frac{e^2 \mu_0}{2m_e r_n} = \frac{e^2 \mu_0 c v}{2\hbar c}. \quad (\text{A-73})$$

Substitution of

$$c = \sqrt{\frac{1}{\epsilon_0 \mu_0}} \quad (\text{A-74})$$

and

$$\alpha = \frac{\mu_0 e^2 c}{2\hbar} \quad (\text{A-75})$$

gives

$$\frac{e^2 \mu_0 c v}{2\hbar c} = 2\pi \alpha \frac{v}{c}. \quad (\text{A-76})$$

The fluxon treads the orbitsphere at $v = c$ (k is the light-like k^0 , so $k = \omega_n/c$). Thus

$$E_{mag}^{fluxon} = 2 \frac{\alpha}{2\pi} \mu_B B. \quad (\text{A-77})$$

A.5.2 Stored Electric Energy

The superposition of the vector projection of the orbitsphere angular momentum on the z axis is $\hbar/2$, with an orthogonal component of $\hbar/4$. Excitation of a resonant Larmor precession gives rise to \hbar on an axis S that precesses about the spin axis at an angle of $\theta = \pi/3$. S rotates about the z axis at the Larmor frequency. S_{\perp} , the transverse projection, is $\pm\sqrt{3}/4 \hbar$ (A-7a), and S_{\parallel} , the projection onto the axis of the applied magnetic field, is $\pm\hbar/2$ (A-7b). As shown in Section A.2, the superposition of the $\hbar/2$, z axis component of the orbitsphere angular momentum and the $\hbar/2$, z axis component of S gives \hbar corresponding to the observed electron magnetic moment of a Bohr magneton, μ_B . The reorientation of S and the orbitsphere angular momentum from parallel to antiparallel to the magnetic field applied along the z axis gives rise to a current. The current is acted on by the flux corresponding to Φ_0 , the magnetic flux quantum, linked by

the electron during the transition, which gives rise to a Hall voltage. The electric field corresponding to the Hall voltage corresponds to the electric power term $\delta/\delta t[(1/2)\epsilon_0 \mathbf{E} \cdot \mathbf{E}]$ of the Poynting power theorem (A-68).

Consider a conductor in a uniform magnetic field and assume that it carries a current driven by an electric field perpendicular to the magnetic field. The current in this case is not parallel to the electric field but is deflected at an angle to it by the magnetic field. This is the Hall effect, and it occurs in most conductors.

A spin-flip transition is analogous to the quantum Hall effect given in the corresponding section of Ref. 3, where the applied magnetic field quantizes the Hall conductance. The current is then precisely perpendicular to the magnetic field, so that no dissipation (that is, no ohmic loss) occurs. This is seen in two-dimensional systems, at cryogenic temperatures, in quite high magnetic fields. Furthermore, the ratio of the total electric potential drop to the total current, the Hall resistance R_H , is precisely

$$R_H = \frac{h}{ne^2}. \quad (\text{A-78})$$

The factor n is an integer in the case of the integral quantum Hall effect and a small rational fraction in the case of the fractional quantum Hall effect. In an experimental plot⁽⁷⁴⁾ as a function of the magnetic field, the Hall resistance exhibits flat steps precisely at these quantized resistance values; however, the regular resistance vanishes (or is very small) at these Hall steps. Thus the quantized Hall resistance steps occur for a transverse superconducting state.

Consider the case that an external magnetic field is applied along the x axis to a two-dimensional superconductor in the yz plane that exhibits the integral quantum Hall effect (see Fig. 27). Conduction electrons align with the applied field in the x direction as the field permeates the material. The normal current carrying electrons experiences a Lorentzian force \mathbf{F}_L due to the magnetic flux. The y -directed Lorentzian force on an electron with velocity \mathbf{v} in the z direction by an x -directed applied flux \mathbf{B} is

$$\mathbf{F}_L = e\mathbf{v} \times \mathbf{B}. \quad (\text{A-79})$$

The electron motion is a cycloid, where the center of mass experiences an $\mathbf{E} \times \mathbf{B}$ drift.⁽⁷⁵⁾ Consequently, the normal Hall effect occurs. Conduction electron en-

ergy states are altered by the applied field and by the electric field corresponding to the Hall effect. The electric force \mathbf{F}_H due to the Hall electric field \mathbf{E}_y is

$$\mathbf{F}_H = e\mathbf{E}_y. \quad (\text{A-80})$$

When these two forces are equal and opposite, conduction electrons propagate in the z direction alone. For this special case, it is demonstrated in Jackson⁽⁷⁵⁾ that the ratio of the corresponding Hall electric field E_H to the applied magnetic flux is

$$\frac{E_H}{B} = v, \quad (\text{A-81})$$

where v is the electron velocity. It is also demonstrated in the Integral Quantum Hall Effect section of Ref. 3 that the Hall resistance R_H in the superconducting state is given by

$$R_H = \frac{h}{ne^2}, \quad (\text{A-82})$$

where n is an integer.

Consider the case of the spin-flip transition of the electron. In the case of an exact balance between the Lorentzian force (A-79) and the electric force corresponding to the Hall voltage (A-80), each superconducting point mass of the electron propagates along a great circle, where

$$\frac{E}{B} = v, \quad (\text{A-83})$$

where v is given by (6). Substitution of (6) into (A-83) gives

$$\frac{E}{B} = \frac{\hbar}{m_e r}. \quad (\text{A-84})$$

Equation (A-84) is the condition for superconductivity in the presence of crossed electric and magnetic fields. The electric field corresponding to the Hall voltage corresponds to the electric energy term E_{ele} of the Poynting power theorem (A-68):

$$E_{ele} = \frac{1}{2} \int_0^{2\pi} \int_0^\pi \int_0^r \epsilon_0 \mathbf{E} \cdot \mathbf{E} r^2 \sin \theta dr d\theta d\phi. \quad (\text{A-85})$$

The electric term for this superconducting state is derived as follows using the coordinate system shown in Fig. 28.

The current is perpendicular to \mathbb{E}_r , so there is no dissipation. This occurs when

$$e\mathbb{E} = ev \times \mathbb{B} \quad (\text{A-86})$$

or

$$\frac{E}{B} = v. \quad (\text{A-87})$$

The electric field corresponding to the Hall voltage is

$$\mathbb{E} = v \times \mathbb{B}. \quad (\text{A-88})$$

Substitution of (A-88) into (A-85) gives

$$E_{ele} = \frac{1}{2} \epsilon_0 \int_0^{2\pi} \int_0^\pi \int_0^r (vB)^2 r^2 \sin \theta dr d\theta d\phi. \quad (\text{A-89})$$

The spin-flip transition may be induced by the absorption of a resonant photon. The velocity is determined from the distance traversed by each point and the time of the transition due to capture of a photon resonant with the spin-flip transition energy. The current i , corresponding to the Hall voltage and \mathbb{E}_r is given by the product of the electron charge and the frequency f of the photon, where the correspondence principle holds, as given in the Photon Absorption section of Ref. 3:

$$i = ef. \quad (\text{A-90})$$

The resistance of free space for the propagation of a photon is the radiation resistance of free space η :

$$\eta = \sqrt{\frac{\mu_0}{\epsilon_0}}. \quad (\text{A-91})$$

The power P_r of the electron current induced by the photon as it transitions from free space to being captured by the electron is given by the product of the corresponding current and the resistance R , which is given by (A-91):

$$P_r = i^2 R. \quad (\text{A-92})$$

Substitution of (A-90) and (A-91) gives

$$P_r = e^2 f^2 \sqrt{\frac{\mu_0}{\epsilon_0}}. \quad (\text{A-93})$$

It follows from the Poynting power theorem (A-68) with spherical radiation that the transition time τ is given by the ratio of the energy to the power of the transition.⁽²⁶⁾

$$\tau = \frac{\text{energy}}{\text{power}}. \quad (\text{A-94})$$

The energy of the transition, which is equal to the energy of the resonant photon, is given by Planck's equation:

$$E = \hbar \omega = hf. \quad (\text{A-95})$$

Substitution of (A-93) and (A-95) into (A-94) gives

$$\tau = \frac{hf}{e^2 f^2 \sqrt{\mu_0 / \epsilon_0}}. \quad (\text{A-96})$$

The distance ℓ traversed by the electron with a kinetic angular momentum change of $\hbar/2$ is

$$\ell = \frac{2\pi r}{2} = \frac{\lambda}{2}, \quad (\text{A-97})$$

where the wavelength is given by (4). The velocity is given by the distance traversed divided by the transition time. Equations (A-96) and (A-97) give

$$\begin{aligned} v &= \frac{\lambda/2}{\tau} = \frac{\lambda/2}{hf / (e^2 f^2 \sqrt{\mu_0 / \epsilon_0})} \\ &= \frac{\sqrt{\mu_0 / \epsilon_0} e^2}{2h} \lambda f. \end{aligned} \quad (\text{A-98})$$

The relationship for a photon in free space is

$$c = \lambda f. \quad (\text{A-99})$$

The fine-structure constant given by (A-75) is the dimensionless factor that corresponds to the relativistic invariance of charge:

Substitution of (A-69) to (A-77) gives

$$\alpha = \frac{1}{4\pi} \sqrt{\frac{\mu_0}{\epsilon_0}} \frac{e^2}{\hbar} = \frac{1}{2} \frac{\sqrt{\mu_0/\epsilon_0}}{h/e^2} = \frac{\mu_0 e^2 c}{2h}. \quad (\text{A-100})$$

$$E_{ele} = 2 \left(\frac{2}{3} \alpha^2 \frac{\alpha}{2\pi} \mu_B B \right). \quad (\text{A-108})$$

It is equivalent to one half the ratio of the radiation resistance of free space, $\sqrt{\mu_0/\epsilon_0}$, to the Hall resistance h/e^2 . The radiation resistance of free space is equal to the ratio of the electric field and the magnetic field of the photon (113). Substitution of (A-99) and (A-100) into (A-98) gives

$$v = \alpha c. \quad (\text{A-101})$$

Substitution of (A-101) into (A-89) gives

$$E_{ele} = \frac{1}{2} \epsilon_0 \int_0^{2\pi} \int_0^\pi \int_0^r (\alpha c \mu_0 H)^2 r^2 \sin \theta dr d\theta d\phi, \quad (\text{A-102})$$

where

$$B = \mu_0 H. \quad (\text{A-103})$$

The relationship between the speed of light c and the permittivity of free space ϵ_0 and the permeability of free space μ_0 is

$$c = \frac{1}{\sqrt{\mu_0 \epsilon_0}}. \quad (\text{A-104})$$

Thus (A-102) may be written as

$$E_{ele} = \frac{1}{2} \alpha^2 \int_0^{2\pi} \int_0^\pi \int_0^r \mu_0 H^2 r^2 \sin \theta dr d\theta d\phi. \quad (\text{A-105})$$

Substitution of (A-29) gives

$$E_{ele} = \alpha^2 \frac{2\pi \mu_0 e^2 \hbar^2}{3m_e^2 r_1^3}. \quad (\text{A-106})$$

The magnetic flux B is quantized in terms of the Bohr magneton because the electron links flux in units of the magnetic flux quantum

$$\Phi_0 = \frac{h}{2e}. \quad (\text{A-107})$$

A.5.3 Dissipated Energy

The $J \cdot E$ energy over time is derived from the electron current corresponding to the Larmor excitation and the electric field given by Faraday's law due to the linkage of the magnetic flux of the fluxon during the spin-flip. Consider the electron current due to the external field. The application of a magnetic field with a resonant Larmor excitation gives rise to a precessing angular momentum vector S of magnitude \hbar directed from the origin of the orbitsphere at an angle of $\theta = \pi/3$ relative to the applied magnetic field. As given in Section A.2, S rotates about the axis of the applied field at the Larmor frequency. The magnitude of the components of S that are parallel and orthogonal to the applied field (A-7b) and (A-7a) are $\hbar/2$ and $\sqrt{3}/4 \hbar$, respectively. Since both the RF field and the orthogonal components shown in Fig. 25 rotate at the Larmor frequency, the RF field that causes a Stern-Gerlach transition produces a stationary magnetic field with respect to these components, as described in Section A.4. The corresponding central field at the orbitsphere surface given by the superposition of the central field of the proton and that of the photon follows from (2.10) to (2.17) of Ref. 3 and is given by (A-48):

$$E = \frac{e}{4\pi\epsilon_0 r^2} [Y_0^0(\theta, \phi) \mathbf{i}_r + \text{Re}\{Y_1^m(\theta, \phi) e^{i\omega_n t}\} \mathbf{i}_y \delta(r - r_1)], \quad (\text{A-109})$$

where the spherical harmonic dipole $Y_1^m(\theta, \phi) = \sin \theta$ is with respect to the S axis. The dipole spins about the S axis at the angular velocity given by (9). The resulting current is nonradiative, as shown in Section 6. Thus the field in the RF is magnetostatic, as shown in Fig. 6, but directed along the S axis. Thus the corresponding current given by (A-17) is

$$K(\rho, \phi, z) = \frac{3}{2} \frac{e\hbar}{m_e r_n^3} \sin \theta \mathbf{i}_\phi. \quad (\text{A-110})$$

Next consider Faraday's equation for the electric field:

$$\oint_C \mathbb{E} \cdot ds = -\frac{d}{dt} \int_S \mu_0 \mathbb{H} \cdot da. \quad (\text{A-111})$$

As demonstrated by Purcell,⁽⁶²⁾ the velocity of the electron changes according to Lenz's law, but the change in centrifugal force is balanced by the change in the central field due to the applied field. The magnetic flux of the electron given by (A-26) is

$$\mathbb{B} = \mu_0 \mathbb{H} = \frac{\mu_0 e \hbar}{m_e r_1^3} (\mathbf{i}_r \cos \theta - \mathbf{i}_\theta \sin \theta) \text{ for } r < r_n. \quad (\text{A-112})$$

From (A-77) the magnetic flux $\mathbb{B}_{J,E}$ of the fluxon is

$$\begin{aligned} \mathbb{B}_{J,E} &= \frac{\alpha}{2\pi} \frac{\mu_0 e \hbar}{m_e r_1^3} (\mathbf{i}_r \cos \theta - \mathbf{i}_\theta \sin \theta) \\ &= \frac{\alpha}{2\pi} \frac{\mu_0 e \hbar}{m_e r_1^3} \mathbf{i}_z. \end{aligned} \quad (\text{A-113})$$

The electric field \mathbb{E} is constant about the line integral of the orbitsphere. Using (A-111) with the change in flux in units of fluxons along the z axis given by (A-113) gives

$$\int_{-r_1}^{+r_1} \oint_C \mathbb{E} \cdot ds dz = \int_{-r_1}^{+r_1} -\pi r^2 \frac{dB}{dt} dz \mathbf{i}_\phi, \quad (\text{A-114})$$

$$\begin{aligned} 2\pi \mathbb{E} \int_0^\pi r_1^2 \sin^2 \theta d\theta &= -\pi \frac{\Delta B}{\Delta t} r_1^2 \sin^3 \theta d\theta \mathbf{i}_\phi \\ &= -\pi r_1^2 \frac{2}{3} \frac{\Delta B}{\Delta t} \mathbf{i}_\phi. \end{aligned} \quad (\text{A-115})$$

Substitution of (A-113) into (A-115) gives

$$\begin{aligned} \pi r_1 \mathbb{E} &= -\pi r_1^2 \frac{2}{3} \frac{\alpha}{2\pi} \frac{\mu_0 e \hbar}{m_e r_1^3 \Delta t} \mathbf{i}_\phi \\ &= -\pi \frac{2}{3} \frac{\alpha}{2\pi} \frac{\mu_0 e \hbar}{m_e r_1 \Delta t} \mathbf{i}_\phi. \end{aligned} \quad (\text{A-116})$$

Thus

$$\mathbb{E} = -\frac{2}{3} \frac{\alpha}{2\pi} \frac{\mu_0 e \hbar}{m_e r_1^2 \Delta t} \mathbf{i}_\phi. \quad (\text{A-117})$$

The dissipative power density $\mathbb{E} \cdot \mathbb{J}$ can be expressed in terms of the surface current density \mathbb{K} as

$$\int_V (\mathbb{E} \cdot \mathbb{J}) \Delta t dv = \int_S (\mathbb{E} \cdot \mathbb{K}) \Delta t da. \quad (\text{A-118})$$

Using the electric field from (A-117) and the current density from (A-110) gives

$$\begin{aligned} &\int_V (\mathbb{E} \cdot \mathbb{J}) \Delta t dv \\ &= \int_0^{2\pi} \int_0^\pi \left(\frac{2}{3} \frac{\alpha}{2\pi} \frac{\mu_0 e \hbar}{m_e r_1^2 \Delta t} \frac{3}{2} \frac{e \hbar}{m_e r_1^3} \right) \Delta t r_1^2 \sin \theta d\theta d\phi \quad (\text{A-119}) \\ &= \frac{4}{3} \frac{\alpha}{2\pi} \frac{\pi \mu_0 e^2 \hbar^2}{m_e^2 r_1^3}. \end{aligned}$$

Substitution of (A-77) into (A-119) gives

$$\int_V (\mathbb{E} \cdot \mathbb{J}) \Delta t dv = 2 \left(\frac{4}{3} \right) \left(\frac{\alpha}{2\pi} \right)^2 \mu_B B. \quad (\text{A-120})$$

A.5.4 Total Energy of Spin-Flip Transition

The principal energy of the transition corresponding to a reorientation of the orbitsphere is given by (A-66). The total energy of the flip transition is the sum of (A-66) with (A-77), (A-108), and (A-120) corresponding to the electric energy, the magnetic energy, and the dissipated energy of a fluxon treading the orbitsphere, respectively:

$$\begin{aligned} \Delta E_{mag}^{spin} &= 2 \left(1 + \frac{\alpha}{2\pi} + \frac{2}{3} \alpha^2 \left(\frac{\alpha}{2\pi} \right) - \frac{4}{3} \left(\frac{\alpha}{2\pi} \right)^2 \right) \mu_B B \quad (\text{A-121}) \\ &= g \mu_B B, \end{aligned}$$

where the stored magnetic energy corresponding to the $\partial/\partial t[(1/2)\mu_0 \mathbb{H} \cdot \mathbb{H}]$ term increases, the stored electric energy corresponding to the $\partial/\partial t[(1/2)\epsilon_0 \mathbb{E} \cdot \mathbb{E}]$ term increases, and the $\mathbb{J} \cdot \mathbb{E}$ term is dissipative. The magnetic moment of (A-66) is twice that from the gyromagnetic ratio, as given by (A-55). The magnetic moment of the electron is the sum of the component corresponding to the kinetic angular momentum $\hbar/2$ and the component corresponding to the vector potential angular momentum $\hbar/2$ (A-64). The spin-flip transition can be considered as involving a magnetic mo-

ment of g times that of a Bohr magneton. The g factor is redesignated the fluxon g factor as opposed to the anomalous g factor, and it is given by (A-121):

$$\frac{g}{2} = 1 + \frac{\alpha}{2\pi} + \frac{2}{3}\alpha^2 \left(\frac{\alpha}{2\pi} \right) - \frac{4}{3} \left(\frac{\alpha}{2\pi} \right)^2. \quad (\text{A-122})$$

For $\alpha^{-1} = 137.036\ 04(11)$,⁽⁷⁶⁾

$$\frac{g}{2} = 1.001\ 159\ 652\ 120. \quad (\text{A-123})$$

The experimental value⁽²³⁾ is

$$\frac{g}{2} = 1.001\ 159\ 652\ 188(4). \quad (\text{A-124})$$

The calculated and experimental values are within the propagated error of the fine-structure constant. Different values of the fine-structure constant have been recorded from different experimental techniques, and α^{-1} depends on a circular argument between theory and experiment.⁽³⁹⁾ One measurement of the fine-structure constant based on the electron g factor is $\alpha^{-1} = 137.036\ 006(20)$.⁽⁷⁷⁾ This value can be contrasted with equally precise measurements employing solid state techniques such as those based on the Josephson effect⁽⁷⁸⁾ ($\alpha^{-1} = 137.035\ 963(15)$) or the quantized Hall effect⁽⁷⁹⁾ ($\alpha_H^{-1} = 137.035\ 300(400)$). A method of determination of α^{-1} that depends on the circular methodology between theory and experiment to a lesser extent is the substitution of the independently measured fundamental constants μ_0 , e , c , and h into (A-100). The following values of the fundamental constants are given by Weast:⁽⁷⁶⁾

$$\mu_0 = 4\pi \times 10^{-7} \text{ Hm}^{-1}, \quad (\text{A-125})$$

$$e = 1.602\ 189\ 2(46) \times 10^{-19} \text{ C}, \quad (\text{A-126})$$

$$c = 2.997\ 924\ 58(12) \times 10^8 \text{ m/s}, \quad (\text{A-127})$$

$$h = 6.626\ 176(36) \times 10^{-34} \text{ J} \cdot \text{Hz}^{-1}. \quad (\text{A-128})$$

For these constants,

$$\alpha^{-1} = 137.036\ 03(82). \quad (\text{A-129})$$

Substitution of the α^{-1} from (A-129) into (A-122) gives

$$\frac{g}{2} = 1.001\ 159\ 652\ 137. \quad (\text{A-130})$$

The experimental value⁽²³⁾ is

$$\frac{g}{2} = 1.001\ 159\ 652\ 188(4). \quad (\text{A-131})$$

The *postulated* QED theory of $g/2$ is based on the determination of the terms of a *postulated* power series in α/π , where each *postulated* virtual particle is a source of *postulated* vacuum polarization that gives rise to a *postulated* term. The algorithm involves scores of *postulated* Feynman diagrams corresponding to thousands of matrices with thousands of integrations per matrix requiring decades to reach a consensus on the "appropriate" *postulated* algorithm to remove the intrinsic infinities. The remarkable agreement between (A-130) and (A-131) demonstrates that $g/2$ may be derived in closed form from Maxwell's equations in a simple straightforward manner that yields a result with 11-figure agreement with experiment — the limit of the experimental capability of the measurement of α directly or the fundamental constants to determine α . In Chapter 1, Appendix II, of Ref. 3, the Maxwellian result is contrasted with the QED algorithm of invoking virtual particles, zero-point fluctuations of the vacuum, and negative energy states of the vacuum. Rather than an infinity of radically different QED models, an essential feature is that *Maxwellian solutions are unique*.

Received 11 December 2002.

Endnotes

¹ The orbitsphere has zero thickness, but in order for the speed of light to be a constant maximum in any frame including that of the gravitational field that propagates out as a light-wave front at particle production, it gives rise to a space-time dilation equal to 2π times the Newtonian gravitational or Schwarzschild radius $r_g = 2Gm_e/c^2 = 1.3525 \times 10^{-57}$ m according to (170) and (194). This corresponds to a space-time dilation of 8.4980×10^{-57} m or 2.8346×10^{-65} s. Although the orbitsphere does not occupy space in the third spatial dimension, its mass discontinuity effectively "displaces" space-time, where the space-time dilation can be considered as a "thickness" associated with its gravitational field.

² The theories of Bohr, Schrödinger, and now CQM all give the identical equation for the principal energy levels of the hydrogen atom:

$$\begin{aligned}
 E_{ele} &= -\frac{Z^2 e^2}{8\pi\epsilon_0 n^2 a_H} \\
 &= -\frac{Z^2}{n^2} \times 2.1786 \times 10^{-18} \text{ J} \\
 &= -Z^2 \times \frac{13.598}{n^2} \text{ eV.}
 \end{aligned} \tag{N-1}$$

In CQM, the two-dimensional wave equation is solved for the charge density function of the electron. And, the Fourier transform of the charge density function is a solution of the three-dimensional wave equation in frequency (k, ω) space. However, the Schrödinger equation solutions are three-dimensional in space-time. The energy is given by

$$\int_{-\infty}^{\infty} \psi H \psi dv = E \int_{-\infty}^{\infty} \psi^2 dv, \quad (\text{N-2})$$

$$\int_{-\infty}^{\infty} \psi^2 dv = 1. \quad (\text{N-3})$$

Thus

$$\int_{-\infty}^{\infty} \psi H \psi dv = E. \quad (\text{N-4})$$

In the case that the potential energy of the Hamiltonian H is a constant times the wave-number, the Schrödinger equation is the well-known Bessel equation. Then with one of the solutions for ψ , (N-4) is equivalent to an inverse Fourier transform. According to the duality and scale change properties of Fourier transforms, the energy equation of CQM and that of QM are identical, i.e., the energy of a radial Dirac delta function of radius equal to an integer multiple of the radius of the hydrogen atom (N-1). Bohr obtained the same energy formula by postulating nonradiative states with angular momentum

$$L_z = m\hbar \quad (\text{N-5})$$

and solving the energy equation classically.

The mathematics for all three theories converge to (N-1). However, the physics is quite different. Only CQM is derived from first principles and holds over a scale of space-time of 85 orders of magnitude. And, the mathematical relationship of CQM and QM is based on the Fourier transform of the radial function. CQM requires that the electron be real and physically confined to a two-dimensional surface that corresponds to a solution of the two-dimensional wave equation plus time. The corresponding Fourier transform is a wave over all space that is a solution of the three-dimensional wave equation (e.g., the Schrödinger equation). *In essence QM may be considered as a theory dealing with the Fourier transform of an electron rather than the physical electron.* By Parseval's theorem the energies may be equivalent, but the quantum-mechanical case is nonphysical — only mathematical. Thus it is nonsensical from this perspective. It may mathematically produce numbers that agree with experimental energies, but the mechanisms

lack internal consistency and conformity with physical laws. If these are the criteria for a valid solution of physical problems, then QM has never successfully solved any problem. The theory of Bohr similarly failed.

Classical revisions may transform Schrödinger's and Heisenberg's quantum theory into what is termed a *classical quantum theory* such that physical descriptions result. For example, in the old quantum theory the spin angular momentum of the electron is called the "intrinsic angular momentum." This term arises because it is difficult to provide a physical interpretation for the electron's spin angular momentum. QED provides somewhat of a physical interpretation by proposing that the "vacuum" contains fluctuating electric and magnetic fields. In contrast, in CQM, spin angular momentum results from the motion of negatively charged mass moving systematically, and the equation for angular momentum $\mathbf{r} \times \mathbf{p}$ can be applied directly to the wave-function (a current density function) that describes the electron. And, quantization is carried by the photon, rather than probability waves of the electron, as demonstrated in this paper.

³ The *second* is currently defined as the time required for 9 192 631 770 vibrations within the cesium-133 atom. The "sec" as defined in (179) is a fundamental constant, namely the metric of space-time (it is almost identically equal to the present value for reasons explained in Ref. 3). A unified theory can only provide the relationships between all measurable observables in terms of a clock defined in terms of fundamental constants according to those observables and used to measure them. The *so-defined "clock" measures "clicks" on an observable in one aspect, and in another, it is the ruler of space-time of the universe with the implicit dependence of space-time on matter-energy conversion*, as shown in Section 29.

⁴ The torque balance can be appreciated by considering that \mathbf{S} is aligned with Z_R if the X_R component is zero, and the three vectors are mutually orthogonal if the X_R component is $\hbar/2$. The balance can be shown by considering the magnetic energies resulting from the corresponding torques when they are balanced. Using (A-50) and (A-52), the potential energy E_V due to the projection of \mathbf{S} 's angular momentum of \hbar along Z_R with $\hbar/2$ of angular momentum is

$$E_V = \mu_B B \cos \theta = \mu_B \frac{1}{2} B_{\mu_B} \cos \theta$$

$$= \frac{1}{2} \hbar \omega_{\mu_B} \cos \theta, \quad (\text{N-6})$$

where B_{μ_B} is the flux due to a magnetic moment of a Bohr magneton and ω_{μ_B} is the corresponding gyromagnetic frequency. The application of a magnetic moment along the X_R axis causes S to precess about the Z_R and X_R axes. In the $X_R Y_R Z_R$ frame rotating at ω_{μ_B} , S precesses about the X_R axis. The corresponding precession energy E_{X_R} of S about the X_R component of $\hbar/4$ is the corresponding Larmor energy

$$E_{X_R} = -\frac{1}{4} \hbar \omega_{\mu_B}. \quad (\text{N-7})$$

The energy E_{Z_R} of the magnetic moment corresponding to S rotating about Z_R with $\hbar/2$ of angular momentum is the corresponding Larmor energy

$$E_{Z_R} = \frac{1}{2} \hbar \omega_{\mu_B}. \quad (\text{N-8})$$

At torque balance the potential energy is equal to the sum of the Larmor energies:

$$E_{Z_R} + E_{X_R} = \hbar \left(\frac{1}{2} - \frac{1}{4} \right) \omega_{\mu_B}$$

$$= \frac{\hbar}{2} \left(1 - \frac{1/4}{1/2} \right) \omega_{\mu_B} \quad (\text{N-9})$$

$$= \frac{1}{2} \hbar \omega_{\mu_B} \cos \theta.$$

Balance occurs when $\theta = \pi/3$. Thus the intrinsic torques are balanced. Furthermore, energy is conserved relative to the external field as well as the intrinsic Z_R and X_R components of the orbitsphere, and the Larmor relationships for both the gyromagnetic ratio and the potential energy of the resultant magnetic moment are satisfied, as shown in Section A.4.

⁵ As shown in Section A.4, the angular momentum of \hbar on the S axis is due to a photon standing wave that is phase-matched to a spherical harmonic source current, i.e., a spherical harmonic dipole $Y_l^m(\theta, \phi) = \sin \theta$ with respect to the S axis. The dipole spins about the S axis at the angular velocity

given by (9). Since the field is magnetostatic in the RF rotating frame, the current is equivalent to current loops along the S axis. Thus the derivation of the corresponding magnetic field is the same as that of the stationary field given in this section.

References

1. F. Laloë, Am. J. Phys. 69, 655 (2001).
2. G. Landvogt, Internat. J. Hydrogen Energy 28, 1155 (2003).
3. R.L. Mills, *The Grand Unified Theory of Classical Quantum Mechanics*, September 2001 Edition, BlackLight Power, Inc., Cranbury, NJ, distributed by Amazon.com. January 2005. Available at <http://www.blacklightpower.com/book.shtml>.
4. *Idem*, Internat. J. Hydrogen Energy 25, 1171 (2000).
5. *Ibid.* 26, 1059 (2001).
6. H. Margenau and G.M. Murphy, *The Mathematics of Physics and Chemistry*, 2nd edition (D. Van Nostrand, New York, 1956), pp. 363–367.
7. H.J. Maris, J. Low Temp. Phys. 120, 173 (2000).
8. C.A. Fuchs and A. Peres, Phys. Today 53, 70 (2000).
9. S. Peil and G. Gabrielse, Phys. Rev. Lett. 83, 1287 (1999).
10. F.J. Dyson, Am. J. Phys. 58, 209 (1990).
11. J. Horgan, Sci. Am. 267, 94 (1992).
12. H.A. Haus, Am. J. Phys. 54, 1126 (1986).
13. R.L. Mills, Global Foundation, Inc., Orbis Scientiae, in *The Role of Attractive and Repulsive Gravitational Forces in Cosmic Acceleration of Particles. The Origin of the Cosmic Gamma Ray Bursts*, 29th Conference on High Energy Physics and Cosmology Since 1964, Dr. Behram N. Kursunoglu, Chairman, 14–17 December 2000, Lago Mar Resort, Fort Lauderdale, FL (Kluwer Academic/Plenum Publishers, New York), pp. 243–258.
14. *Idem*, Internat. J. Hydrogen Energy 27, 565 (2002).
15. D.A. McQuarrie, *Quantum Chemistry* (University Science Books, Mill Valley, CA, 1983), pp. 206–225.
16. J. Daboul and J.H.D. Jensen, Z. Phys. 265, 455 (1973).
17. T.A. Abbott and D.J. Griffiths, Am. J. Phys. 53, 1203 (1985).
18. G. Goedecke, Phys. Rev. B 135, 281 (1964).
19. P. Pearle, Found. Phys. 7, 931 (1977).

20. L.C. Shi and J.A. Kong, *Applied Electromagnetism* (Brooks/Cole Engineering Division, Monterey, CA, 1983), pp. 170–209.
21. J.D. Jackson, *Classical Electrodynamics*, 2nd edition (John Wiley & Sons, New York, 1975), pp. 739–779.
22. Ref. 15, pp. 238–241.
23. R.S. Van Dyck, Jr., P. Schwinberg, and H. Dehmelt, *Phys. Rev. Lett.* **59**, 26 (1987).
24. M. Mizushima, *Quantum Mechanics of Atomic Spectra and Atomic Structure* (W.A. Benjamin, Inc., New York, 1970), p. 17.
25. Ref. 21, pp. 739–752.
26. *Ibid.*, pp. 758–763.
27. E.M. Purcell, *Electricity and Magnetism* (McGraw-Hill, New York, 1965), pp. 156–167.
28. D. Clark, *J. Chem. Educ.* **68**, 454 (1991).
29. J. Gribbin, *New Scientist*, **153**, 2066 (1997).
30. I. Levine et al., *Phys. Rev. Lett.* **78**, 424 (1997).
31. C.E. Moore, “Ionization Potentials and Ionization Limits Derived from the Analyses of Optical Spectra,” *Nat. Stand. Ref. Data Ser.-Nat. Bur. Stand. (U.S.)*, No. 34, 1970.
32. R.C. Weast, *CRC Handbook of Chemistry and Physics*, 58th edition (CRC Press, West Palm Beach, FL, 1977), p. E-68.
33. P.J. Bromberg, *J. Chem. Phys.* **50**, 3906 (1969).
34. J. Geiger, *Z. Phys.* **175**, 530 (1963).
35. A. Beiser, *Concepts of Modern Physics*, 4th edition (McGraw-Hill, New York, 1978), pp. 2–10.
36. E.G. Adelberger, C.W. Stubbs, B.R. Heckel, Y. Su, H.E. Swanson, G. Smith, and J.H. Gundlach, *Phys. Rev. D* **42**, 3267 (1990).
37. G.R. Fowles, *Analytical Mechanics*, 3rd edition (Holt, Rinehart, and Winston, New York, 1977), pp. 154–155.
38. K. Hagiwara et al., *Phys. Rev. D* **66**, 010001 (2002). Also available at <http://pdg.lbl.gov/2002/s035.pdf>.
39. P.J. Mohr and B.N. Taylor, *Rev. Modern Phys.* **72**, 351 (2000).
40. T. Van Flandern, *Phys. Lett. A* **250**, 1 (1998).
41. R. Cowen, *Sci. News* **153**, 292 (1998).
42. M. Chown, *New Scientist* **154**, 50 (1997).
43. B. Schwarzschild, *Phys. Today* **51**, 19 (1998).
44. J.C. Mather and E.S. Cheng, *Astrophys. J. Lett.* **354**, L37 (1990).
45. W. Saunders and C. Frenk, *Nature* **349**, 32 (1991).
46. R.P. Kirshner, A. Oemler, Jr., P.L. Schechter, and S.A. Shectman, *Astron. J.* **88**, 1285 (1983).
47. V. de Lapparent, M.J. Geller, and J.P. Huchra, *Astrophys. J.* **332**, 44 (1988).
48. A. Dressler, S.M. Faber, D. Burstein, R.L. Davies, D. Lynden-Bell, R.J. Terlevich, and G. Wegner, *Astrophys. J.* **313**, L37 (1987).
49. S. Flamsteed, *Discover* **16**, 66 (1995).
50. J. Glanz, *Science* **273**, 581 (1996).
51. S.D. Landy, *Sci. Am.* **280**, 38 (1999).
52. W.L. Freeman, B.F. Madore, and G.D. Illingworth, *Nature* **371**, 757 (1994).
53. R.M. Wald, *General Relativity* (University of Chicago Press, Chicago, 1984), pp. 114–116.
54. P.J.E. Peebles and J. Silk, *Nature* **346**, 233 (1990).
55. W. McC. Siebert, *Circuits, Signals, and Systems* (The MIT Press, Cambridge, MA, 1986), pp. 597–603.
56. J. Glanz, *Science* **279**, 1298 (1998).
57. R. Cowen, *Sci. News* **153**, 344 (1998).
58. *Ibid.* **154**, 277 (1998).
59. P. de Bernardis et al., *Nature* **404**, 955 (2000). Also available at <http://www.phys.cwru.edu/boomerang/papers.html/debernardis00.pdf>.
60. N.W. Halverson, E.M. Leitch, C. Pryke, J. Kovac, J.E. Carlstrom, W.L. Holzapfel, M. Dragovan, J.K. Cartwright, B.S. Mason, S. Padin, T.J. Pearson, M.C. Shepard, and A.C.S. Readhead, “DASI First Results: A Measurement of the Cosmic Microwave Background Angular Power Spectrum,” *arXiv:astro-ph/0104489*, 30 April 2001.
61. B. Holverstott and R. Mills, “Modeling the Orbitsphere.” Available at <http://www.blacklightpower.com/pdf/technical/animations/Appendix%20III%20-%20Orbitsphere%20020905.pdf>.
62. Ref. 27, pp. 370–375, 447.
63. R.L. Mills, “The Fallacy of Feynman’s Argument on the Stability of the Hydrogen Atom According to Quantum Mechanics,” submitted.
64. Ref. 15, pp. 238–241.
65. Ref. 21, p. 178.
66. Ref. 37, p. 196.
67. Ref. 15, pp. 206–221.
68. Ref. 21, pp. 194–197.
69. Ref. 27, pp. 370–379.
70. Ref. 21, pp. 84–102; 752–763.
71. S. Patz, *Cardiovasc. Interven. Radiol.* **8**(25), 225 (1986).
72. Ref. 27, pp. 361–367.
73. C.E. Gough, M.S. Colclough, E.M. Forgan, R.G. Jordan, M. Keene, C.M. Muirhead, A.I.M. Rae,

- N. Thomas, J.S. Abell and S. Sutton, *Nature* **326**, 855 (1987).
74. S. Das Sarma and R.E. Prange, *Science* **256**, 1284 (1992).
75. Ref. 21, pp. 582–584.
76. R.C. Weast, *CRC Handbook of Chemistry and Physics*, 68th Edition (CRC Press, Boca Raton, FL, 1987–88), pp. F-186–F-187.
77. G.P. Lepage, *Proceedings of the International Conference on Atomic Physics* (World Scientific, Singapore, 1981), p. 297.
78. E.R. Williams and P.T. Olsen, *Phys. Rev. Lett.* **42**, 1575 (1979).
79. K.V. Klitzing, G. Dorda, and M. Pepper, *Phys. Rev. Lett.* **45**, 494 (1980).

Randell L. Mills

BlackLight Power, Inc.
493 Old Trenton Road
Cranbury, NJ 08648 U.S.A.

e-mail: rmills@blacklightpower.com

Figure Captions

Figure 1. The orbitsphere is a two-dimensional spherical shell of zero thickness with the Bohr radius of the hydrogen atom, $r = a_H$.

Figure 2. The current pattern of the orbitsphere shown with 6° increments of the infinitesimal angular variables $\pm\Delta\alpha_r$ and $\pm\Delta\alpha_\phi$ looking along the z axis. The current and charge density are confined to two dimensions at $r_n = nr_1$. The corresponding charge density function is uniform.

Figure 3. The orbital function modulates the constant (spin) function (shown for $t = 0$, three-dimensional view).

Figure 4. The normalized radius as a function of the velocity due to relativistic contraction.

Figure 5. Far field approximation.

Figure 6. The magnetic field of an electron orbitsphere (z axis defined as the vertical axis).

Figure 7. Broadening of the spectral line due to the rise time and shifting of the spectral line due to the radiative reaction. The resonant line shape has width Γ . The level shift is $\Delta\omega$.

Figure 8. The Cartesian coordinate system, where the first great circle magnetic field line lies in the $x'z'$ plane and the second great circle electric field line lies in the $y'z'$ plane, is designated the photon orbitsphere reference frame.

Figure 9. The field line pattern along the z axis of a right-handed circularly polarized photon.

Figure 10. The electric field of a moving point charge ($v = 4c/5$).

Figure 11. The electric field lines of a right-handed circularly polarized photon orbitsphere as seen along the axis of propagation in the lab inertial reference frame as it passes a fixed point.

Figure 12. The front view of the magnitude of the mass (charge) density function in the xy plane of a free electron; side view of a free electron along the axis of propagation (z axis).

Figure 13. The experimental results for the elastic differential cross-section for the elastic scattering of electrons by helium atoms and a Born approximation prediction.

Figure 14. The closed-form function ((139) and (140)) for the elastic differential cross-section for the elastic scattering of electrons by helium atoms. The scattering amplitude function $F(s)$ (138) is shown as an inset.

Figure 15. The radius of the universe as a function of time.

Figure 16. The expansion/contraction rate of the universe as a function of time.

Figure 17. The Hubble constant of the universe as a function of time.

Figure 18. The density of the universe as a function of time.

Figure 19. The power of the universe as a function of time.

Figure 20. The temperature of the universe as a function of time during the expansion phase.

Figure 21. The differential expansion of the light sphere due to the acceleration of the expansion of the cosmos as a function of time.

Figure 22. Step 1. Each point or coordinate position on the continuous two-dimensional electron orbitsphere defines an infinitesimal charge (mass) density element that moves along a geodesic orbit making up a great circle. Two such infinitesimal charges (masses) at points 1 (moving counterclockwise on the great circle in the

$y'z'$ plane) and 2 (moving clockwise on the circle in the $x'z'$ plane) of two orthogonal great circle current loops in the basis frame are considered as sub-basis elements to generate the current density corresponding to the spin quantum number, $s = 1/2$, $m_s = \pm 1/2$. The xyz system is the laboratory frame, and the orthogonal current loop basis set is rigid with respect to the $x'y'z'$ system that undergoes transformations to generate the elements of the electron current density function. The angular momentum of the orthogonal great circle current loops in the $x'y'$ plane is $\hbar/(2\sqrt{2})$.

Figure 23. Step 2. The orthogonal great circle basis set is rotated $\Delta\alpha_x = \pi/2$ with respect to the basis set of Step 1 shown in Fig. 22, and the direction of the current of the loop in the $y'z'$ plane is reversed. Point 1 now moves clockwise on the great circle in the $y'z'$ plane, and point 2 moves counterclockwise on the great circle in the $x'y'$ plane. The angular momentum of the orthogonal great circle current loops in the $-xz$ plane is $\hbar/(2\sqrt{2})$, corresponding to each of the z and $-x$ components of magnitude $\hbar/4$.

Figure 24. The trajectory of the resultant angular momentum vector of the orthogonal great circle current loops of magnitude $\hbar/(2\sqrt{2})$ during Step 1.

Figure 25. The angular momentum components of the orbitsphere and S in the rotating coordinate system X_R , Y_R , and Z_R that precess at the Larmor frequency about Z_R such that the vectors are stationary.

Figure 26. The angular momentum components of the orbitsphere and S in the stationary coordinate system. S and the components in the xy plane precess at the Larmor frequency about the z axis.

Figure 27. Coordinate system of crossed electric field E_y corresponding to the Hall voltage, magnetic flux B_x due to the applied field, and superconducting current i_z .

Figure 28. Coordinate system of crossed electric field E_r corresponding to the Hall voltage, magnetic flux B_θ due to the applied field, and superconducting current i_ϕ .

Tables

Table I: The Calculated Electric (per electron), Magnetic (per electron), and Ionization Energies for Some Two-Electron Atoms

Atom	r_1 (a_0) ^a	Electric Energy ^b (eV)	Magnetic Energy ^c (eV)	Calculated Ionization Energy ^d (eV)	Experimental Ionization ^(31,32) Energy (eV)
He	0.567	-23.96	0.63	24.59	24.59
Li ⁺	0.356	-76.41	2.54	75.56	75.64
Be ²⁺	0.261	-156.08	6.42	154.48	153.89
B ³⁺	0.207	-262.94	12.96	260.35	259.37
C ⁴⁺	0.171	-396.98	22.83	393.18	392.08
N ⁵⁺	0.146	-558.20	36.74	552.95	552.06
O ⁶⁺	0.127	-746.59	55.35	739.67	739.32
F ⁷⁺	0.113	-962.17	79.37	953.35	953.89

^a from (130)^b from (132)^c from (133)^d from (131) and (134)**Table II:** The Maxwellian Closed-Form Calculated and Experimental Parameters of H₂, D₂, H₂⁺, and D₂⁺

Parameter	Calculated	Experimental	Equations ⁽³⁾
H ₂ bond energy	4.478 eV	4.478 eV	(12.251)
D ₂ bond energy	4.556 eV	4.556 eV	(12.253)
H ₂ ⁺ bond energy	2.654 eV	2.651 eV	(12.220)
D ₂ ⁺ bond energy	2.696 eV	2.691 eV	(12.222)
H ₂ total energy	31.677 eV	31.675 eV	(12.247)
D ₂ total energy	31.760 eV	31.760 eV	(12.248)
H ₂ ionization energy	15.425 eV	15.426 eV	(12.249)
D ₂ ionization energy	15.463 eV	15.466 eV	(12.250)
H ₂ ⁺ ionization energy	16.253 eV	16.250 eV	(12.218)
D ₂ ⁺ ionization energy	16.299 eV	16.294 eV	(12.219)
H ₂ ⁺ magnetic moment	$9.274 \times 10^{-24} \text{ J} \cdot \text{T}^{-1} (\mu_B)$	$9.274 \times 10^{-24} \text{ J} \cdot \text{T}^{-1} (\mu_B)$	(14.1)–(14.7)
Absolute H ₂ gas-phase NMR shift	-28.0 ppm	-28.0 ppm	(12.362)
H ₂ internuclear distance ^a	$0.748 \text{ X}(\sqrt{2} a_0)$	0.741 X	(12.238)
D ₂ internuclear distance ^a	$0.748 \text{ X}(\sqrt{2} a_0)$	0.741 X	(12.238)
H ₂ ⁺ internuclear distance ^b	$1.058 \text{ X}(2a_0)$	1.06 X	(12.207)
D ₂ ⁺ internuclear distance ^a	$1.058 \text{ X}(2a_0)$	1.0559 X	(12.207)
H ₂ vibrational energy	0.517 eV	0.516 eV	(12.259)
D ₂ vibrational energy	0.371 eV	0.371 eV	(12.264)
H ₂ $\omega_e x_e$	120.4 cm ⁻¹	121.33 cm ⁻¹	(12.261)
D ₂ $\omega_e x_e$	60.93 cm ⁻¹	61.82 cm ⁻¹	(12.265)
H ₂ ⁺ vibrational energy	0.270 eV	0.271 eV	(12.228)
D ₂ ⁺ vibrational energy	0.193 eV	0.196 eV	(12.232)
H ₂ $J = 1$ to $J = 0$ rotational energy ^a	0.0148 eV	0.015 09 eV	(14.45)
D ₂ $J = 1$ to $J = 0$ rotational energy ^a	0.007 41 eV	0.007 55 eV	(14.37)–(14.45)
H ₂ ⁺ $J = 1$ to $J = 0$ rotational energy ^b	0.007 40 eV	0.007 39 eV	(14.49)
D ₂ ⁺ $J = 1$ to $J = 0$ rotational energy ^a	0.003 70 eV	0.003 723 eV	(14.37)–(14.43), (14.49)

^a The internuclear distances are not corrected for the reduction due to \bar{E}_{osc} .

^b The internuclear distances are not corrected for the increase due to \bar{E}_{osc} .

Table III: Predicted Harmonic Parameters ℓ and Relative Intensities $I(n)$ as a Function of Peak n

n	ℓ^a	Angle ($^\circ$) ^a	$I(n)^b$
1	197	0.91	1
2	591	0.30	0.50
3	788	0.23	0.33
4	985	0.18	0.25
5	1182	0.15	0.20
6	1379	0.13	0.17

^a from (217)

^b from (221)

Table IV: Summary of the Results of the Matrix Transformations of the Two Orthogonal Current Loops to Generate the Orbitsphere

Step	Initial Direction of Angular Momentum Components $(\hat{r} \times \hat{K})^a$	Final Direction of Angular Momentum Components $(\hat{r} \times \hat{K})^a$	Sign of $\Delta\alpha_x$	Sign of $\Delta\alpha_y$	Initial to Final Axis Transformation	L_{xy}	L_z
1	$\hat{x}, -\hat{y}$	$-\hat{x}, \hat{y}$	$+\Delta\alpha_x$	$+\Delta\alpha_y$	$+x' \rightarrow +y$ $+y' \rightarrow +x$ $+z' \rightarrow -z$	0	$\hbar/4$
2	$-\hat{x}, \hat{z}$	$-\hat{x}, \hat{z}$	$-\Delta\alpha_x$	$+\Delta\alpha_x$	$+z' \rightarrow -x$ $+x' \rightarrow -z$ $+y' \rightarrow -y$	$\hbar/4$	$\hbar/4$
Total						$\hbar/4$	$\hbar/2$

^a \mathbf{K} is the current density, \mathbf{r} is the polar vector of the great circle, and $\hat{\cdot}$ denotes unit vectors, e.g., $\hat{u} \equiv \mathbf{u}/|\mathbf{u}|$.

Figure 1. The orbitsphere is a two dimensional spherical shell of zero thickness with the Bohr radius of the hydrogen atom, $r = a_H$.

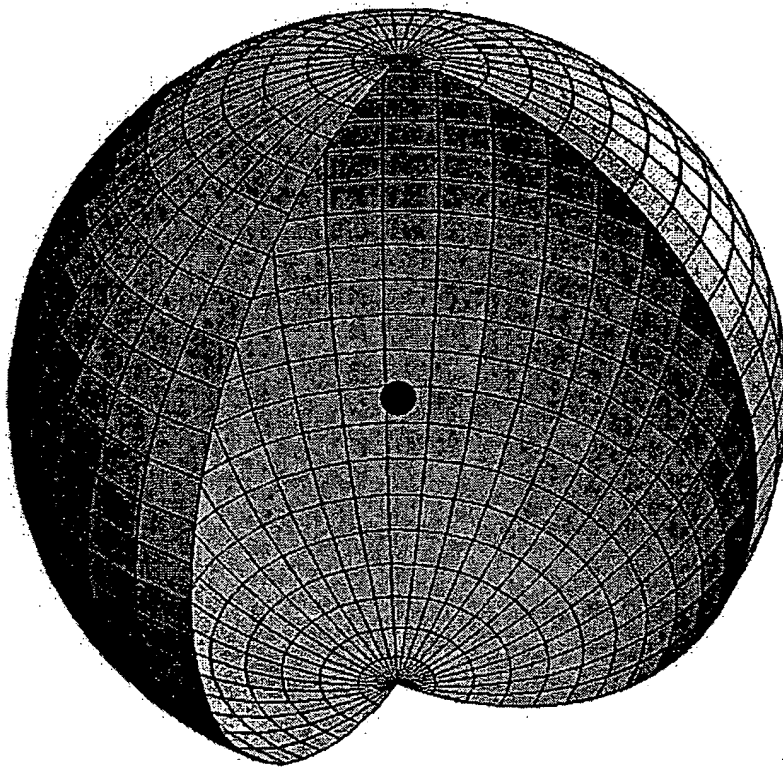
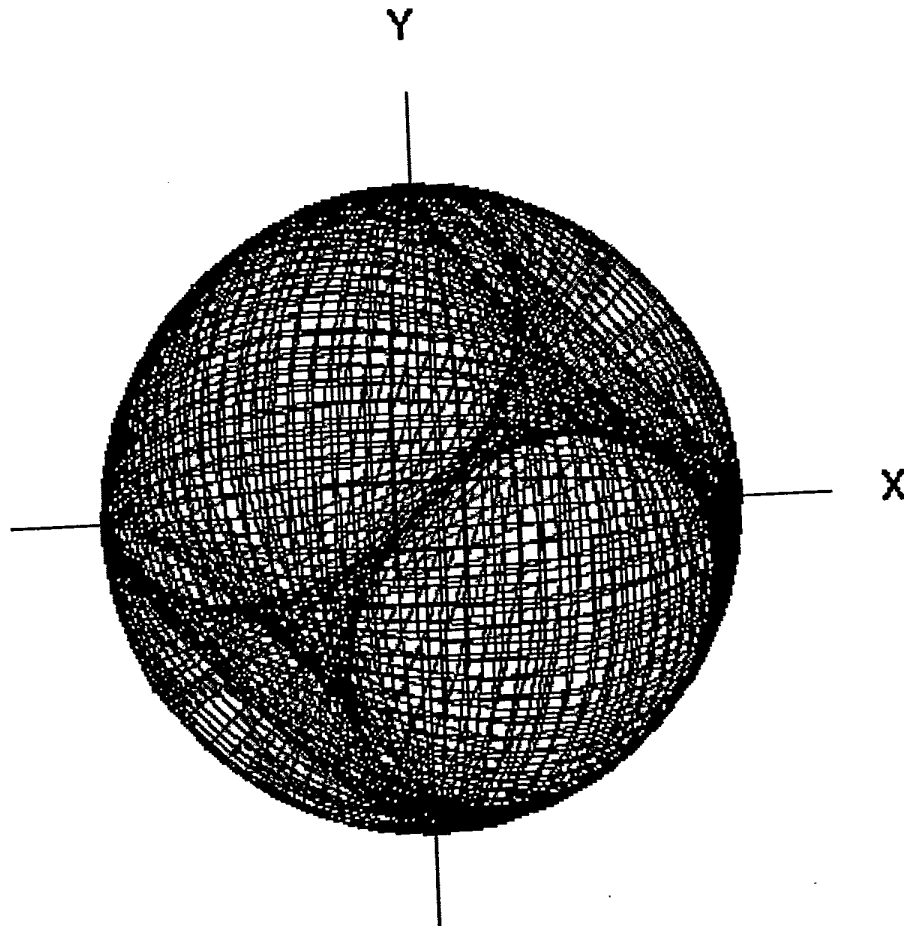


Fig. 2. The current pattern of the orbitsphere shown with 6 degree increments of the infinitesimal angular variables $\pm\Delta\alpha_r$ and $\pm\Delta\alpha_j$, from the perspective of looking along the z-axis. The current and charge density are confined to two dimensions at $r_n = nr_1$. The corresponding charge density function is uniform.



View Along the Positive Z Axis

Fig. 3. The orbital function modulates the constant (spin) function (shown for $t = 0$; three-dimensional view).

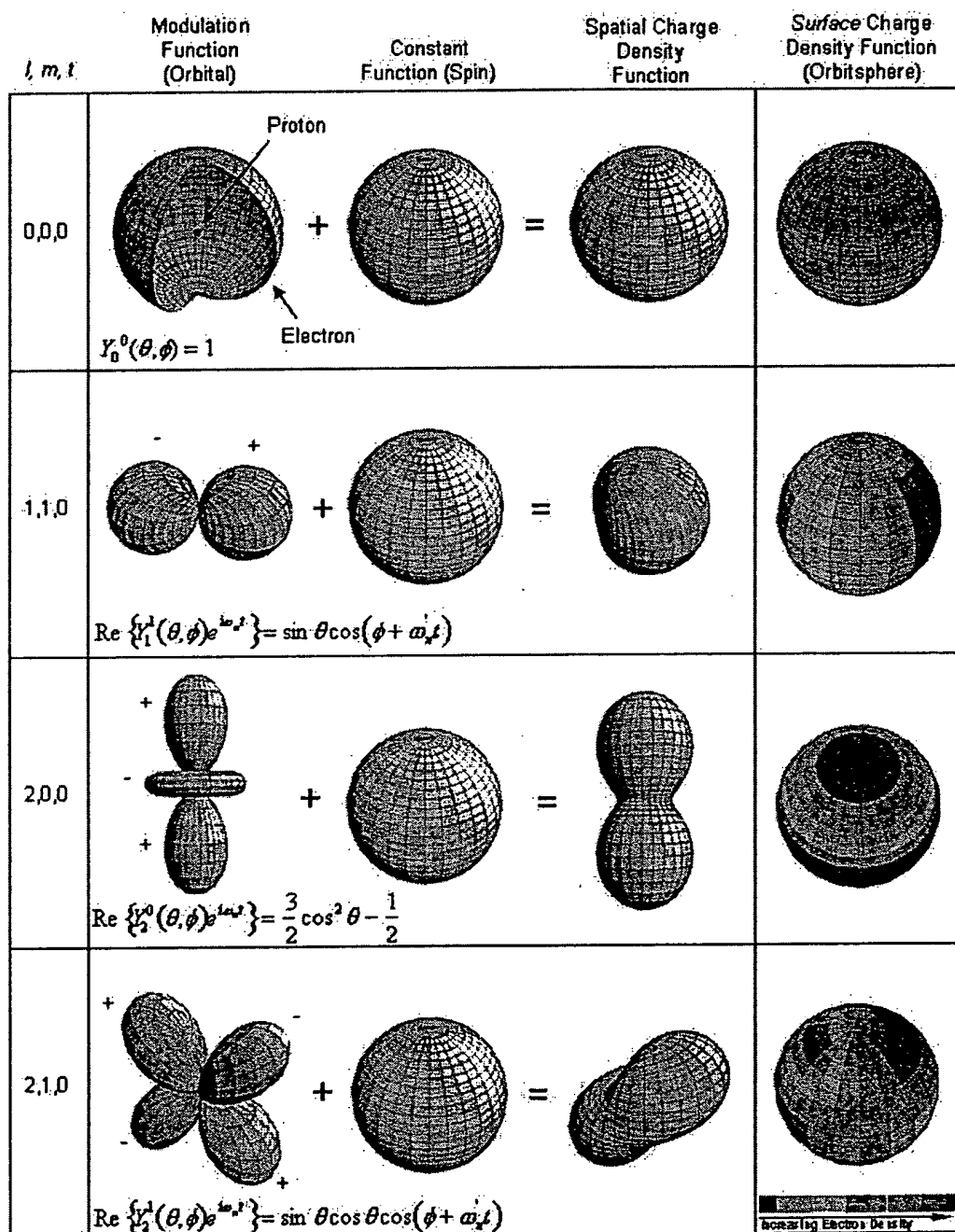


Fig. 4. The normalized radius as a function of the velocity due to relativistic contraction.

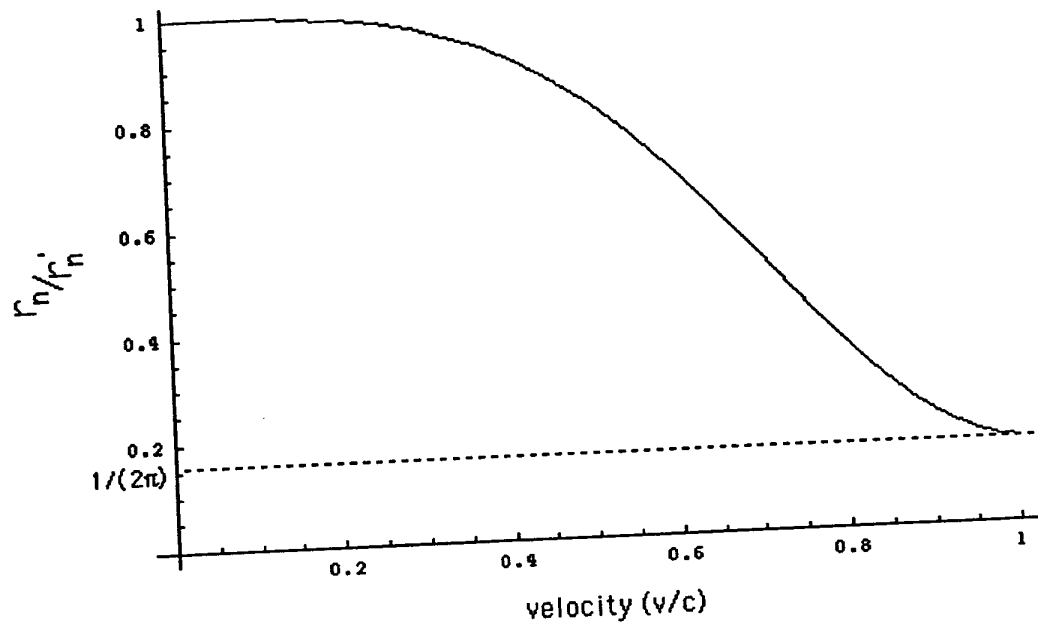


Fig. 5. Far field approximation.

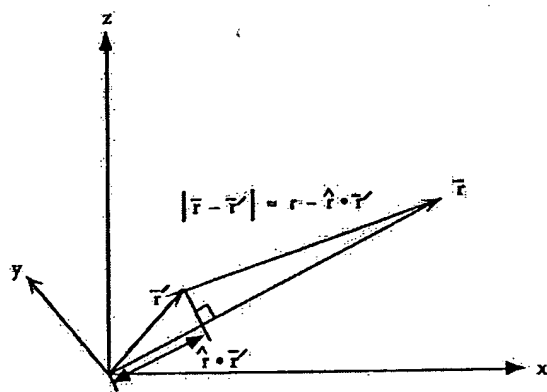


Fig. 6. The magnetic field of an electron orbitsphere (z-axis defined as the vertical axis).

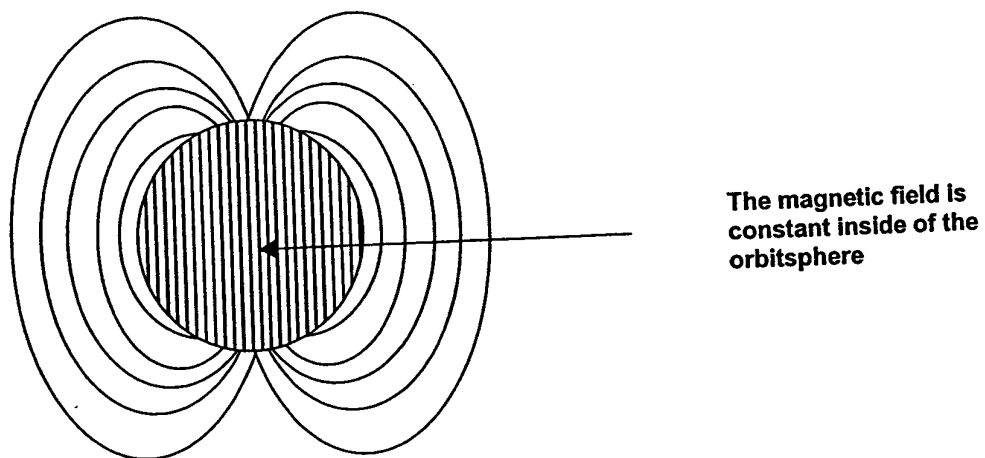


Fig. 7. Broadening of the spectral line due to the rise-time and shifting of the spectral line due to the radiative reaction. The resonant line shape has width Γ . The level shift is $\Delta\omega$.

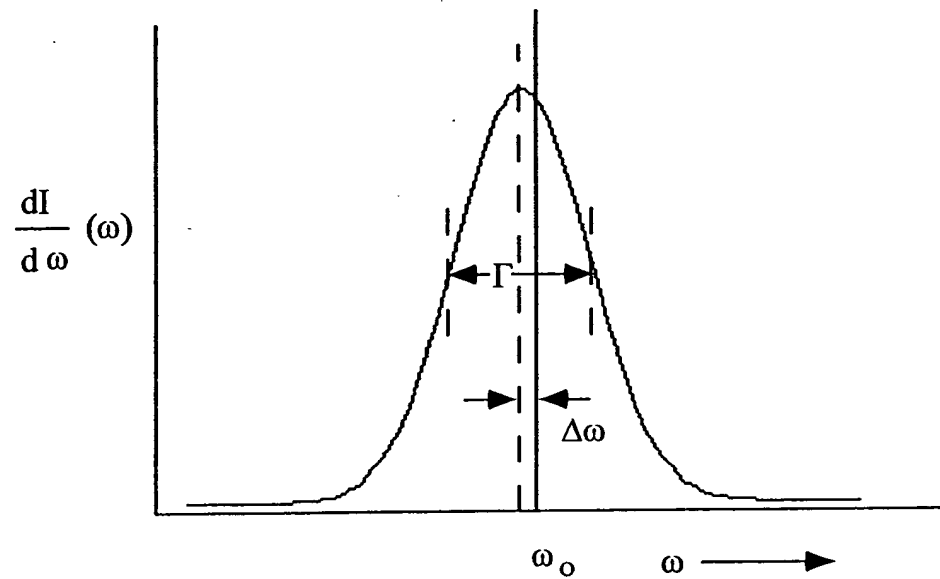


Fig. 8

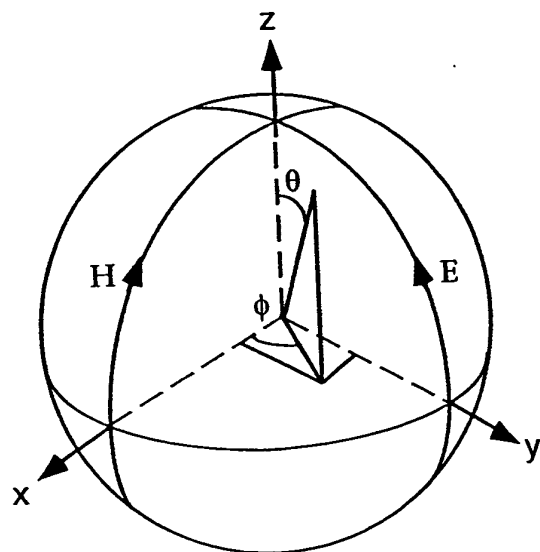


Fig. 9

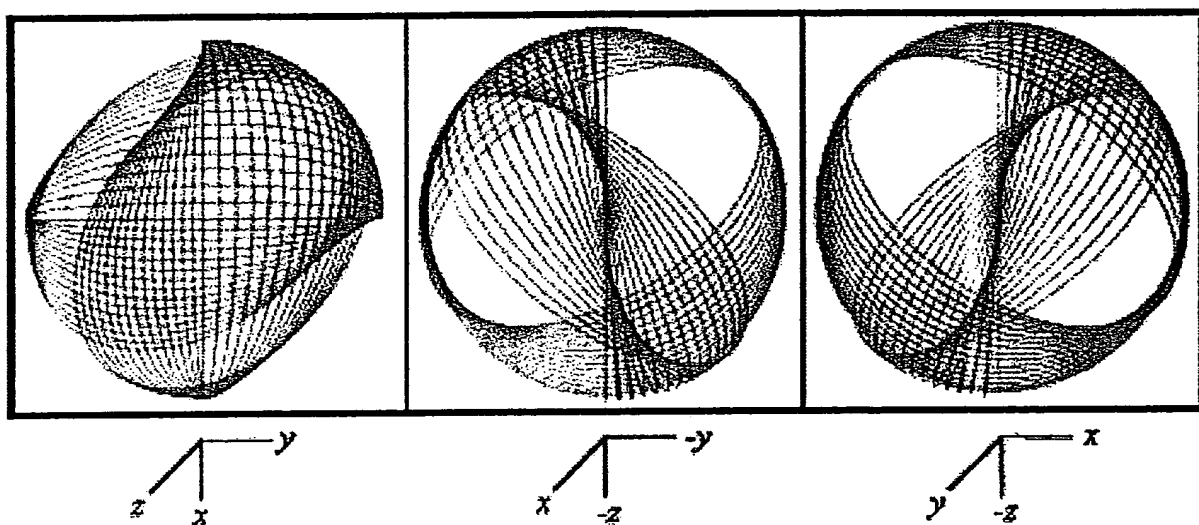


Fig. 10. The electric field of a moving point charge ($v = \frac{4}{5}c$).

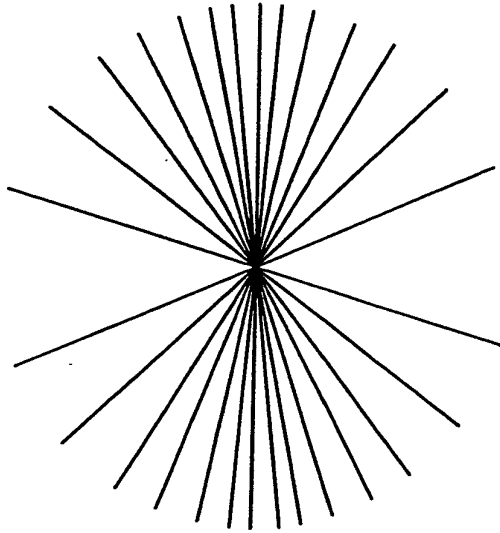


Fig. 11. The electric field lines of a right-handed circularly polarized photon orbitsphere as seen along the axis of propagation in the lab inertial reference frame as it passes a fixed point.

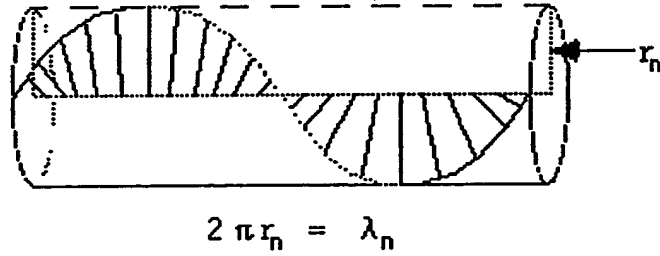


Fig. 12

The Free Electron

$$\rho_0 = \frac{\hbar}{m_e v_x}$$

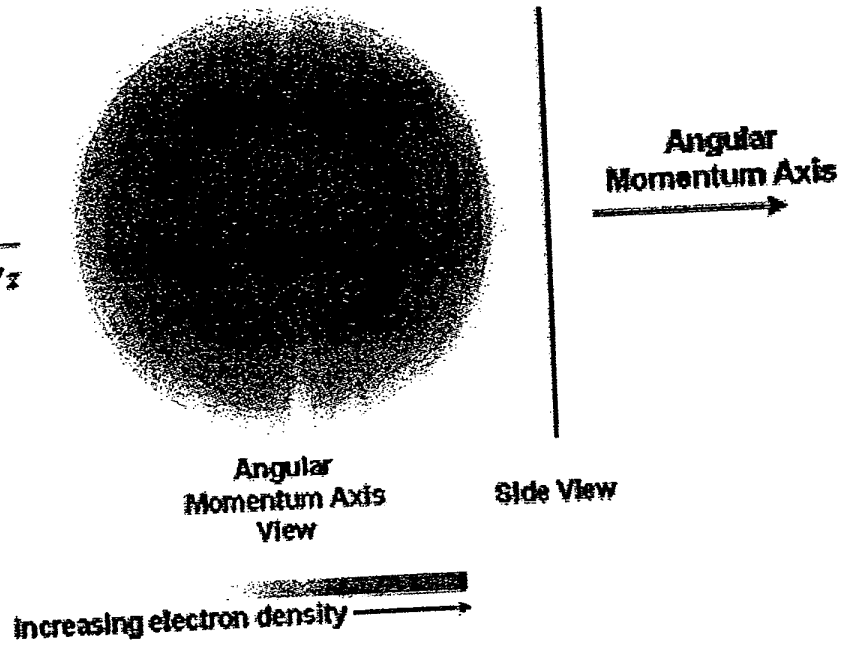


Fig. 13. The experimental results for the elastic differential cross section for the elastic scattering of electrons by helium atoms and a Born approximation prediction.

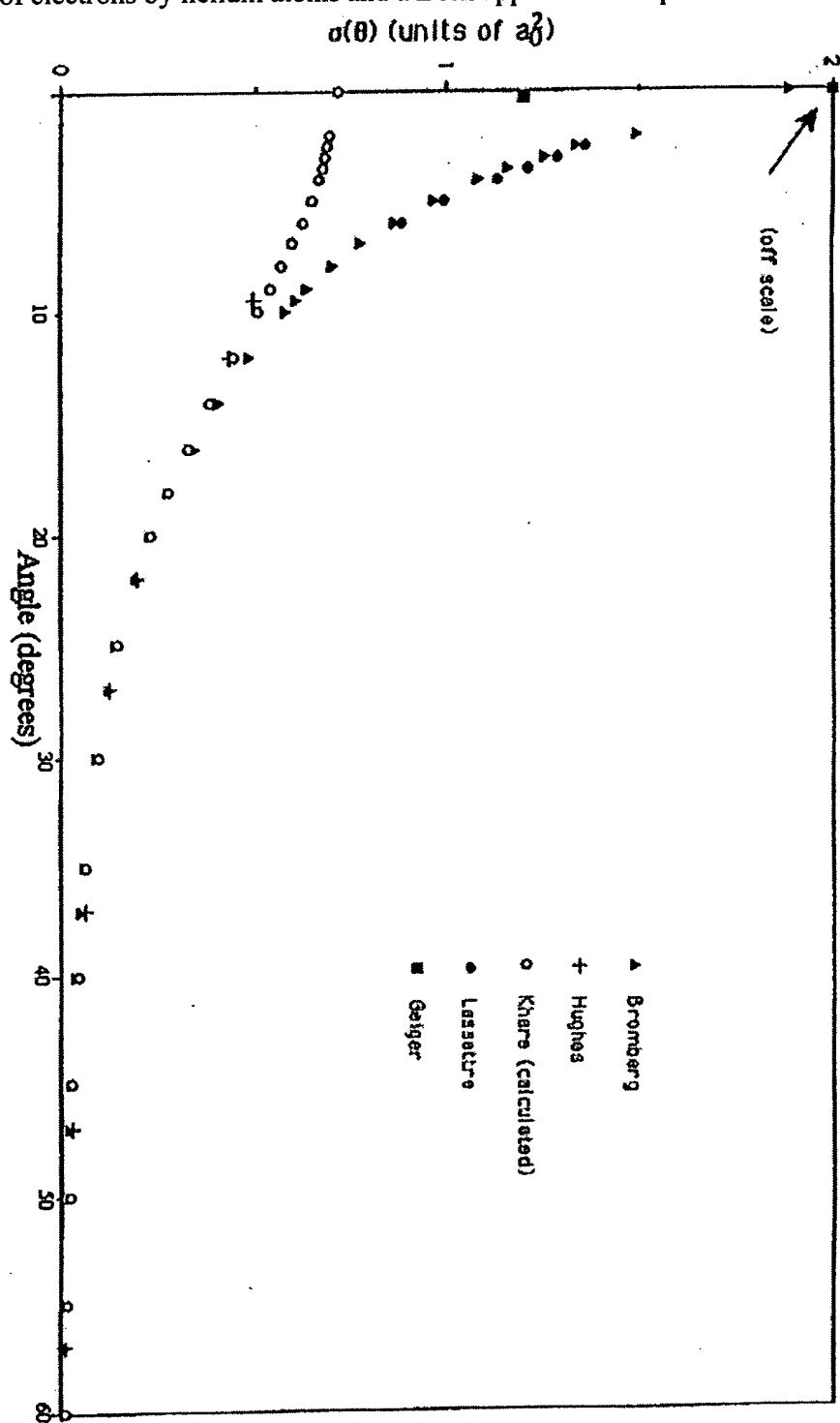


Fig. 14. The closed form function (Eqs. (146) and (147)) for the elastic differential cross section for the elastic scattering of electrons by helium atoms. The scattering amplitude function, $F(s)$ (Eq. (145)), is shown as an insert.

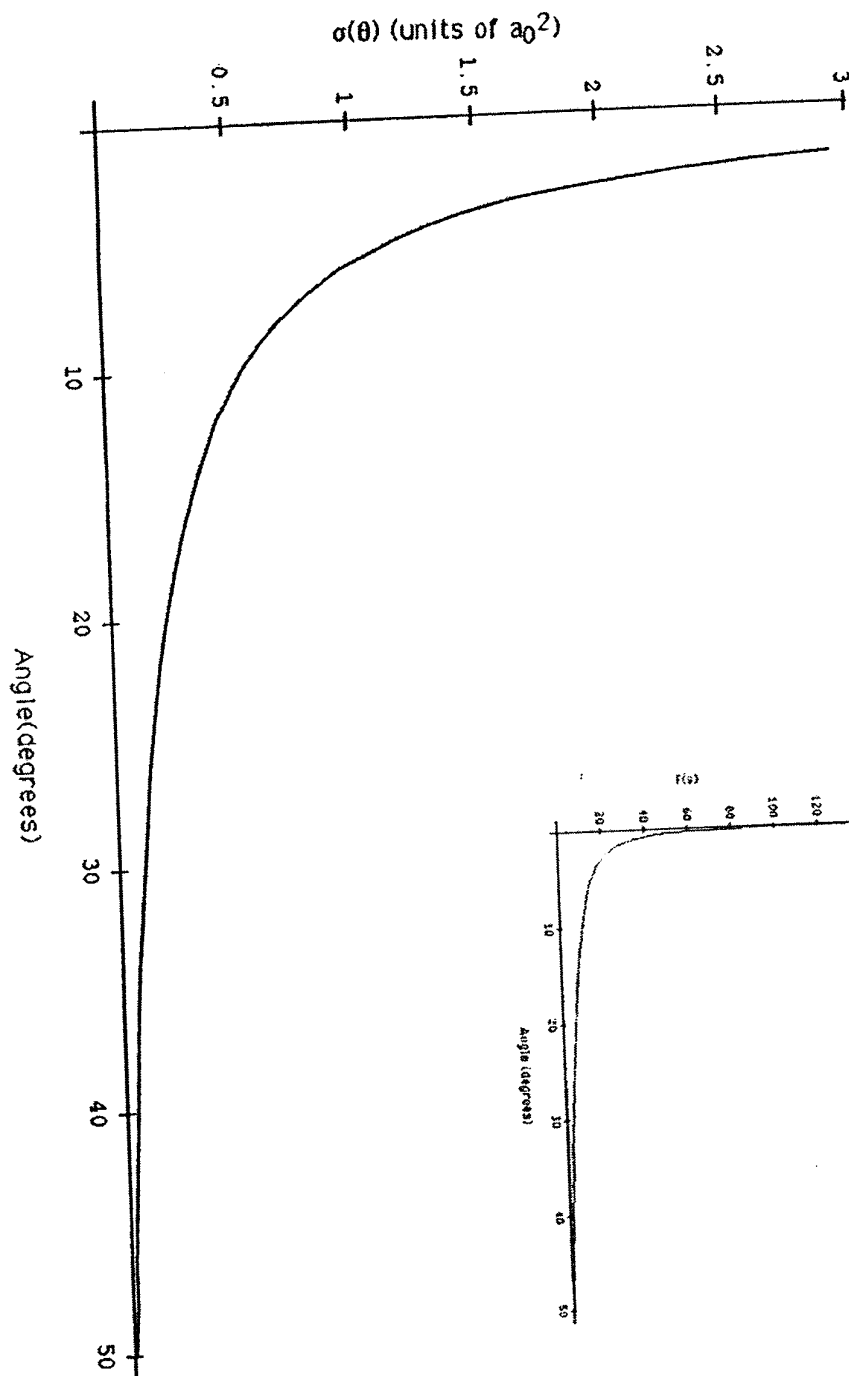


Fig. 15. The radius of the universe as a function of time.

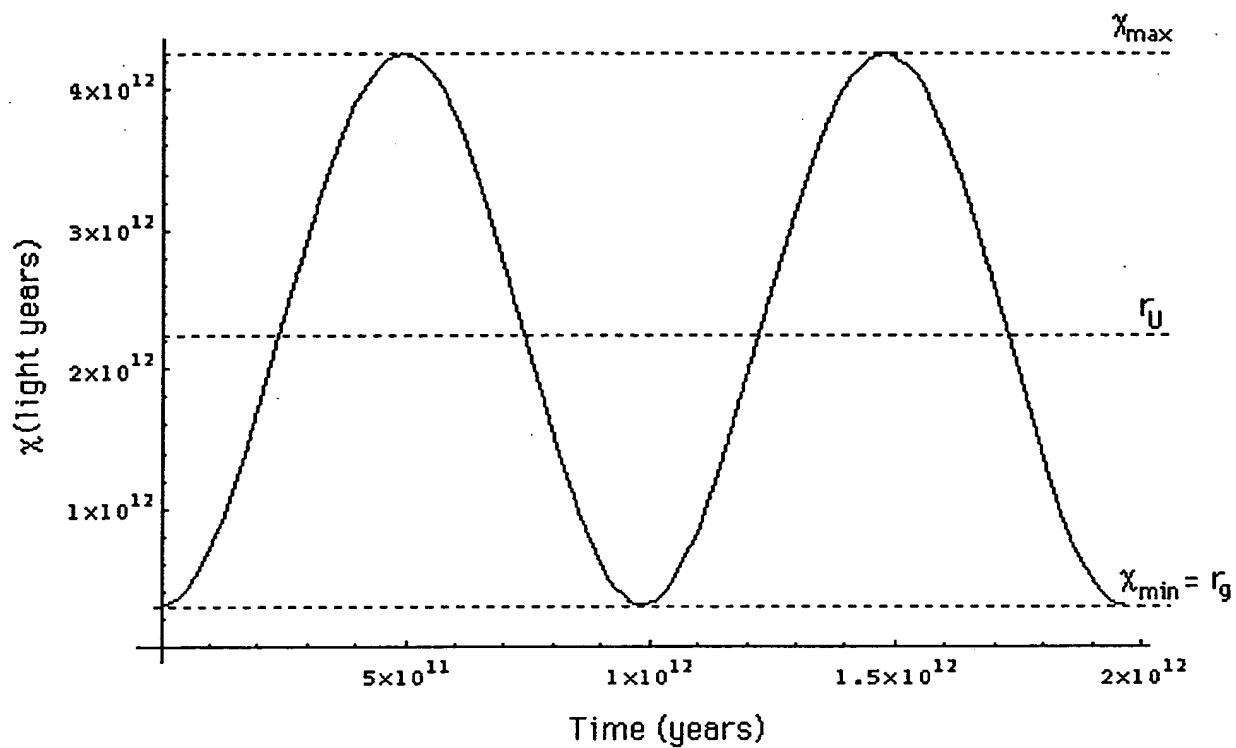


Fig. 16. The expansion/contraction rate of the universe as a function of time.

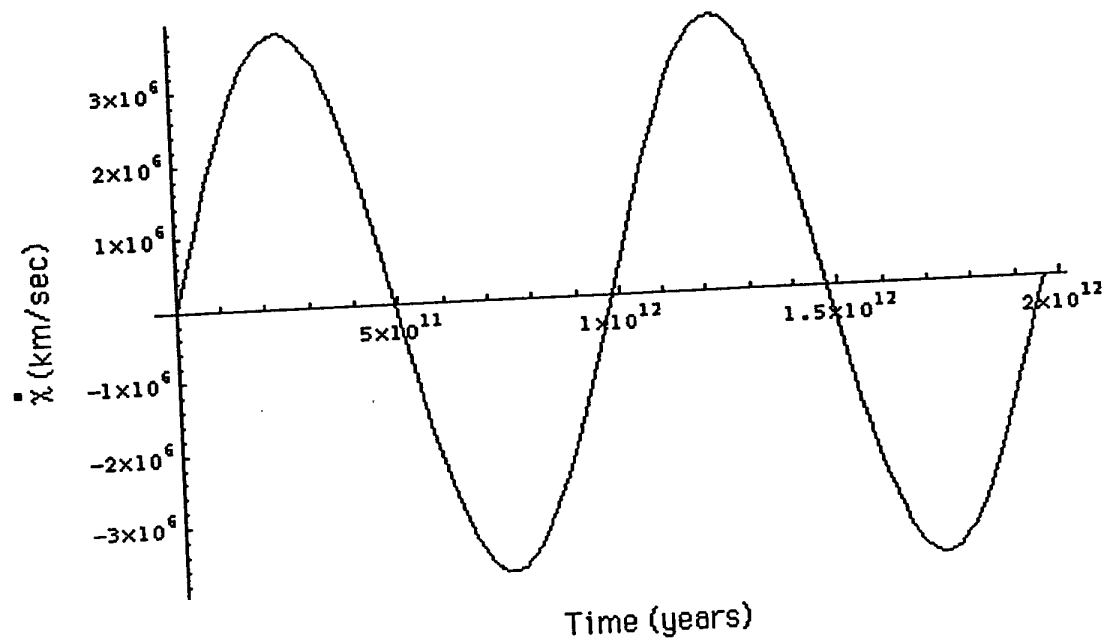


Fig. 17. The Hubble constant of the universe as a function of time.

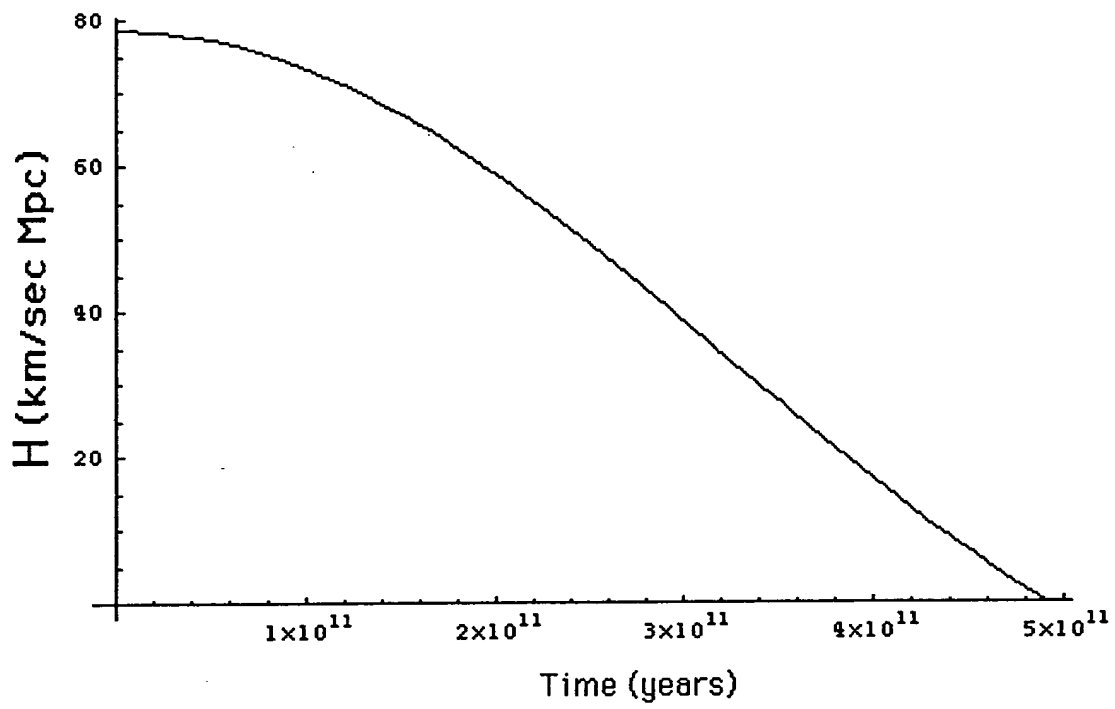


Fig. 18. The density of the universe as a function of time.

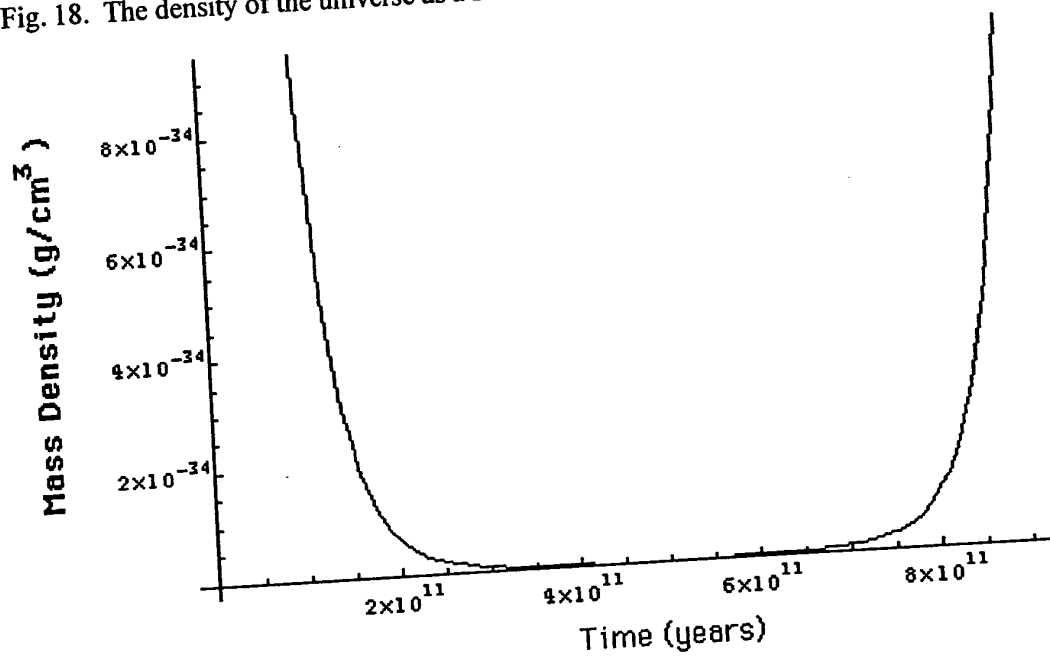


Fig. 19. The power of the universe as a function of time.

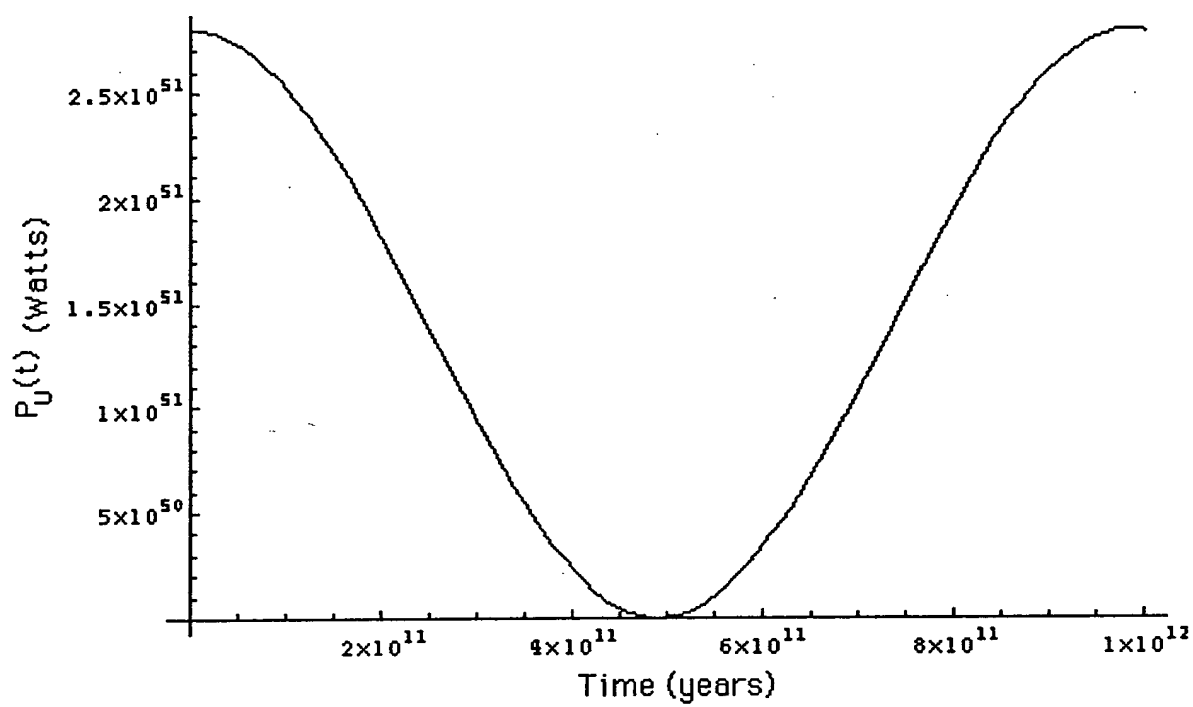


Fig. 20. The temperature of the universe as a function of time during the expansion phase.

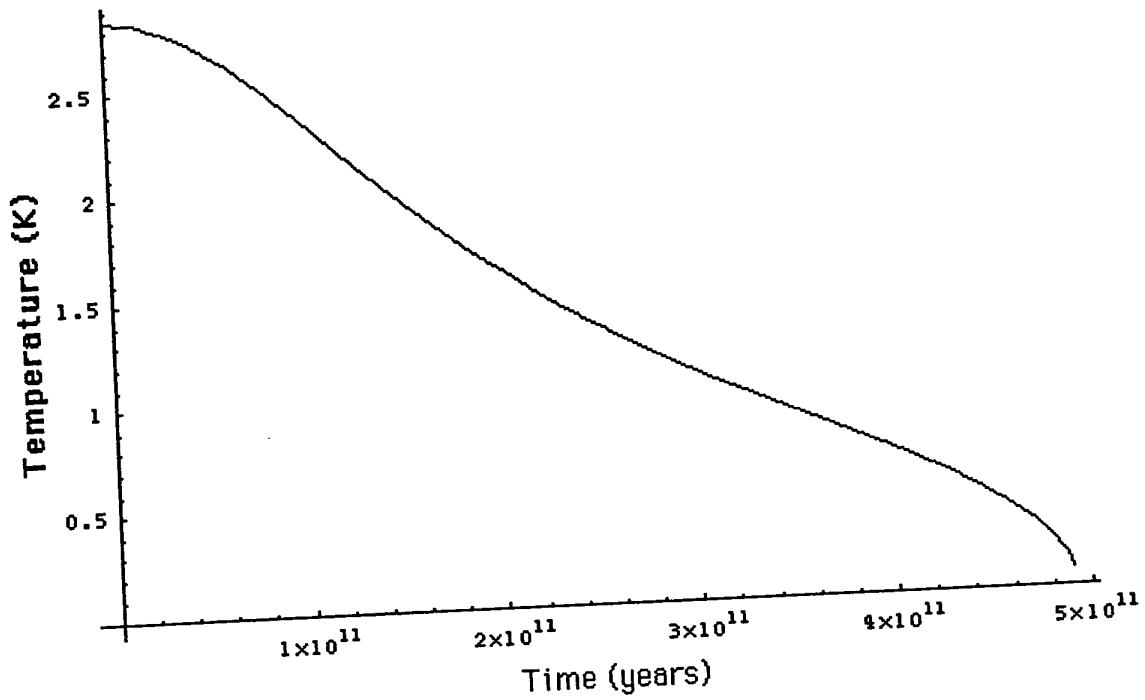


Fig. 21. The differential expansion of the light-sphere due to the acceleration of the expansion of the cosmos as a function of time.

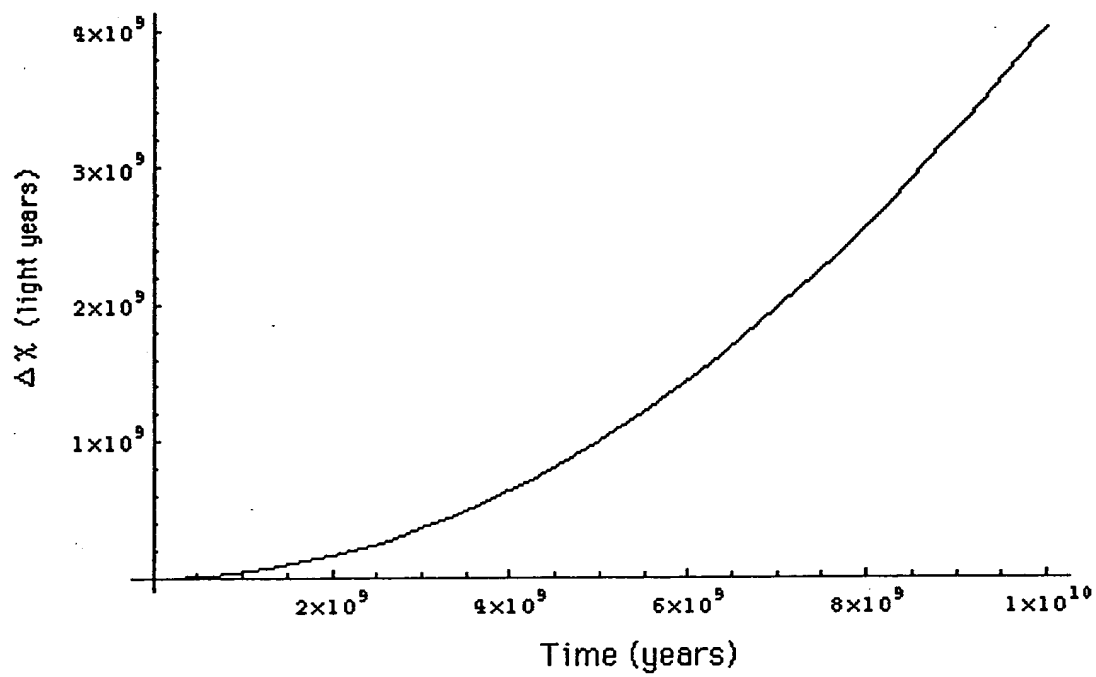


Fig. 22. Step One. Each point or coordinate position on the continuous two-dimensional electron orbitsphere defines an infinitesimal charge (mass)-density element which moves along a geodesic orbit comprising a great circle. Two such infinitesimal charges (masses) at points one (moving counter clockwise on the great circle in the $y'z'$ -plane) and two (moving clockwise on the great circle in the $x'z'$ -plane) of two orthogonal great circle current loops in the basis frame are considered as sub-basis elements to generate the current density corresponding to the spin quantum number, $s = \frac{1}{2}$; $m_s = \pm \frac{1}{2}$. The xyz -system is the laboratory frame, and the orthogonal-current-loop basis set is rigid with respect to the $x'y'z'$ -system that undergoes transformations to generate the elements of the electron current density function. The angular momentum of the orthogonal great circle current loops in the $x'y'$ -plane is $\frac{\hbar}{2\sqrt{2}}$.

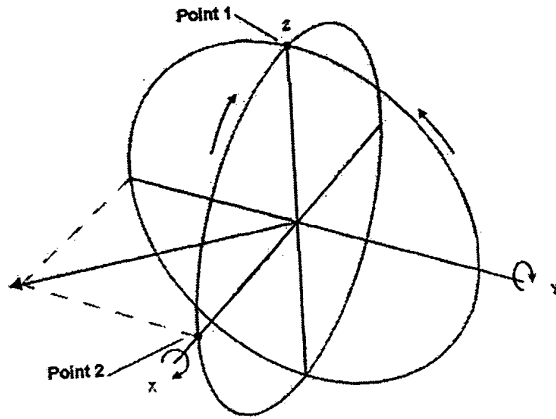


Fig. 23. Step Two. The orthogonal great circle basis set is rotated $\Delta\alpha_x = \frac{\pi}{2}$ with respect to the basis set of Step One shown in Figure 22 and the direction of the current of the loop in the $y'z'$ -plane is reversed. Point one now moves clockwise on the great circle in the $y'z'$ -plane, and point two moves counter clockwise on the great circle in the $x'y'$ -plane. The angular momentum of the orthogonal great circle current loops in the $-xz$ -plane is $\frac{\hbar}{2\sqrt{2}}$ corresponding to each of the z and $-x$ -components of magnitude $\frac{\hbar}{4}$.

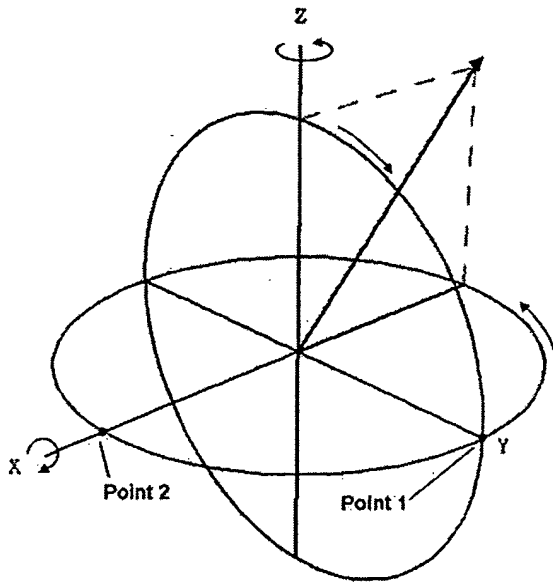


Fig. 24. The trajectory of the resultant angular momentum vector of the orthogonal great circle current loops of magnitude $\frac{\hbar}{2\sqrt{2}}$ during Step One.

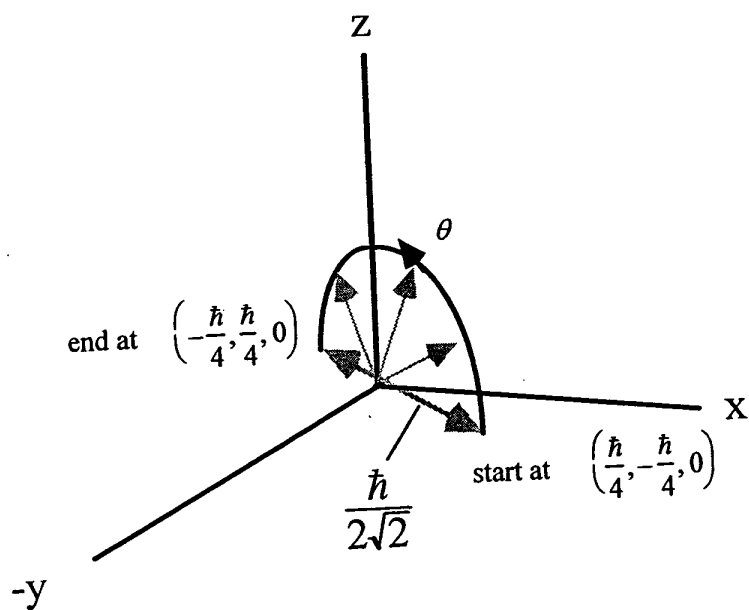


Fig. 25. The angular momentum components of the orbitsphere and S in the rotating coordinate system X_R , Y_R , and Z_R that precesses at the Larmor frequency about Z_R such that the vectors are stationary.

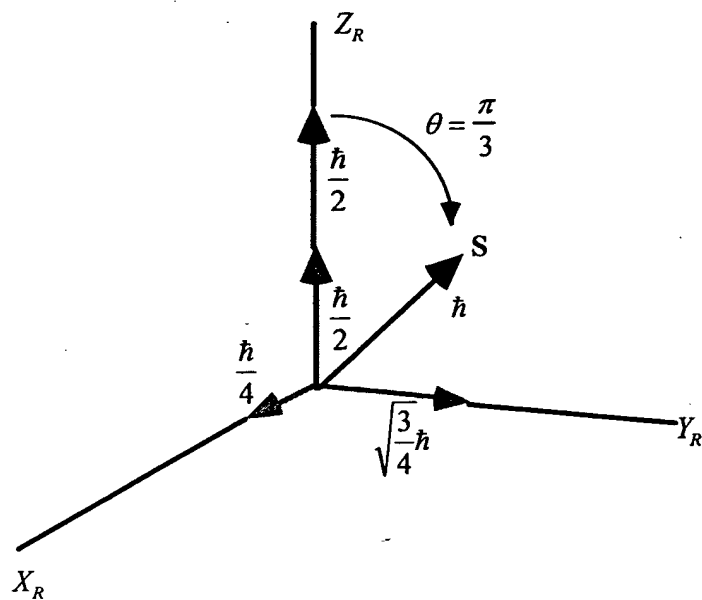


Fig. 26. The angular momentum components of the orbitsphere and S in the stationary coordinate system. S and the components in the xy -plane precesses at the Larmor frequency about the z -axis.

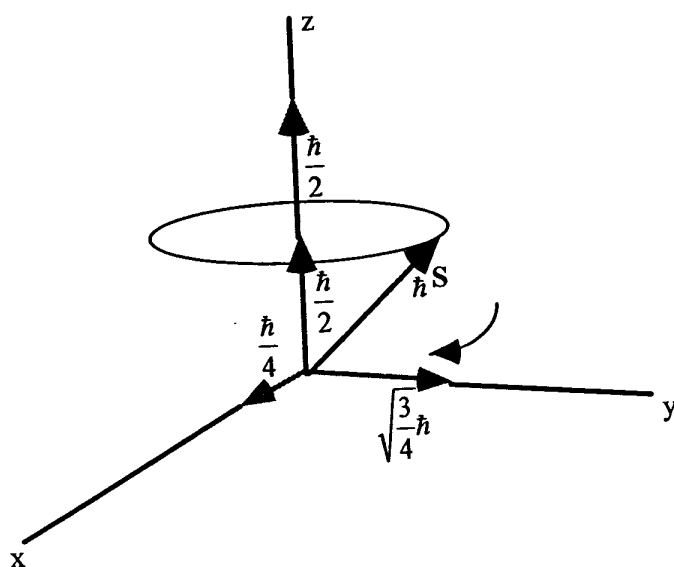


Fig. 27. Coordinate system of crossed electric field, E_y , corresponding to the Hall voltage, magnetic flux, B_x , due to applied field, and superconducting current i_z .

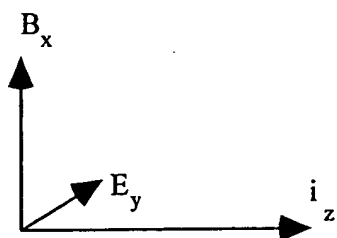
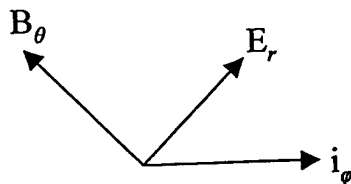


Fig. 28. Coordinate system of crossed electric field, E_r , corresponding to the Hall voltage, magnetic flux, B_θ , due to applied field, and superconducting current i_ϕ .



**This Page is Inserted by IFW Indexing and Scanning
Operations and is not part of the Official Record**

BEST AVAILABLE IMAGES

Defective images within this document are accurate representations of the original documents submitted by the applicant.

Defects in the images include but are not limited to the items checked:

- ☐ BLACK BORDERS
- ☐ IMAGE CUT OFF AT TOP, BOTTOM OR SIDES
- ☐ FADED TEXT OR DRAWING
- ☒ BLURRED OR ILLEGIBLE TEXT OR DRAWING
- ☐ SKEWED/SLANTED IMAGES
- ☐ COLOR OR BLACK AND WHITE PHOTOGRAPHS
- ☐ GRAY SCALE DOCUMENTS
- ☐ LINES OR MARKS ON ORIGINAL DOCUMENT
- ☐ REFERENCE(S) OR EXHIBIT(S) SUBMITTED ARE POOR QUALITY
- ☐ OTHER: _____

IMAGES ARE BEST AVAILABLE COPY.

As rescanning these documents will not correct the image problems checked, please do not report these problems to the IFW Image Problem Mailbox.

This Page Blank (uspto)